

AD-A078 057

PRATT AND WHITNEY AIRCRAFT GROUP EAST HARTFORD CONN
EXPERIMENTAL EVALUATION OF A LOW EMISSIONS HIGH PERFORMANCE
JAN 79 R P LOHMANN , R J MADOR

F/G 21/5
DUC--ETC(U)

UNCLASSIFIED

PWA-5513-32

NASA-CR-159694

NL

1 OF 2
AD-
A078057



AD A078057

NASA CR-159694
PWA 5513-32



**EXPERIMENTAL EVALUATION OF A LOW EMISSIONS
HIGH PERFORMANCE DUCT BURNER FOR VARIABLE CYCLE ENGINES (VCE)**

FINAL REPORT

by

R. P. Lohmann and R. J. Mador

UNITED TECHNOLOGIES CORPORATION
Pratt & Whitney Aircraft Group
Commercial Products Division

DDC FILE COPY

Prepared for

National Aeronautics and Space Administration
NASA Lewis Research Center
Contract NAS3-20602

REPRODUCED BY
NATIONAL TECHNICAL
INFORMATION SERVICE
U.S. DEPARTMENT OF COMMERCE
SPRINGFIELD, VA. 22161

79 11 05-268

1. Report No. NASA CR-159694	2. Government Accession No.	3. Recipient's Catalog No.
4. Title and Subtitle Experimental Evaluation of a Low Emissions High Performance Duct Burner for Variable Cycle Engines (VCE)		5. Report Date
7. Author(s) Robert P. Lohmann Ronald J. Mador		6. Performing Organization Code
8. Performing Organization Name and Address UNITED TECHNOLOGIES CORPORATION Pratt & Whitney Aircraft Group - CPD East Hartford, Connecticut		9. Performing Organization Report No. PWA-5513-32
12. Sponsoring Agency Name and Address NASA Lewis Research Center VCE Projects Office 21000 Brookpark Road Cleveland, OH 44135		10. Work Unit No.
15. Supplementary Notes		11. Contract or Grant No. NAS3-20602
16. Abstract An experimental evaluation was conducted with a three-stage Vorbix duct burner to determine the performance and emissions characteristics of this concept and to refine the configuration to provide acceptable durability and operational characteristics for its use in the VCE Testbed Program. The tests were conducted at representative takeoff, transonic climb and supersonic cruise inlet conditions for the VSCE-502R study engine. The carbon monoxide and unburned hydrocarbon emissions were low at all three operating conditions with combustion efficiencies in excess of 99.7 percent, as compared to the goal of 99.0 percent. NO _x emissions were moderate but in excess of the program goal of 1 gm/kg at takeoff. The thrust efficiency exceeded the goal level of 94.5 percent reaching a value of 97 percent at supersonic cruise. soft ignition, the absence of combustion generated acoustic instabilities and liner temperature levels acceptable for experimental hardware were also demonstrated. The total pressure loss across the duct burner, at 6.76 the loss mechanisms have been identified and, in one configuration 40 percent of this excess loss was eliminated without compromising the emissions or thrust efficiency.		13. Type of Report and Period Covered
17. Key Words (Suggested by Author(s)) 07 Aircraft Propulsion & Power		14. Sponsoring Agency Code
19. Security Classif. (of this report) Unclassified	20. Security Classif. (of this page) Unclassified	

* For sale by the National Technical Information Service, Springfield, Virginia 22161

TABLE OF CONTENTS (Cont'd)

Section	Title	Page
7.0	EXPERIMENTAL RESULTS - DUCT BURNER EVOLUTION	63
	7.1 Introduction	63
	7.2 Burner Liner Durability	63
	7.3 Effect of Fuel Injections on Emissions	68
	7.4 Total Pressure Loss Reduction	73
	7.5 Effect of Total Pressure Loss on Emissions and Other Performance Parameters	76
8.0	SUMMARY OF EXPERIMENTAL RESULTS	78
9.0	CONCLUDING REMARKS	79
	APPENDIX A - DUCT BURNER CONFIGURATIONS	80
	APPENDIX B - EXHAUST GAS ANALYSIS	92
	APPENDIX C - EXPERIMENTAL DATA SUMMARY	97
	APPENDIX D - FUEL INJECTOR SPRAY EVALUATION	102
	NOMENCLATURE	107
	REFERENCES	107

LIST OF ILLUSTRATIONS

Figure No.	Title	Page
3-1	Crosssection of the VSCE -502B Variable Stream Control Engine	5
3-2	Operating Modes of Variable Stream Control Engine	6
3-3	Effect of Duct burner Emissions on Overall Engine Emissions Characteristics During EPA Landing and Takeoff Cycle	9
3-4	Effect of Duct Burner Emissions Characteristics on Overall Engine NO _x Emissions at Supersonic Cruise	10
3-5	Three Stage Vorbix Duct Burner in the VSCE-502B Engine	11
3-6	Effect of Reference Velocity on Momentum Pressure Loss and Radial Duct Height	13
3-7	Fuel Schedule for the Three Stage Duct Burner	15
3-8	Crosssection of the VCE Testbed	17
3-9	Duct Burner Segment Rig Components	20
3-10	VCE Duct Burner Segment Rig Partially Assembled	21
3-11	Dimensions of the VCE Segment Duct Burner Rig	21
3-12	Design Airflow and Pressure Distribution in the Duct Burner Rig at the Takeoff Condition	24
4-1	Schematic of X-127 Airflow System	25
4-2	Diagram of Fuel Supply and Distribution System in Stand X-127 Stand	27
4-3	Duct Burner Rig Pressure and Temperature Instrumentation	28
4-4	Details of Steam Cooled Gas Sampling Rake	30
4-5	Location of Gas Sampling Probes	31
4-6	Emissions Sample Selection System	31
4-7	Water Flow Visualization Model Duct Burner	33

LIST OF ILLUSTRATIONS (Cont'd)

Figure No.	Title	Page
4-8	Swirler Flow Calibration Rig	33
4-9	Fuel Injector Flow Visualization Rig	34
5-2	Comparison of Exit Gas Temperature Calculated From Local Carbon Balance Fuel-Air Ratio and the Thermocouple Probe Measurement	38
5-3	Analytical Model for Computing Thrust Efficiency	39
6-1	Airflow Distribution in Configuration 11 of the Duct Burner Rig	40
6-2	Effect of Fuel Air Ratio on Airflow Distribution in the Duct Burner	47
6-3	Emissions Characteristics of the Duct Burner	51
6-4	Effect of Fuel Flow Split on the Emissions Characteristics of the Combined Prechamber and Pilot Secondary Stages	53
6-5	Effect of Fuel Split Between Prechamber/Pilot Secondary Stages and the High Power Stage on Emissions	53
6-6	Total Pressure Loss Across Configuration 11 of the Duct Burner Rig	54
6-7	Comparison of Predicted and Measured Static Pressure Distributions	55
6-8	Total Pressure and Temperature Profiles at the Exit of the Duct Burner Rig (Configuration 11)	56
6-9	Ignition and Lean Blow Out Characteristics of the Duct Burner	59
6-10	Duct Burner Ignition Pressure Pulse	60
6-11	Spectral Distribution of Pressure Variation in the High Power Stage of the Duct Burner	61
7-1	Metal Temperature History on Louver 8 of the Outer Liner	64
7-2	Swirler Tube Orientation in the Duct Burner	64
7-3	Measured Liner Temperature Distribution in Configuration 11 of the Duct Burner	67

LIST OF ILLUSTRATIONS (Cont'd)

Figure No.	Title	Page
7-4	Effect of Conical Spray (Configuration 7) Vs Flat Spray (Configuration 11) High Power Fuel Nozzles on Emissions Takeoff Inlet Conditions	70
7-5	VCE Duct Burner Rig Exit Emissions Profiles at Transonic Climb Conditions	72
7-6	Capped Swirler Centertube Employed in Duct Burner Rig Configuration 11	74
7-7	Reduced Diameter and Cant Angle Swirler Tubes Employed in Duct Burner Rig Configuration 12	74
7-8	Effect of Modifications on the Total Pressure Loss Across the Duct Burner	75
A-1	Liner Hole Pattern for Duct Burner Configuration 1	83
A-2	Liner Hole Pattern for Duct Burner Configuration 2	84
A-3	Liner Hole Pattern for Duct Burner Configuration 3	85
A-4	Liner Hole Pattern for Duct Burner Configurations 4 and 5	86
A-5	Liner Hole Pattern for Duct Burner Configurations 6 and 7 and 8	87
A-6	Liner Hole Pattern for Duct Burner Configurations 9 and 10	88
A-7	Liner Hole Pattern for Duct Burner Configuration 11	89
A-8	Liner Hole Pattern for Duct Burner Configuration 12	90
B-1	Mobile Laboratory Gas Analysis System	94
B-2	Smoke Meter (78-8047)	98
D-1	Fuel Injector Spray Penetration Characteristics	106
D-2	Fuel Injector Spray Patterns	107

LIST OF TABLES

Table	Title	Page
3-I	Duct Burner Operating Conditions at Three Key Flight Modes	7
3-II	Duct Burner Performance Goals	8
3-III	Duct Burner Emissions Goals	9
3-IV	Analytically-Projected Duct Burner Aerothermodynamic Performance and Exhaust Emissions Characteristics	16
3-V	Fan Stream Conditions at Takeoff Conditions for the VCE Testbed and VSCE-502B Study Engine	18
5-I	Summary of Duct Burner Performance Parameters	35
5-II	Duct Burner Segment Rig Test Conditions	42
6-I	Bulk Equivalence Ratios in Initial Reaction Zones at the Takeoff Operating Condition	45
6-II	Duct Burner Emissions Characteristics	48
6-III	Projected Thrust Efficiency of Duct Burner Test Configuration 11	57
7-I	Effect of High Power Stage Fuel Injector on Duct Burner Emissions Characteristics	69
7-II	Effect of Duct Burner Modifications on Emissions Characteristics	77
B-I	Instrumentation	95
B-II	Calibration Gases	97
C-I	Test Results - Aerodynamic Performance	100
C-2	Test Results Emissions and Combustion Performance	103
D-1	Fuel Injectors Evaluated in Spray Visualization Tests	105

FOREWORD

This report presents the results of an experimental evaluation of a duct burner for an advanced supersonic propulsion system conducted for NASA by Pratt & Whitney Aircraft. This program was conducted in the period from March 1977 to January 1979 under Contract NAS3-20602.

The NASA Project Manager for this contract was Mr. Albert G. Powers. NASA Project Coordinators were Carl T. Norgren, Combustion and Pollution Research Branch, and Rene Chambellan, V. C. E. Project Office of Lewis Research Center, Cleveland, Ohio. Key P&WA personnel include: John Westmoreland, VCE Program Manager, Dr. Robert P. Lohmann, Deputy Program Manager and Ronald J. Mador. Dr. Lohmann and Mr. Mador were the principal investigators.

SECTION 1.0

1.0 SUMMARY

This report presents the results of an experimental evaluation of a three-stage Vorbix type duct burner intended to provide low emissions and high performance for fan stream augmentation in advanced supersonic engines. The objectives of this program were to determine the feasibility of this duct burner concept and to refine the configuration to provide acceptable performance, operational characteristics and durability for its use in the VCE (Variable Cycle Engine) Testbed Program.

This effort was preceded by a study, conducted under NASA contract, that involved analytical screening of a number of different combustor concepts to identify those having the greatest potential for meeting the performance, environmental and geometric constraints on a duct burner for advanced supersonic aircraft powerplants. The three-stage Vorbix duct burner concept was identified and selected under this study on the basis of its potential for meeting the study goals while maintaining a low level of development risk compatible with the schedule of the VCE Testbed Program.

The effort in this program was initiated with the design and fabrication of a rectangular segment rig that simulated a 55-degree sector of the three-stage Vorbix duct burner in an airflow size consistent with the F100-based VCE testbed demonstrator. A total of twelve configurational variations of this duct burner was evaluated during the program, which involved more than 200 hours of testing. The tests were conducted at inlet conditions representative of takeoff, transonic climb and supersonic cruise operation in the VSCE-502B advanced supersonic study engine.

The results indicated that the final configurations of the duct burner satisfied the overall program objectives in that acceptable durability and operational characteristics were demonstrated and the majority of the emissions and performance goals were met and, in some cases, exceeded by wide margins.

The experimental results demonstrated that the emissions of carbon monoxide and unburned hydrocarbons from the duct burner were substantially below the program goals and analytical projections. These led to combustion efficiencies in excess of 99.7 percent as opposed to a goal of 99 percent at all three operation conditions -supersonic cruise, transonic climb and takeoff. The emissions of oxides of nitrogen were moderate but in excess of the program goals stipulated by NASA. However, analysis indicates that because overall engine NO_x emissions are dominated by the main burner, duct burner NO_x emissions of the level observed would not significantly compromise the ability of the engine to comply with the proposed Environmental Protection Agency emissions standards for Class T-5 engines in the airport vicinity.

The thrust efficiency of the duct burner, as defined by analysis of the experimentally observed burner exit total temperature and pressure profiles, is in excess of 97 percent at supersonic cruise as compared to a goal level of 94.5 percent. Similar analysis of data obtained at the transonic climb and takeoff conditions indicate thrust efficiencies of 92 and 94 percent which are 4 to 6 percent higher than initial analytical projections.

The total pressure loss across the duct burner exceeded the program goal with the measured loss at supersonic cruise being 6.76 percent as opposed to a goal of 4.5 percent. However, the mechanisms causing this elevated pressure loss have been identified. In one of the configurations evaluated, 40 percent of the excess total pressure loss was eliminated without significantly compromising the above cited emissions and thrust efficiency characteristics. The mechanism causing the excess pressure loss appears parasitic in nature and further reduction in pressure loss without compromising other performance or emission aspects should be achievable.

Soft ignition capability of the duct burner was demonstrated. Ignition was achieved at a fuel/air ratio as low as 0.002 with resulting static pressure pulses of less than two percent of the burner inlet total pressure. The absence of any combustion-related acoustic instabilities was also demonstrated over the entire duct burner operating range.

The heat load on the duct burner liners, particularly in the upstream end of the pilot secondary and high power stage, were found to be sensitive to swirler tube and fuel injector configuration as a result of interactions between the fuel spray and the combustion air jets. However, acceptable metal temperature levels were achieved through judicious modifications to the liner cooling system and the use of fuel injector configurations with improved spray characteristics.

The overall emissions and performance levels demonstrated during this program have added more substantiating evidence that the duct burner is a viable concept for a second-generation, supersonic commercial transport. The levels of emissions and aerothermal performance documented show that a multistage duct burner based on Vorbix technology warrants continued technology development.

SECTION 2.0

INTRODUCTION

Pratt & Whitney Aircraft has been conducting advanced supersonic propulsion studies under the National Aeronautics and Space Administration (NASA) sponsored Supersonic Cruise Airplane Research (SCAR) Program. Results of this work have identified the Variable Stream Control Engine (VSCE) as a promising approach to meet the stringent operational and environmental demands for a second-generation, supersonic propulsion system.

The VSCE is an advanced duct burning turbofan engine concept. The use of duct augmentation, in conjunction with other advanced technology components, provides a unique throttle schedule for independent control of both the fan and core streams. This results in substantial gains in jet noise reduction and propulsive efficiency.

The duct burner is a critical component and is being studied under several VCE-related technology programs. The initial selection and aerothermal-mechanical definition of a duct burner concept for a VSCE application was accomplished under the NASA-sponsored Duct Burner Analytical Study Program (ref. 1). This work consisted of a screening of combustor concepts as well as preliminary design and performance analyses of selected concepts. On the basis of these results, a three-stage Vorbix duct burner system was selected for more comprehensive experimental rig evaluation and eventual use in the VCE testbed demonstrator. This concept is a moderate risk approach based on Vorbix combustion technology demonstrated under the NASA/P&WA Experimental Clean Combustor Program.

The Duct Burner Segment Rig Test Program, the subject of this report, was directed towards experimental evaluation of the three stage duct burner configuration. Technical objectives addressed characterization and refinement of combustor aerothermal performance, mechanical integrity and exhaust emissions. The scope of work consisted of the following Tasks:

Task I Design of a two-dimensional, 55-degree duct burner segment rig

Task II Fabrication of rig components, procurement of unique instrumentation, and rig installation

Task III Experimental evaluation of twelve test configurations

Task IV Documentation

Task V Investigation of fuel nozzle designs.

Accomplishments from the rig test program have provided both fundamental guidelines and technical insight for the three-stage duct burner in the related VCE Testbed Program (ref. 2). The Testbed Program is aimed at demonstrating duct burner technology as well as the coannular exhaust nozzle technology. This technology demonstration is being successfully completed through a series of emissions and aero/acoustic tests. In addition to providing a technology base for designing the duct burner in the VCE testbed, the rig evaluations have been instrumental in identifying where design improvements can be implemented to more closely approach the intent for a future flight system.

SECTION 3.0

DUCT BURNER CONCEPTUAL DEFINITION AND TEST RIG DESCRIPTION

3.1 INTRODUCTION

The design of the three-stage Vorbix duct burner rig was made to be as close as possible to the duct burner system in the Variable Stream Control Engine (VSCE), study designation VCSE-502B (ref. 3). In addition, it was designed to simulate the preliminary duct burner design for the VCE testbed engine. The scale of the test rig is equivalent to a 55-degree sector of the full annular duct burner in the testbed engine. In this way, testing served a dual purpose of substantiating the technology and concepts defined in the analytical screening study, while providing an opportunity to resolve any operational or durability problems which could compromise the test objectives established for the VCE Testbed Program.

3.2 VARIABLE STREAM CONTROL ENGINE - AN OVERVIEW

Mechanically, the Variable Stream Control Engine (VSCE) is a twin spool configuration similar to a conventional turbofan. Figure 3-1 shows the basic mechanical arrangement of major components. The low pressure spool consists of an advanced multistage, variable-geometry fan and a two-stage turbine. The high-pressure spool has a variable-geometry compressor driven by a single-stage turbine with high temperature capability. Both the primary combustor and duct burner utilize low emissions/high performance concepts. The exhaust nozzle is coannular (concentric annular), featuring variable throat areas in both fan and core streams. The nozzle is also equipped with an ejector/reverser system. Integration and coordination of the various engine/nozzle control functions are managed by a full-authority, digital, electronic control system.

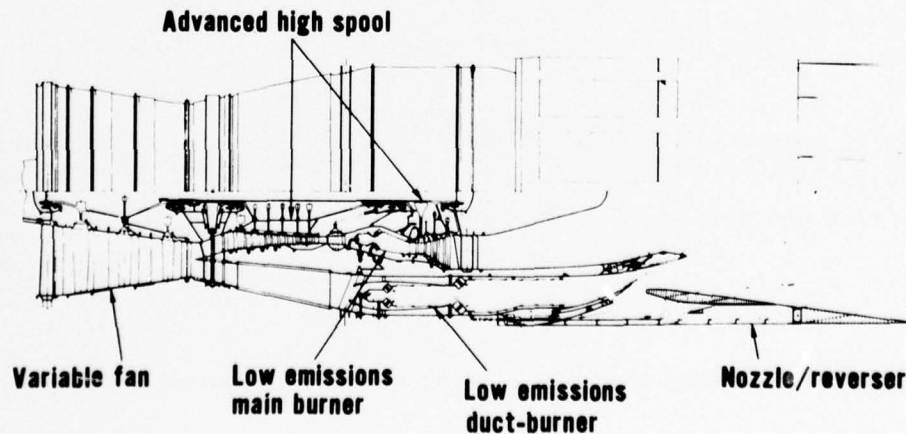


Figure 3-1 Crosssection of the VSCE 502-B Variable Stream Control Engine

The capability to independently control temperature and velocity in both core and fan streams through the use of duct augmentation and a variable-geometry coannular exhaust nozzle is the dominant feature of the VSCE. The flexibility to operate the engine at a fan stream velocity that is significantly higher than the core stream velocity produces an inverse velocity profile for effective noise suppression at takeoff and climb-out. The inverse velocity profile of the VSCE-502B is illustrated in Figure 3-2. At these conditions the core stream is throttled to an intermediate power setting so that jet noise associated with the core is low. To provide both the required thrust and inverted velocity profile, the duct burner operates at the maximum exit temperature of approximately 1700°K (2600°F). Compared to military engine augmentor systems, which approach stoichiometric combustion, peak duct burner temperature levels for a VSCE are relatively low.

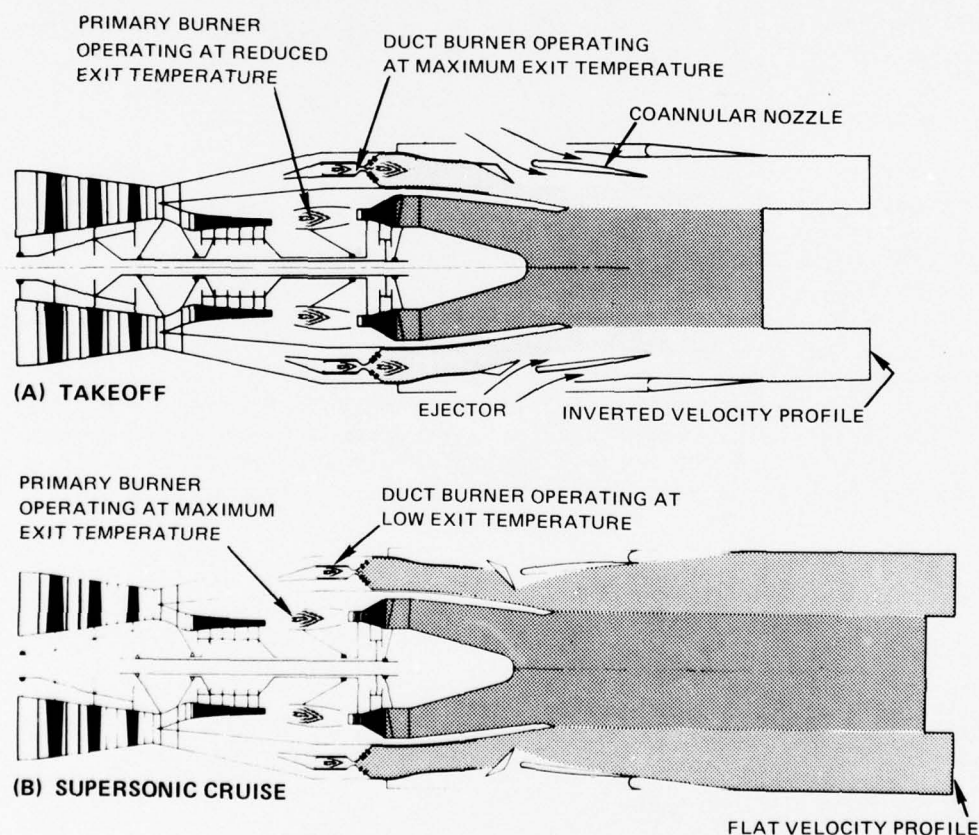


Figure 3-2 Operating Modes of Variable Stream Control Engine

At supersonic cruise, the primary combustor exit temperature is increased and the high-pressure spool speed and the flow rate are matched to the exit temperature. This matching technique is referred to as the inverse throttle schedule - inverse relative to conventional subsonic engines which cruise at much lower temperatures and rotor speeds than required at takeoff. In addition, exhaust temperatures from the co-annular streams are nearly equal, and the exit velocity profile is flat to optimize propulsive efficiency. As a result, fuel consumption at cruise approaches that of a turbojet cycle designed exclusively for supersonic operation. Thus, the inverse throttle schedule enables sizing the engine for optimum supersonic cruise performance, while meeting Federal Aviation Regulations (FAR) noise levels at the other end of the operating spectrum by means of the coannular noise benefit (ref.4).

3.3 DUCT BURNER DESIGN REQUIREMENTS AND CONSTRAINTS

Duct burner operating conditions in the VSCE-502B are listed in Table 3-I for the critical flight conditions of takeoff, transonic climb and supersonic cruise. Duct Mach numbers and airflows are consistent with a 410 kg/sec (900 lb/sec) airflow size engine, a fan duct radial height of 33 cm (13 in) and a duct inner radius of 70 cm (27.6 in). The fuel/air ratio at takeoff could vary between 0.030 and 0.040, depending on the optimization between duct burner combustion and exhaust jet noise. For the purpose of this program, however, a fuel/ air ratio of 0.0385 was selected as the nominal value.

TABLE 3-I

DUCT BURNER OPERATING CONDITIONS AT THREE
KEY FLIGHT MODES
VSCE-502B Flow Size 410 kg/sec (900 lb/sec)

	Operating Conditions		
	Takeoff	Transonic Climb	Cruise
Flight Mn	0.3	1.3	2.4
Alt. - m (ft)	0	11110 (36500)	16130 (53000)
Duct Burner			
Inlet P_t - MPa (psia)	0.26 (37.8)	0.182 (26.4)	0.0254 (36.8)
Inlet T_t - °K (°F)	438(330)	445 (342)	604 (628)
Duct Mn (ref)	0.161	0.119	0.120
Airflow - kg/sec (lb/sec)	247 (543)	127 (279)	154 (338)
Fuel/Air Ratio	0.0385	0.030	0.013
Exit T_t - °K (°F)	1603 (2430)	1500 (2240)	998 (1340)
Fuel Flow - kg/sec	9.5	3.81	1.99
(lb/sec)	(20.91)	(8.37)	(4.39)

Performance goals established for the duct burner are presented in Table 3-II. The supersonic cruise operating condition is critical to the economic operation of the aircraft, and fan duct pressure loss and thrust efficiency are specified at this condition. Since the fan duct diffuser and exhaust nozzle were not investigated during this program, it was assumed that the total pressure loss across these components would be a total of two percent of the fan discharge total pressure at supersonic cruise. Consequently, the goal of a 6.5 percent overall duct loss was considered equivalent to a 4.5 percent total pressure loss across the duct burner at supersonic cruise.

TABLE 3-II

DUCT BURNER PERFORMANCE GOALS

Thrust Efficiency at Supersonic Cruise (%)	94.5
Fan Duct Total Pressure Loss at Supersonic cruise(%)	6.5
Ignition Fuel/Air Ratio	0.002

The low ignition fuel/air ratio is dictated by operational constraints. Although the duct nozzle area is varied to match the exit temperature, the pressure pulse produced by the initiation of combustion, if severe enough, could stall the fan. While the actual soft ignition criterion is the magnitude of the pressure pulse at the fan discharge, experience with conventional duct burners indicates that if ignition occurs at an overall fuel/air ratio of 0.002 or lower, the pressure pulse will be sufficiently small to avoid perturbing the fan. Consequently, this fuel/air ratio was selected as a temporary goal until pressure pulse data could be obtained.

Exhaust emissions goals for this program are listed in Table 3-III. The goals for carbon monoxide (CO) and total unburned hydrocarbon (THC) emission indices are representative in that they are typical of those necessary to achieve the more general combustion efficiency goal. These goals were established at the start of the program and were not related directly to any proposed or established regulation. More recently, analyses have been conducted (ref.2) to establish the duct burner emissions requirements from the point of view of compliance with the proposed Environmental Protection Agency 1984 Regulations for Class T-5 engines. These analyses recognized both the duct burner and the main burner as emissions sources and evaluated the tradeoff in emissions characteristics of both combustors on those of the entire engine. The analysis was based on the use of a Vorbix main burner in the VSCE-502B engine and the emission characteristics were defined by scaling those of the burner evaluated under Phase III of the PWA/NASA Experimental Clean Combustor Program (ref.5).

TABLE 3-III
DUCT BURNER EMISSIONS GOALS

Flight Condition	Pollutant	Emissions Index (g pollutant/kg fuel)
Supersonic Cruise and Sea Level Takeoff	NO _x	1.0
	CO	30.0
	THC	2.5
	Smoke (SAE No.)	15.0

Note: Combustion efficiency at all operating conditions = 99 percent

Figure 3-3 shows the projected emissions levels of the VSCE-502B for the EPA landing and takeoff cycle as a function of chemical combustion efficiency and NO_x emissions of the duct burner. The shaded area depicts emissions from the main combustor, while the unshaded area depicts the emissions from the duct burner. The projections of the different pollutants are based on direct scaling, and do not reflect any allowance for deviation from a nominal engine, deterioration or additional development of the combustors.

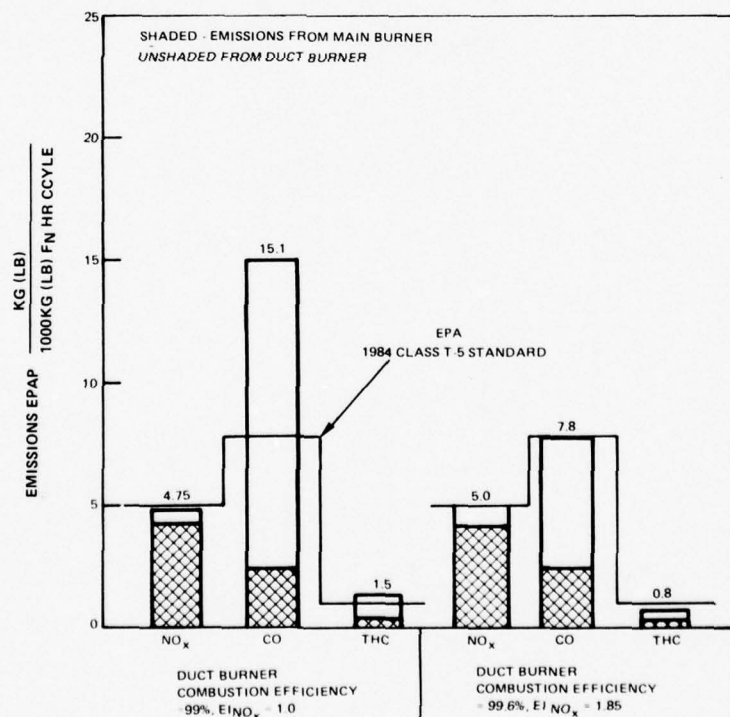


Figure 3-3 Effect of Duct Burner Emissions on Overall Engine Emissions Characteristics During EPA Landing and Takeoff Cycle

The results indicate that by incorporating the program goal of a duct burner NO_x emissions index of unity, the engine is capable of meeting the 1984 NO_x emissions requirements for Class T-5 engines by some margin and that, during the landing and takeoff cycle, the majority of the NO_x is generated in the main burner. However, when the duct burner combustion efficiency is established at the program goal of 99 percent, carbon monoxide (CO) pollutants are nearly twice and the unburned hydrocarbons (THC) 50 percent above the Environmental Protection Agency Parameter (EPAP) required levels (ref.6). The excessive CO and THC emissions are attributable to duct burner operation at takeoff and climbout. To reduce the overall output of these pollutants to the required airport vicinity levels, it is necessary to increase the chemical combustion efficiency of the duct burner from 99 percent to 99.6 percent. The figure also shows that this increase in combustion efficiency could be accompanied by an 85 percent increase in the NO_x emissions levels from the duct burner beyond the program goal. This would be accomplished without exceeding the proposed maximum allowable EPAP level for NO_x emissions.

Figure 3-4 shows the effect of the NO_x emissions from the duct burner on the overall NO_x emissions index of the engine at supersonic cruise and compares these emissions levels with the proposed CIAP goal (ref.7). An 85 percent increase in the duct burner NO_x emissions beyond the program goal of unity is shown to produce a minimal impact on engine emissions because more than 90 percent of the total NO_x is generated in the main burner.

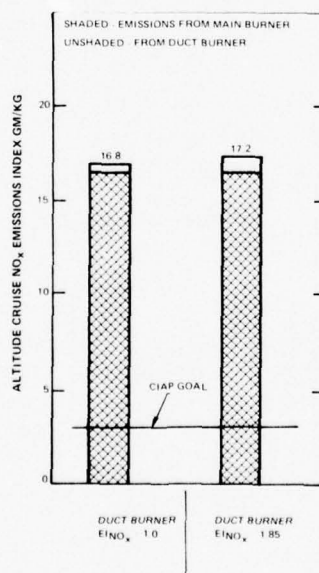


Figure 3-4 Effect of Duct Burner Emissions Characteristics on Overall Engine NO_x Emissions at Supersonic Cruise

On the basis of these observations it appears that some latitude in meeting the program goal for NO_x emissions is available without seriously compromising duct burner performance but that the combustion efficiency goal of 99 percent must be exceeded by substantial margins at the takeoff conditions.

3.4 DUCT BURNER CONCEPTUAL DEFINITION

3.4.1 Mechanical Definition

Figure 3-5 shows the three-stage Vorbix duct burner in the fan duct of the 410 kg/sec (900 lb/sec) airflow size VSCE-502B study engine and depicts the overall structure, principal components and airflow distribution. The duct burner utilizes a prechamber stage, a pilot secondary stage, and a high power stage. During takeoff, all three stages are operative, while at supersonic cruise only the prechamber and pilot secondary stages are operative.

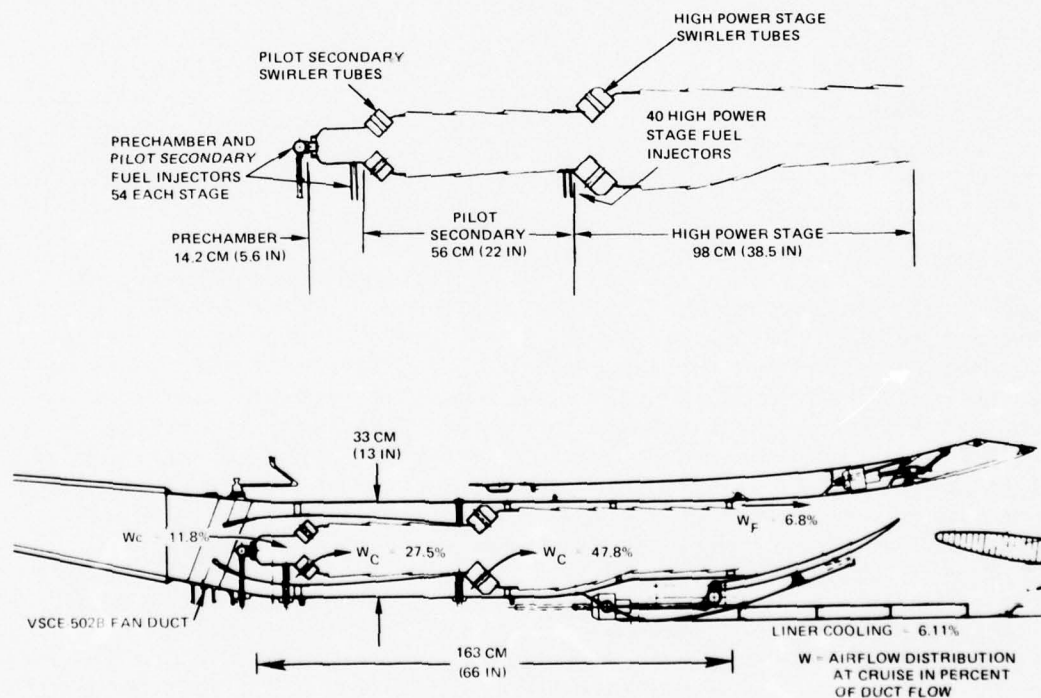


Figure 3-5 Three Stage Vorbix Duct Burner in the VSCE-502B Engine

The prechamber and pilot secondary stages are enclosed by a hood to ensure positive air management for combustion. The prechamber consists of a conventional annular combustor volume with direct fuel injection through the front bulkhead. Combustion air enters the pilot secondary stage through a row of swirler tubes that promotes rapid mixing of air with combustion gases exiting from the prechamber stage. The rapid turbulent mixing produced by the swirling jets enhances complete combustion to reduce exhaust pollutants. A similar arrangement is also employed in the high power combustion zone. As indicated in Figure 3-5, fuel injectors in the pilot secondary and high power stages are located at the exit of the previous stage so that fuel may be rapidly vaporized in the hot combustion products. The combustor liners in both low and high power stages are a louvered design, passing slightly more than 6 percent of the airflow for cooling at cruise. This cooling flow increases to 9-10 percent of the duct flow at takeoff because of the redistribution of the pressure drop through the combustor.

3.4.2 Aerothermal Definition for the VSCE-502B Study Engine

The requirements for lighting at very low fuel/air ratios and smooth modulation to high fuel/air ratios dictated the need for a piloted or multistage combustor system. The overall stability of the combustion process, including lighting at low fuel/air ratios and adequate lean blowout margin, is a constraint unique to the pilot stage. Furthermore, when considering the fuel/air ratio turndown between maximum augmentation and supersonic cruise, stability as well as emissions constraints necessitate that only the pilot stage be operational at the cruise condition.

The frontal area of the duct burner is constrained because of engine diameter effects on drag and introduces the need for considerably higher reference velocities and shroud Mach numbers than encountered in primary combustors. At the high fuel/air ratios of sea level takeoff and climb-out, this can lead to substantial momentum total pressure losses associated with mixing and heat release processes. This imparts a strong interdependence among the duct burner parameters of pressure loss, radial height and reference velocity. The effect is illustrated by Figure 3-6 by showing the variation of the momentum total pressure loss and required fan duct height with the reference velocity in the pilot and higher power stages. These trends were generated using realistic assumptions regarding the clearance between the liners and duct cases and shroud Mach numbers.

The pilot stage is compatible with a 33 cm (13 in) radial duct height and a relatively small (0.5 percent) heat addition momentum loss will be incurred if this stage is designed with a reference velocity of approximately 46 m/sec (150 ft/sec). This velocity is only slightly higher than the 30 to 40 m/sec (90 to 120 ft/sec) reference velocity at which most experience has been acquired with primary combustor systems. With a momentum total pressure loss of only 0.5 percent, the pressure loss goal for supersonic cruise can be achieved with a 4 percent pressure loss across the pilot stage liners. In the high power stage, a duct height on

the order of 50 cm (20 in) would be necessary to maintain reference velocities comparable to primary combustors. This, however, would produce intolerable increases in the engine diameter. Thus, to meet the 33 cm (13 in) duct height goal, the power stage was designed for a reference velocity of 73 m/sec (240 ft/sec) at takeoff.

At the high power stage reference velocities necessary to achieve the desired duct height, the trends shown in Figure 3-6 indicate that the momentum total pressure loss across the duct burner, as a result of heat addition, is approximately 7.1 percent at the sea level takeoff condition. The 4 percent liner pressure loss previously established for the pilot stage at supersonic cruise increases to approximately 7 percent at takeoff because of the 33 percent increase in the duct reference Mach number at this condition. Consequently, an overall duct burner total pressure loss of the magnitude of 14 percent can be anticipated at sea level takeoff.

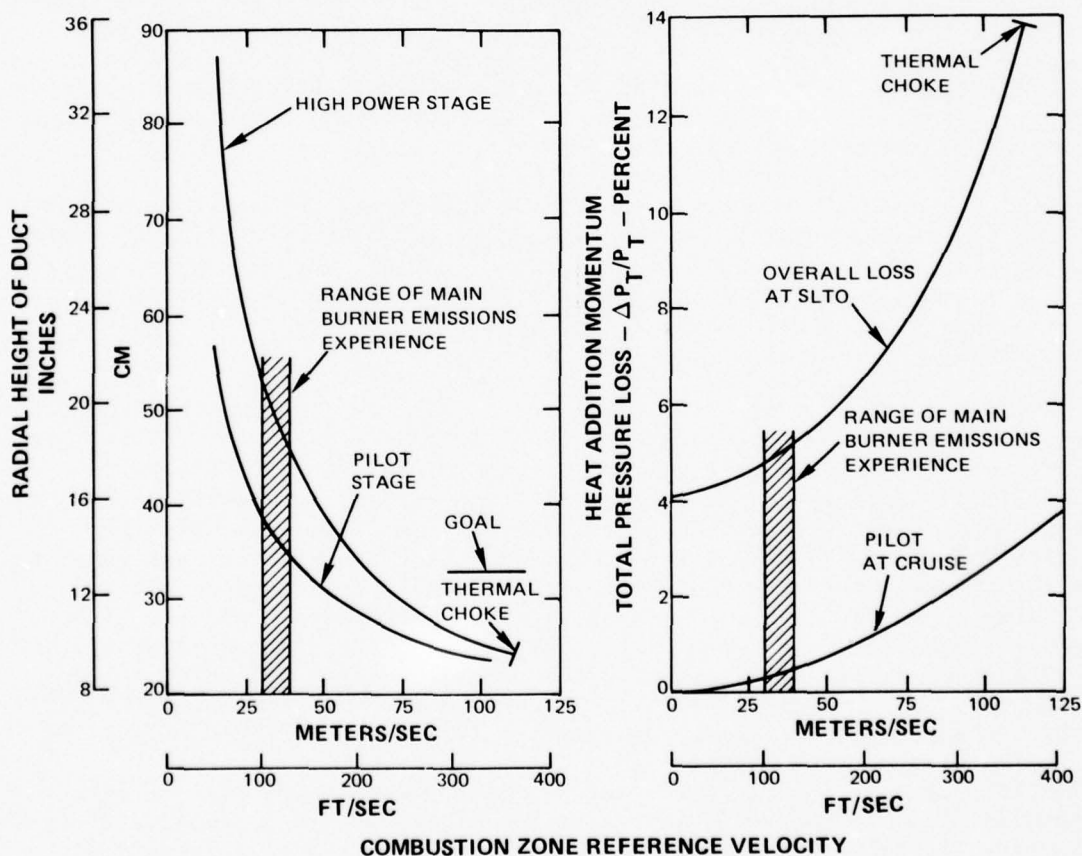


Figure 3-6 Effect of Reference Velocity on Momentum Pressure Loss and Radial Duct Height

The general approach employed to attain low emissions and high thrust efficiency at supersonic cruise involved sizing the pilot stage for adequate residence time to achieve a 99 percent combustion efficiency within the pilot stage proper. Also, a high power stage is required that produces rapid and intensive mixing of the pilot exhaust flow and the bypass air. This accomplishes a dual purpose of generating the mixing necessary to achieve uniform exhaust temperature profiles consistent with high thrust efficiency, while quenching pilot exhaust gases to suppress residual NO_x production. The rapid and intense mixing achievable in the high power stage with the Vorbix concept, as opposed to more conventional piloted-V gutter approaches, was a significant factor in selecting this configuration.

The duct burner aerothermal design was based on the results obtained with the Vorbix primary combustor system tested under the NASA/P&WA Experimental Clean Combustor Program (refs. 5, 8, 9) and other exploratory programs (refs. 10 and 11). The pilot prechamber stage was designed to operate at an equivalence ratio of about unity at supersonic cruise to ensure adequate turndown capability to satisfy the soft ignition requirement. When combined with an optimum prechamber/pilot secondary stage fuel flow split, this led to utilization of approximately 12 percent of the duct airflow in the prechamber stage.

Sizing the prechamber stage was based on considerations of ignition and stability margin, spatial heat release rate and sufficient length/radial height ratio for recirculation zone stabilization. Consideration of these variables led to selection of a reference velocity of 19.5 m/sec (64 ft/sec) and a stage length of 14.2 cm (5.6 in) at the supersonic cruise condition.

The pilot prechamber stage was designed to provide a combined prechamber and pilot secondary equivalence ratio of 0.41 at supersonic cruise. This would produce an estimated gas temperature of 1650°K (2500°F), which is sufficiently high to permit CO oxidation without generating excessive NO_x . To provide this environment at a 0.013 fuel/air ratio for supersonic cruise, the combined prechamber and pilot secondary stages require about 46 percent of the duct flow. Only a small percentage of the remaining duct flow is used for cooling the exhaust nozzle and the high power stage liner, and most of the flow is admitted as combustion air in the high power stage. At takeoff, this air scheduling produces gas temperatures on the order of 1750°K (2700°F) in the high power stage. This is also conducive to CO consumption with low production of NO_x .

The lengths of the pilot secondary and high power stages were selected to provide sufficient residence time for mixing and carbon monoxide oxidation. The pilot secondary stage length was selected to achieve the combustion efficiency goal at supersonic cruise within that stage, since the severe quenching in the high power stage would prohibit further CO conversion. The length of the high power stage was predicated on similar considerations at the takeoff condition. The resultant lengths of these stages are indicated in Figure 3-5.

Liner cooling flow was defined by an augmentor thermal analysis. The inner and outer liners were defined as louver-cooled panels. The nominal panel length was 18 cm (7.1 in), but shorter length louvers were employed in the front end of the stages and in the prechamber where nonhomogeneity of the mixture was expected to produce locally hot regions. The nominal height of the louver lips was 0.64 cm (0.25 in). Cooling requirements were predicated on maintaining a maximum liner metal temperature of 1115°K (1550°F) for durability in a commercial application. Results of this analysis indicated that a total of 9.5 to 10 percent of the duct air would be required for the duct burner liners at takeoff. Cooling requirements for the duct exhaust nozzle were estimated by scaling on a flow per unit surface area basis from an existing nozzle design.

A hood is incorporated over the prechamber and pilot secondary stages to recover the full inlet total pressure and maintain a high liner pressure drop in these stages. The capture area of the hood was sized for minimum total pressure losses at the supersonic cruise condition. The flow bypassing the pilot stages reaches a Mach number of 0.30 at takeoff at the minimum shroud height location of the pilot hood. Beyond this point the shrouds diverge gradually to form diffusers of area ratio 1.75 and length/inlet radial height ratio of 13.5. These proportions are well below accepted stall boundaries for annular diffusers, and the total pressure recovered in the shrouds at the inlet to the high power stage was expected to be within 1 to 3 percent of that upstream of the duct burner at takeoff.

Figure 3-7 shows the fuel schedule for the duct burner. This schedule is based on: (1) achieving the optimum fuel flow split between combustion stages at supersonic cruise and takeoff conditions, (2) continuous modulation, (3) and capabilities for realistic fuel system flow turndown.

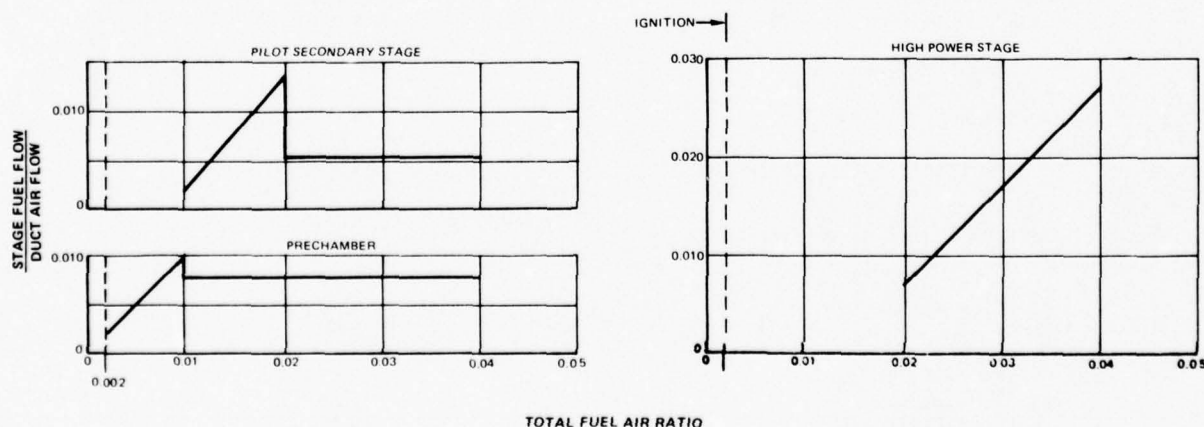


Figure 3-7 Fuel Schedule for the Three Stage Duct Burner

Ignition is accomplished in the prechamber stage, and as augmentation increases, the fuel/air ratio in the prechamber stage increases correspondingly until an overall fuel/air ratio of 0.010 is achieved. After this point, further augmentation is satisfied by activating the pilot secondary fuel system. The schedule in this stage is established so as to satisfy the optimum prechamber and pilot secondary fuel flow split at the supersonic cruise fuel/air ratio, while the pilot secondary stage is operated progressively richer at high fuel/air ratios. When a fuel/air ratio of about 0.020 is reached, the high power stage is activated and the fuel flow split between this stage and the pilot secondary system is adjusted to the optimum levels at transonic climb and takeoff. Fuel flow overshoots prior to staging are required to maintain realistic fuel flow turndown ratios on the simplex pressure atomizing fuel injector employed in the pilot secondary and high power stage. Aerating fuel injectors are employed in the prechamber stage to provide good atomization at ignition in combination with a 5:1 or higher fuel flow turndown requirement.

The analytically-projected performance and emissions characteristics of the three-stage Vorbix duct burner in the VSCE-502B study engine are summarized in Table 3-IV. As indicated, the duct burner is projected to meet all of the performance goals, including pressure loss, thrust efficiency and soft ignition, and be compatible with the engine duct geometry. While the projected NO_x emissions exceed the program goal, the estimates are consistent with those of the most advanced-technology, experimental main combustors evaluated to date.

TABLE 3-IV

ANALYTICALLY-PROJECTED DUCT BURNER AROTHERMODYNAMIC
PERFORMANCE AND EXHAUST EMISSIONS CHARACTERISTICS

	Program Goal	Three-Stage Design
<u>Geometry:</u>		
Maximum Duct Height - cm (in)	33 (13)	33 (13)
Length - cm (in)	163 (66)	163 (66)
<u>Cruise Performance:</u>		
Total Pressure Loss (%)	4.5	4.5
Thrust Efficiency (%)	94.5	94.5
<u>Sea Level Takeoff Performance:</u>		
Total Pressure Loss (%)	None Req'd	14.0
Thrust Efficiency (%)	None Req'd	88.0
Maximum Ignition Fuel/Air Ratio	0.002	0.002
<u>Cruise Emissions:</u>		
EI NO_x - gm/kg	1.0	2.75
Combustion Efficiency (%)	99.0	99.0
<u>Sea Level Takeoff Emissions:</u>		
EI NO_x - gm/kg	1.0	1.78
Combustion Efficiency (%)	99.0	99.0
<u>Transonic Climb Emissions:</u>		
EI NO_x - gm/kg	None Req'd	1.22
Combustion Efficiency (%)	99.0	92.5

3.4 3 Scaling to the VCE Testbed Airflow Size

The duct burner and the variable geometry coannular exhaust nozzle will be evaluated in large scale at representative VSCE conditions during the NASA-sponsored VCE Testbed Program. The VCE testbed demonstrator vehicle is shown schematically in Figure 3-8. A Pratt & Whitney Aircraft F100 engine is used as the basic gas generator for the testbed components, the duct burner and coannular nozzle/ejector system, which are located behind the engine.

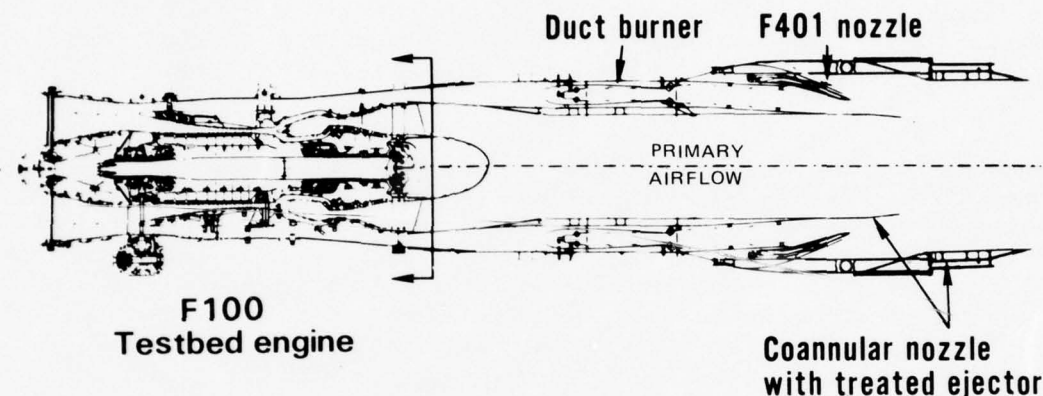


Figure 3-8 Cross Section of the VCE Testbed

Table 3-V shows the fan stream design point conditions in the F100 engine, which with the exception of the airflow rate, are essentially identical to the VSCE-502B. When differences in the fan duct mean diameter are recognized, the duct height in the F100 is about half that in the VSCE-502B at comparable duct Mach numbers. Consequently, resizing of the duct burner for the VCE Testbed Program involved reducing the radial height dimensions of the burner and shroud passages. More specifically, recognizing that scaling the size of burner components is not linear the duct burner was redesigned to operate at the same pressure drop, combustion zone reference velocities and shroud Mach numbers as the VSCE-502B study engine.

The shrouds for bypass airflow around the pilot stage were designed to reproduce the axial Mach number distribution anticipated in the VSCE502B configuration. This assured equal pressure losses to the entrance to the swirler tubes in the high power stage and, when combined with equal velocity levels inside the burner, produced the same pressure drop across these components. Similarity of the aerodynamic aspects critical to emissions was also maintained in the aerothermal definition.

TABLE 3-V

FAN STREAM CONDITIONS AT TAKEOFF CONDITIONS FOR THE
VCE TESTBED
AND VSCE-502B STUDY ENGINE

	<u>VCE Testbed</u>	<u>VSCE-502B</u>
Duct Total Pressure - MPa (psia)	0.283 (41.0)	0.26 (37.8)
Duct Total Temperature - °K (°F)	441 (335)	438 (330)
Duct Airflow - kg/sec (lb/sec)	48.6 (107)	247 (543)
Fuel/Air Ratio	0.0385	0.0385
Duct Exit Total Temperature - °K (°F)	1605 (2434)	1603 (2430)
Approx Mean Rad of Fan Duct - cm (in)	43.6 (17.2)	86.5 (34)

In scaling from the VSCE size to the testbed size, mixing in the vicinity of the swirler tubes and total residence time in the particular stage were the major considerations. Mixing of the vortex jet is controlled by jet penetration and swirl strength. This similarity is retained by maintaining identical pressure drop across the swirler tube and gaspath velocity. The geometric proportions of circumferential spacing and diameter of the jets relative to the duct height was also maintained invariant. The success in maintaining simultaneous similarity with the geometric parameters is largely due to the unique combination of radial height and mean gas path radius that is preserved between the VSCE-502B and testbed configurations.

While local velocities in the combustion zones of the testbed duct burner were maintained equal to those of study engine design, the annular shrouds outside the combustor were modified in some locations because of dimensional constraints. Scaling the shroud annuli in the high power stage and those under the pilot hood on the basis of equal velocities resulted in wall gaps of about 0.38 to 0.65 cm (0.15 to 0.25 in). The sensitivity of such heights to fabrication tolerances and thermal distortion could result in maldistribution or restriction of cooling airflow. To avoid these potential problems, the radial gaps between these walls were limited to a minimum of 1.27 cm (0.50 in). The change in pressures due to reduced shroud velocities only affects the pressure drop across the cooling liners in the pilot secondary stage and was compensated by reducing the size of the cooling air holes. These passage height adjustments led to a total radial height of the fan duct of 15.5 cm (6.1 in), approximately 10 percent greater than required for similarity in duct burner inlet Mach number.

Since the liner cooling flow per unit surface area is essentially invariant with burner size, the smaller size of the F100 engine required an increase in the fraction of duct air used for this purpose. Analysis of cooling requirements indicated that the 9.5 to 10 percent of duct flow required to cool the liners in a full size VSCE-502B duct burner at takeoff increased to 18 to 19 percent in the F100-sized duct burner.

This increase influences both emissions and thrust efficiency. The use of more air for liner cooling increases the nominal equivalence ratio in the combustion air in the high power stage by about five percent, which can increase the sea level takeoff NO_x emissions from the rig over that of the equivalent burner sized for the VSCE-502B.

3.5 TEST RIG DESCRIPTION

The duct burner segment rig duplicates as closely as possible the preliminary definition of the VCE testbed duct burner and the design intent of the duct burner in the VSCE-502B study engine. The rig is a rectangular representation of a 55-degree sector of the VCE testbed duct burner. However, in conforming with component development practices, the rig is designed to demonstrate only aerothermal-mechanical concepts and does not address the durability and structural integrity standards required for flight engine applications. Rig construction conformed to standard manufacturing techniques, and materials used for fabricating conventional combustion systems were employed.

The duct burner rig was designed and constructed in five sections to facilitate assembly, routing of instrumentation lead wiring and for liner support considerations. These sections are: (1) the prechamber liner, including the inlet to the pilot secondary stage; (2) the remainder of the pilot secondary stage, including the downstream portion of the hood; (3) the front hood segment; (4) the inlet section of the high power stage; and (5) the high power stage liner. Figure 3-9 identifies these major subassemblies, and the partially assembled rig is illustrated in Figure 3-10.

Figure 3-11 shows critical rig dimensions and design features. The overall burner length is 177.8 cm (70 in), as measured from the leading edge of the pilot hood to the end of the last louver. The nominal width is 43.2 cm (17 in), and the radial height is 15.5 cm (6.1 in). The axial length and radial heights of the combustion volumes in each stage are consistent with the reference velocity and residence time requirements established during the aerothermal definition, as discussed earlier in Section 3.4.2. To avoid excessive pressure loss in the test facility exhaust system and minimize mechanical complexity, the segment rig did not incorporate a variable-geometry exhaust nozzle as in both the testbed demonstrator and study engine concept. However, the axial location of the bosses for exit instrumentation rakes was based on providing the additional residence time that would occur in the convergent section upstream of the nozzle throat area. In addition, the quantity of air used to cool the louvers downstream of these instrumentation rakes is representative of the fraction of duct air that bypasses the duct burner to cool the exhaust nozzle in the VSCE-502B.

The liners are constructed of 0.132 0.191 cm (0.060 0.075 in) thick Hastelloy X material with 0.229 cm (0.090 in) thick endwall panels. The entire burner is enclosed in two cases constructed of 0.640 cm (0.250 in) thick stainless steel plate. Effective flow areas of all air metering components are documented in Appendix A.

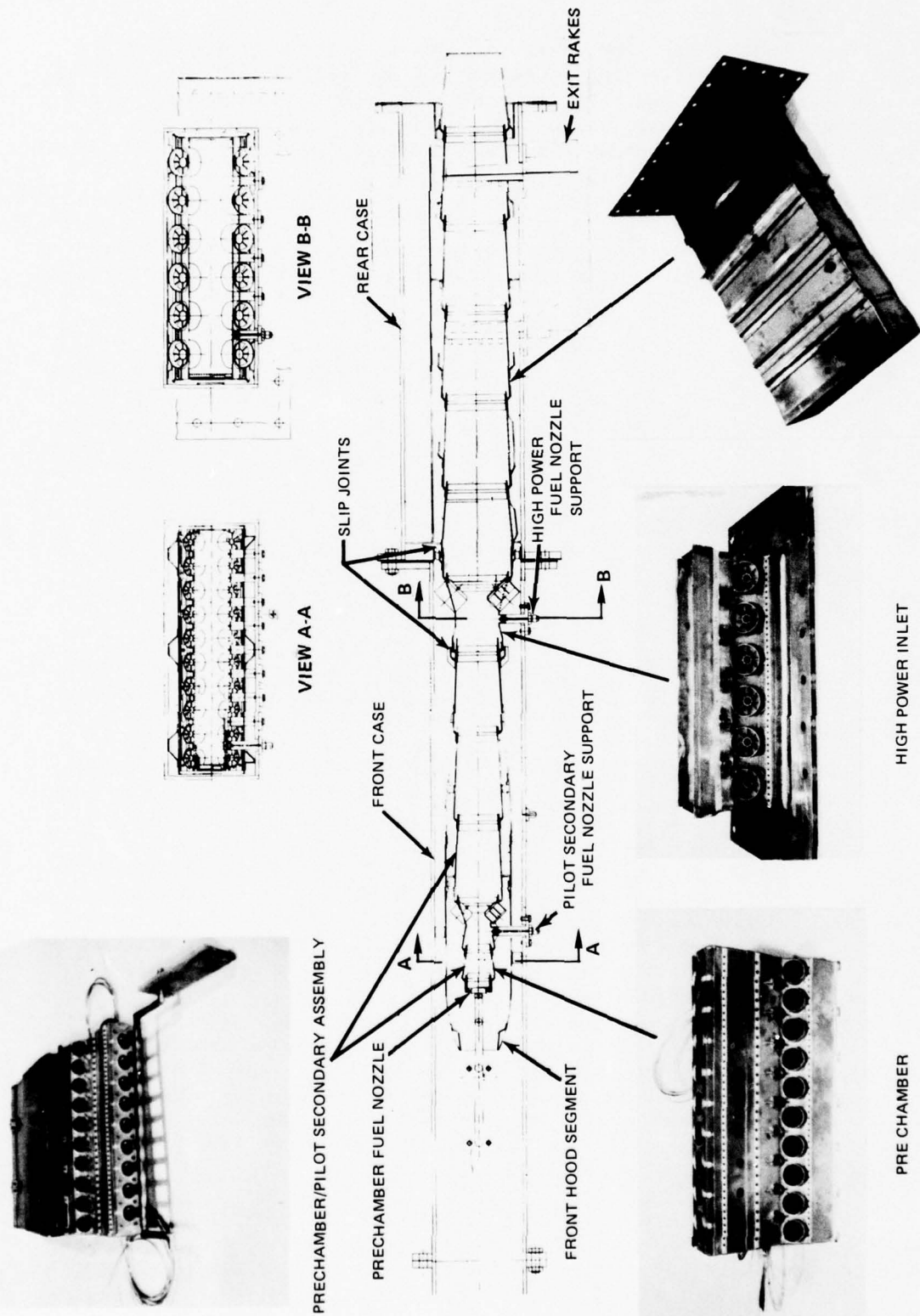


Figure 3-9 Duct Burner Segment Rig Components

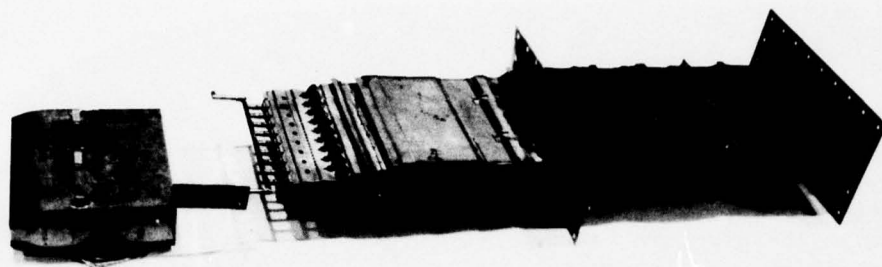


Figure 3-10 VCE Duct Burner Segment Rig Partially Assembled

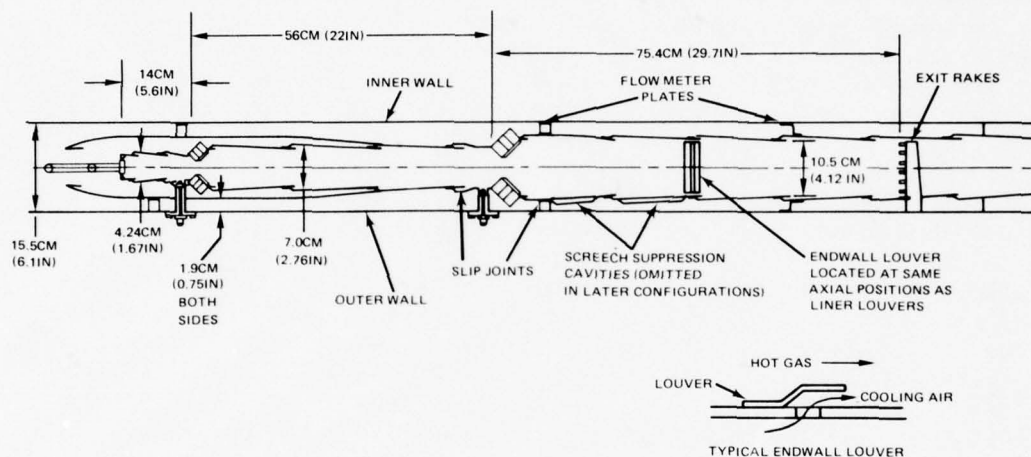


Figure 3-11 Dimensions of the VCE Segment Duct Burner Rig

3.5.1 Prechamber Stage

Aerating fuel injectors are employed in the prechamber stage to provide good atomization at the low starting fuel flows and to satisfy the 5:1 flow turndown requirements.

The prechamber fuel manifold, constructed of stainless steel tubing and positioned inside the burner hood, supplies fuel to the nine aerating fuel nozzles that protrude through floating collars mounted on the prechamber bulkhead. This positioning mechanism facilitates installation and removal of the fuel manifold as well as provides a certain degree of freedom of the prechamber bulkhead for allowable thermal expansion.

A 20-joule ignitor is located immediately downstream of the second fuel injector from the endwall. This ignitor is mounted on the outer case wall and penetrates both the hood and prechamber liner.

3.5.2 Pilot Secondary Stage

Fuel to the pilot secondary stage is injected through nine pressure atomizing nozzles mounted on individual fuel nozzle supports. These supports provide sufficient structural strength to axially locate the entire prechamber, pilot secondary and hood subassemblies. A slip joint is located at the juncture between the pilot secondary stage and the inlet to the high power stage to accommodate liner thermal expansion.

Combustion air is introduced into the pilot secondary stage through ten swirler tubes installed on each side as shown in Figure 3-10. These components are welded to the second louver panel, downstream of the pilot secondary fuel injectors, at a 45-degree inclination to the duct burner axis. The swirler tubes were fabricated as castings and have an outer diameter of 3.23 cm (1.31 in). This dimension allows approximately 30 percent more flow capacity than required in order to provide a margin for varying combustor flow rates if desirable during optimization testing. Conical skirts were installed on the discharge end of the tubes to restrict the flow rate to the desired level. In addition, these skirts provided the advantage of coalescing the swirling jet.

A flange was incorporated into the third louver to facilitate disassembly of the pilot section. This flange is slotted to permit the flow of cooling air to downstream liners. The flange is constructed to engage clips welded to the front hood segment, thereby assuring a positive but nonrigid hood to burner liner retention. This type of retention prevents deflection of both the hood and liner panels against the opposing pressure loads of each wall. Similar clip arrangement was installed downstream, attaching the rear part of the hood to the fourth louver. During assembly, the front hood segment is riveted to the rear hood wall.

3.5.3 High Power Stage

The inlet section to the high power stage is supported from the rig cases by separators welded between the inlet liners and flange plate. The plate is clamped between the front and rear cases flanges resulting in a rigid radial and lateral positioning of this component. The flange plate to which the separators are attached is sized to form the flow metering area required for shroud flow pressure control at this axial location.

The high power stage liner is retained at the downstream end. The inlet and exit surfaces on the high power stage inlet section serve to position and support the rear of the prechamber/pilot secondary subassembly and the upstream end of the high power stage liner. Slip joints permit liner thermal expansion into the high power inlet section. Additional radial support and positioning is provided by the shroud separators welded to the outer surfaces of the front hood segment.

Fuel to the high power stage is injected through five pressure atomizing nozzles mounted on fuel nozzle supports in the inlet section. Although similar in construction to the pilot secondary fuel nozzle supports, these supports do not transmit mechanical loads.

Six swirler tubes, similar in construction to the configuration in the pilot secondary stage, are welded on each side of the sixth louver. Dimensionally, the swirlers have an outer diameter of 5.08 cm (2.0 in), which is oversized for the nominal airflow requirements. The tubes incorporate a conical skirt for flow control and are installed at a 45-degree angle to the axis of the burner.

Because of a potential for the occurrence of a high intensity, combustion-generated noise, referred to as "screech", sound absorbing cavities were initially installed in the outer side of the seventh and eighth louvers. These "screech liners" consist of a perforated liner, backed by a sound absorbing cavity (a type of Helmholtz resonator) formed by enclosing the space on the shroud side of the liner wall. In subsequent test configurations, in which no acoustic instabilities were evident, the screech suppression system was removed and the perforated liner panels were replaced with solid panels.

The long and wide burner liner louvers are subject to buckling under the relatively high operating pressure loadings. Therefore, strengthening techniques were employed to ensure rigidity. While the rear hood, shroud flow metering plates, screech liner and flange plate weldments provide wall stiffness, additional zee strips and doubler strips were incorporated on the high power stage liner to prevent buckling. To avoid excessive pressure losses in the shroud flow, holes were drilled through the raising surface of all the zee strips.

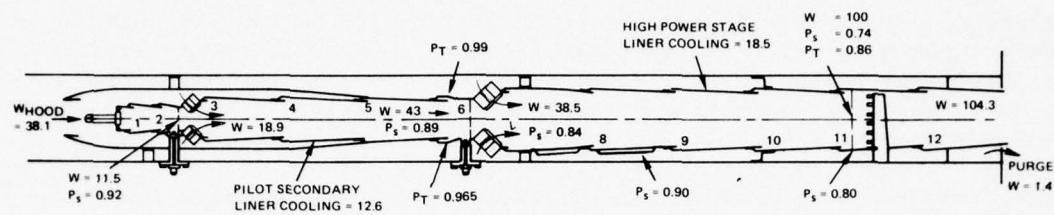
3.5.4 Design Airflow Distribution

Figure 3-12 presents a listing of the rig design airflow and pressure distribution when operating at the takeoff condition (fuel/air ratio of 0.0385). Airflow is referenced to the total flow inside the high power stage at the exit rake location, including that introduced through the louver immediately upstream of the rakes.

Approximately 10 percent of the combustor airflow is utilized for cooling the endwalls and to accommodate leakage at the liner slip joints. Relative to the preliminary design of the full annular duct burner for the VCE Testbed Program, combustion airflow through the swirlers in both the pilot secondary and high power stages was reduced proportionately to offset this flow and maintain the desired level of velocity at the downstream locations of these stages. As a result, both stages operate at a slightly higher equivalence ratio at the upstream end in comparison to the full annular configuration.

Fuel injectors in the pilot secondary and high power stages were a simplex pressure atomizing type that produced an 85-degree hollow cone spray. Injectors in the pilot secondary stage had a flow number of 10.38 kg/hr/MPa^{1/2} (1.89 lb/hr/psi^{1/2}), while those in the high power stage with initial configurations were rated at 45.5 kg/hr/MPa^{1/2} (8.3 lb/hr/psi^{1/2}). In subsequent test configurations, different injectors

were used in the high power stage with other flow numbers and spray patterns. These injector changes are documented in Appendix A and the effect on duct burner operation is discussed in Sections 6.0 and 7.0.



PRECHAMBER COMBUSTION
AIR DISTRIBUTION W

FUEL NOZZLE	2.00
BULKHEAD COOLING	0.96
COMBUSTION AIR JETS IN LOUVER 1	3.70

W = PERCENT OF TOTAL FLOW IN BURNER
AT EXIT RAKE PLANE

P_s, P_T = LOCAL PRESSURES AS FRACTION OF
BURNER INLET TOTAL PRESSURE

COOLING FLOWS

LOUVER NUMBER	FLOW FOR FOUR WALLS - W	FLOW THROUGH ENDWALLS - W
1	1.94	0.214
2	2.90	0.348
3	2.70	0.337
4	2.50	0.530
5	2.50	0.530
6	4.90*	0.580
7	4.80*	1.330
8	3.26	0.857
9	3.26	0.890
10	3.54	0.928
11	3.62	0.960
12	2.90	0.746
TOTAL ENDWALL COOLING W = 8.25		

*INCLUDES LEAKAGE IN SLIP
JOINTS IN THESE LOUVERS

Figure 3-12 Design Airflow and Pressure Distribution in the Duct Burner Rig at the Takeoff Condition

SECTION 4.0

TEST FACILITIES AND INSTRUMENTATION

4.1 INTRODUCTION

This section presents a description of the test facilities and test instrumentation used in conducting the various experimental investigations during the program.

All experimental testing of the three-stage duct burner rig was conducted in Stand X-127 at the Pratt & Whitney Aircraft Group Commercial Products Division in East Hartford, Connecticut. This facility has the capability to examine the aerothermal-mechanical performance of this advanced combustion system over a range of conditions envisioned for a VSCE application. The measurement of exhaust emissions was obtained with a gas sampling instrumentation system.

In addition to stand X-127, supporting flow visualization rigs were used for diagnostic testing to establish and demonstrate the feasibility of specific concepts. These rigs included a water tunnel flow visualization rig, a swirler calibration rig and a fuel injector rig.

4.2 TEST STAND X-127

An illustration and schematic diagram of Stand X-127 are presented in Figure 4-1 to identify the components of some of the major functional stand systems. Such systems include the air supply system, the rig inlet and test section, the exhaust system, and the fuel system.

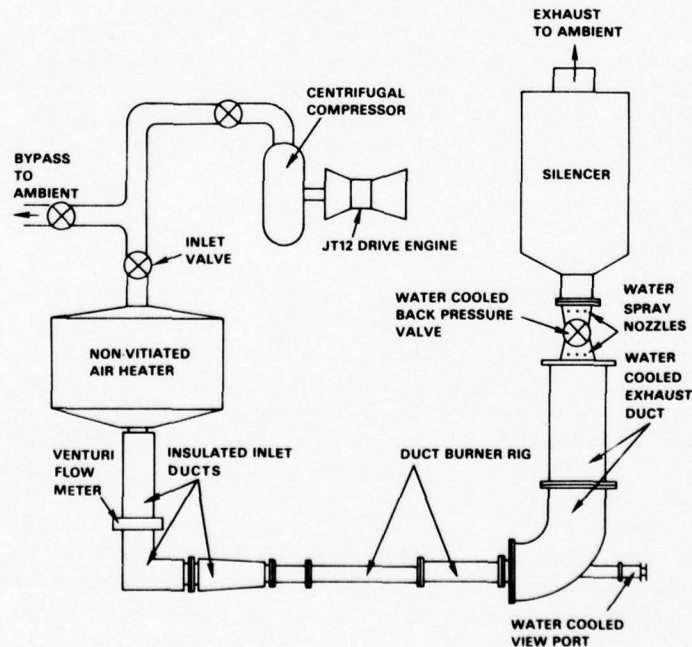


Figure 4-1 Schematic of X-127 Airflow System

The air supply system furnishes air from either of two JT12-driven centrifugal compressors located close to the stand. Air supply pressure is controlled by a bypass to ambient valve. The rig inlet valve is located in the air supply system. This valve operates in conjunction with the backpressure valve at the rig exit to regulate the rig inlet pressure and airflow.

The pressurized air is heated to a predetermined temperature in a non-vitiated preheater furnace before introduction to the test rig. The non-vitiated preheater furnace is a natural gas-fired system with an air side temperature capability of 920°K (1200°F). The maximum rig inlet temperature required during testing was 605°K (628°F), which corresponds to supersonic cruise operation. The furnace provides nonvitiated air to permit measurement of emissions produced solely by the duct burner. After discharge from the furnace, the air flows through a series of insulated ducts to the test rig. Enroute, the flow rate is measured with a venturi flow meter that is accurate to within 0.5 percent.

An insulated transition duct, designed particularly for this application, directs the flow from the 25.4 cm (10 in) diameter circular duct to the 15.5 cm by 44.7 cm (6.1 by 17.6 in) rectangular cross section of the rig cases. Accessibility to the duct burner rig for expedient on-stand maintenance as well as visual inspection of test hardware is provided by removing a short inlet case at the front of the test rig. A fine mesh screen is welded to the exit of this inlet case to ensure uniform flow distribution to the rig inlet. Downstream of the screen are two rectangular cases having a total length of 2.06 m (81 in) that enclose the three-stage segment rig.

The facility's exhaust system has provisions to cool rig exhaust gases and suppress exhaust noise. A water-cooled adapter flange provides a transition from the rectangular exit case of the rig to a circular elbow on the stand exhaust system. As indicated by Figure 4-1, the circular elbow contains a water-cooled viewing port for visual examination and photo acquisition of duct burner flame properties and propagation rates during testing. This port has a quartz window purged with nitrogen gas to ensure cleanliness.

A total of six nozzles, located above and below the backpressure valve, directs a spray of water onto the hot surface of the circular exhaust ducts and into the gas stream exiting the duct burner rig. In this manner, surface temperatures and exhaust gas temperatures are maintained at acceptable levels. Before the gases are expelled into the atmosphere, they pass through a silencer. This chamber, located downstream of the backpressure valve, effectively reduces the rig exhaust noise with a series of internal baffles.

Fuel to each of the three duct burner stages is metered independently in a highly filtered system. The fuel supply and distribution system for stand X-127 is diagramed in Figure 4-2. Jet A fuel flows from external storage tanks through an isolation valve, cartridge-type filter and high flow capacity pump. Fuel pressure is controlled by a bypass valve, and a pressure relief valve set at 4.91 MPa (715 psi) prevents overpressurization of the system.

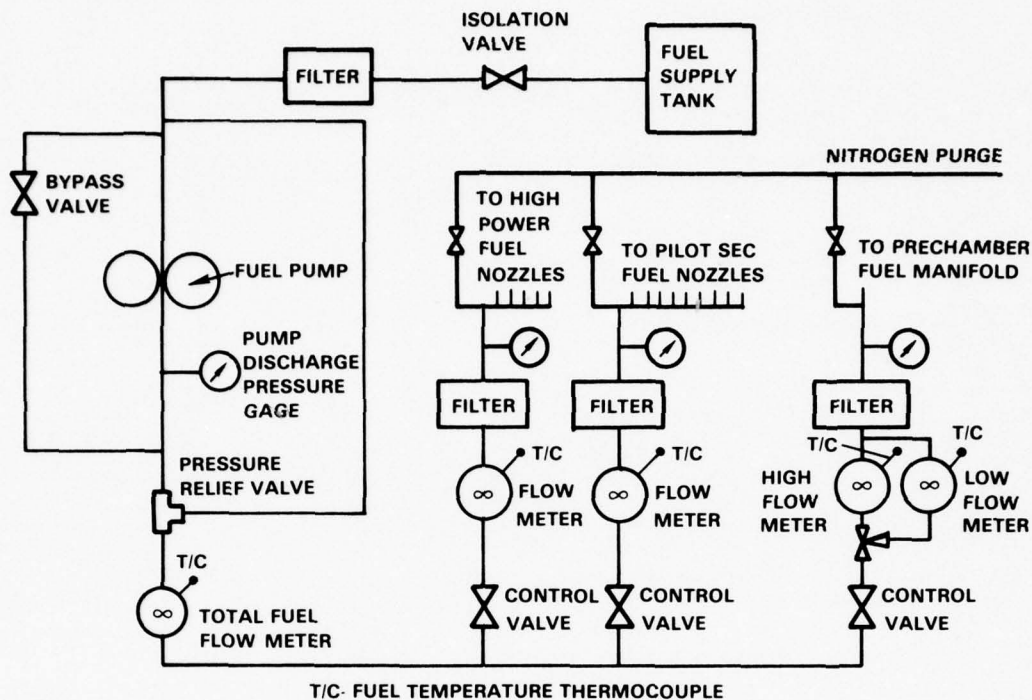


Figure 4-2 Diagram of Fuel Supply and Distribution System in Stand X-127 Stand

Total fuel flow to the duct burner is measured by turbine flow meters prior to distribution to the three rig fuel systems. Flow to each fuel line is manually controlled, individually measured with turbine meters, and filtered. For this program, an additional low-flow turbine meter was installed in the prechamber stage fuel line to improve measurement accuracy during testing to determine ignition and blowout characteristics. Fuel temperature levels are monitored by thermocouples installed in the turbine meters. Also, nitrogen gas is available to purge the fuel lines and manifolds and provide fuel nozzle cooling when no fuel is flowing in the stage.

4.3 TEST INSTRUMENTATION

4.3.1 Aerothermal and Structural Instrumentation

Pressure and temperature instrumentation was installed at predefined locations to acquire aerothermodynamic data and to provide early indication of any incipient problem. Figure 4-3 depicts the different locations of this instrumentation in the test rig.

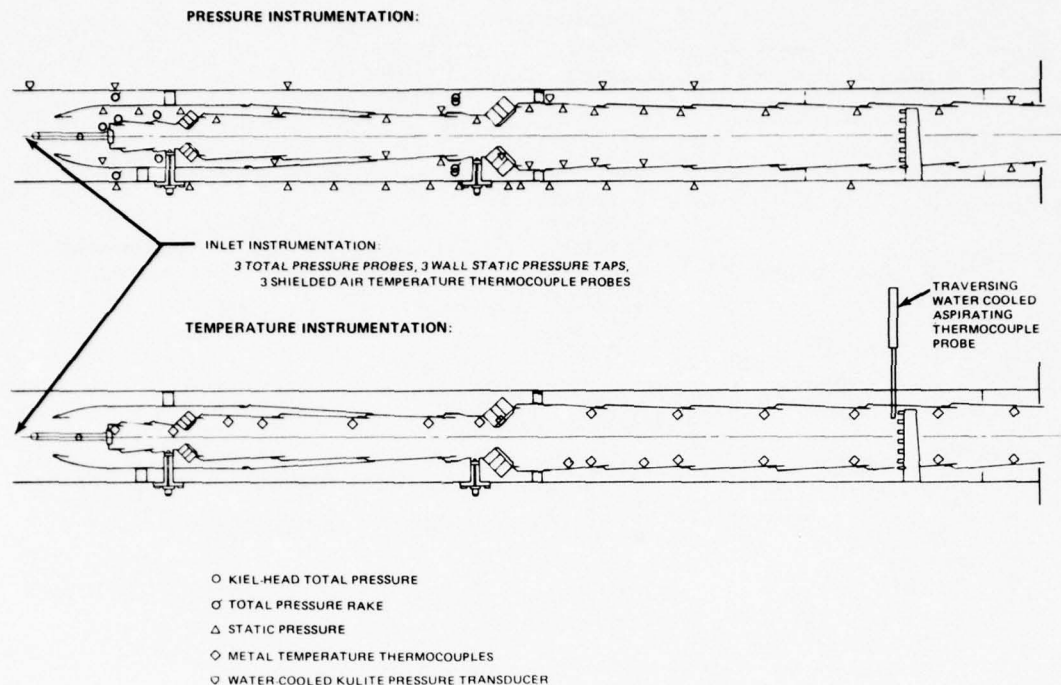


Figure 4-3 Duct Burner Rig Pressure and Temperature Instrumentation

The location of sensors for measuring static and total pressure permitted an accurate assessment of shroud pressure loss, overall system pressure loss, duct burner airflow, and pressure distributions. The total pressure probes were a Keil-head type and insensitive to flow direction at air incidence angles as high as 30 degrees off axis. Typically, two sensors were positioned at each measurement location.

Conventional chromel-alumel thermocouples were installed at selected liner locations for diagnostic purposes. Typically, two thermocouples were located at each position. The burner inlet air temperature was measured with single shielded chromel-alumel thermocouple probes. In addition, a traversing aspirating probe was installed forward of the fixed exit rakes during one series of tests for verification of gas temperature measurement accuracy. This probe has a water-cooled support with a platinum/platinumrhodium thermocouple in an uncooled platinum tip and provides an accuracy to within ± 2 percent for measuring gas temperatures below 1813°K (2800°F).

Rig inlet conditions were carefully monitored by three fixed Kiel-head total pressure probes, three static pressure taps and three air temperature thermocouples. Inlet total pressure and venturi total pressure were read on mercury manometers. All remaining pressure taps or probes, including the venturi throat static pressure, were connected to three forty-eight port scanivalves to allow individual readout with a single

meter. Scanivalve pressures were measured as a differential value relative to the venturi total pressure by a 0 12.7 m (0 500 in) of water capacity differential pressure digital gauge. For diagnostic purposes, the pressure drop across the duct burner liner at seven critical locations was also monitored on differential manometers.

Two water-cooled Kulite pressure transducers were incorporated in the rig, one at the inlet and the second in the high power stage, to monitor and record combustion noise or instability. Electrical signals from this instrumentation were processed through an amplifier and monitored on a root-mean-square voltmeter. The signal was also processed and recorded on magnetic tape for subsequent evaluation. To more accurately identify the potentially damaging screech mode, signals from the Kulite probe in the high power stage were processed through two electronic filters yielding individual signals in narrow bands between 1000 Hz to 4000 Hz, the frequencies at which screech is most prominent. These signals were recorded on a Magnetic Automatic Recording System (MARS). Because of the uncertainty of occurrence of this acoustic phenomenon, several rig parameters were also recorded continuously on magnetic tape with the MARS when operating at high fuel/air ratios. These parameters included burner airflow, fuel flow, liner pressure drop at louver 7 in the high power stage and metal temperatures from 14 selected locations.

4.3.2 Emissions Sampling and Analysis Equipment

Emissions sampling instrumentation consisted of three fixed rakes at preselected circumferential or transverse locations. Besides emissions, the rakes were also used to measure total pressure at the exit plane for calculating system pressure loss. The sampling rake design is shown in Figure 4-4, along with other pertinent design details. As indicated, the rake contains six radially spaced sampling probes and associated transfer lines. The probes are designed to choke the gas sample at the throat area, thereby reducing the static temperature.

The rakes are cooled with high pressure steam in order to withstand the high temperature environment at the duct burner exit. Steam is introduced at the leading edge, as shown in Figure 4-4, circulates throughout the rake body and is expelled into the mainstream. The platinum rhodium probe tips are cooled by conduction from the internal tubes and the leading edge structure. In addition to cooling, the steam also reduces the gas sample temperature to levels which suppress further chemical reactions.

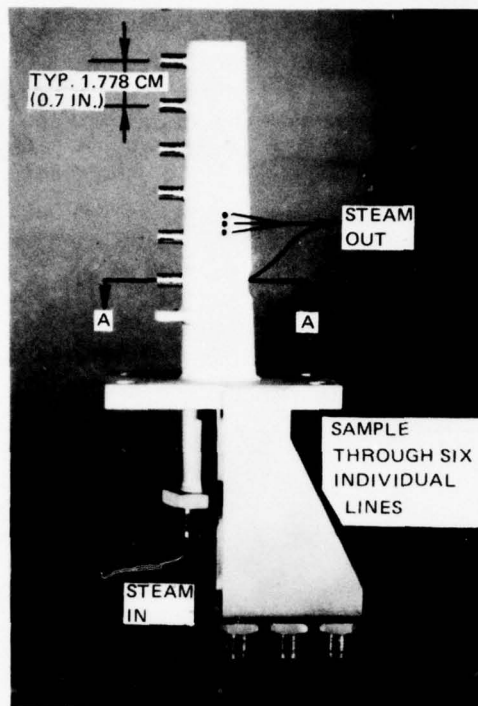
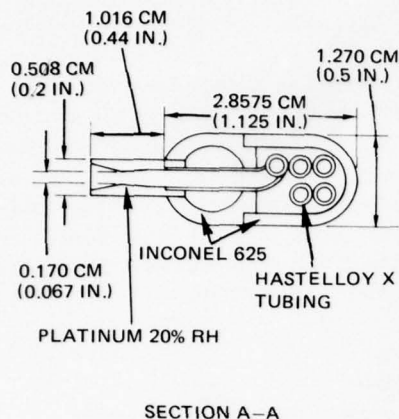


Figure 4-4 Details of Steam Cooled Gas Sampling Rake

The rakes are designed to extend through the outer case and burner shroud and radially span the exit flow field. The installation locations are depicted in Figure 4-5 by showing a cross section of the high power stage and the placement of the radial sampling elements. Rake orientation relative to upstream components was of primary importance. One rake is positioned behind a high power stage fuel nozzle, a second midspan between the high power stage nozzles, and the third in a position one-fourth of the way between nozzles. These rakes were located with the probe tips 76.6 cm (30.2 in) downstream of the fuel injectors in the high power stage. This length was selected to provide a residence time in the high power stage equivalent to that upstream of the exhaust nozzle throat in a flight engine.

Upon leaving the rake, the gas sample enters insulated and heated transfer lines that maintain a sample temperature of about 425°K (300°F). A total of eighteen on/ off selector valves located within a steam-heated, insulated chamber can be positioned to obtain sampling from an individual probe, or mixtures of sample from radial and/ or circumferentially-spaced probes or from the entire exit plane. For mixed sampling, individual gas samples are mixed in a chamber designed to insure a representative sample. A diagram of the sample selection system is shown in Figure 4-6.

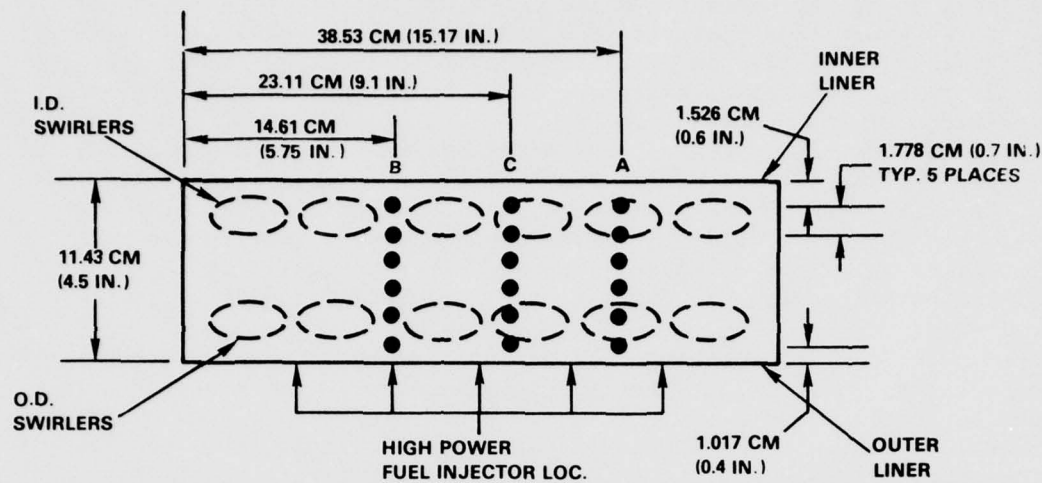


Figure 4-5 Location of Gas Sampling Probes

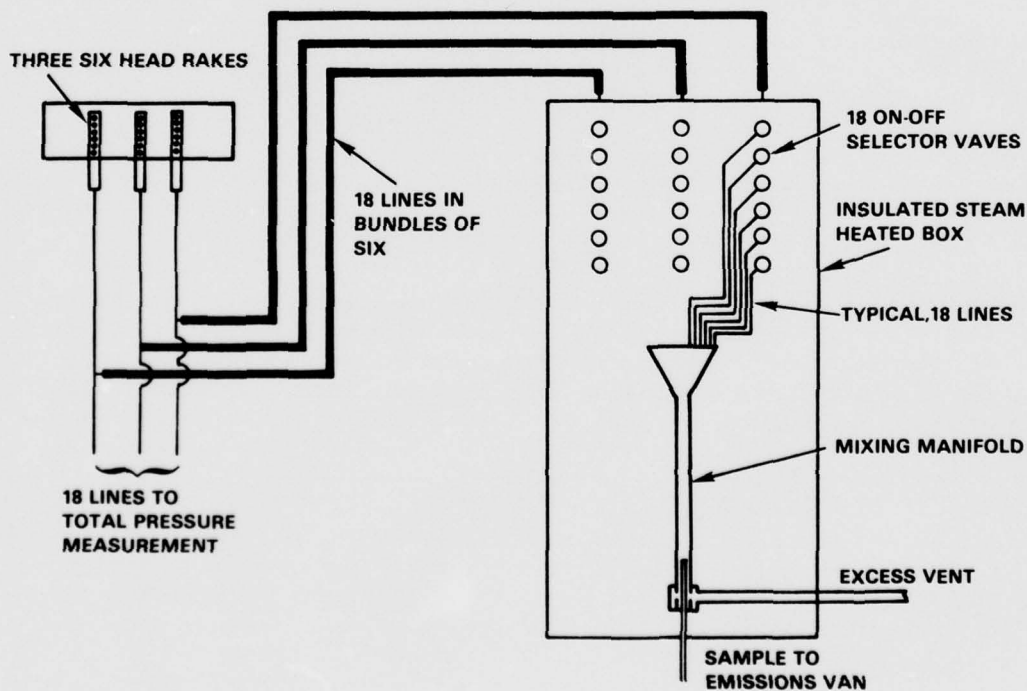


Figure 4-6 Emissions Sample Selection System

The Pratt & Whitney Aircraft Mobile Emissions Laboratory used in this program for emissions analysis is a completely self-contained unit and incorporates the latest on-line equipment for measuring carbon monoxide, carbon dioxide, oxides of nitrogen, total hydrocarbons, hydrogen, and water vapor. Instrumentation and sample handling equipment were designed to conform with the specifications described in Federal Register Vol. 38 No. 136 Part II, July 17, 1973, "Control of Air Pollution from Aircraft and Aircraft Engines". Each instrument is provided with "sample" and "calibration" operating modes. Also, the laboratory carries its own calibration gases and maintains standard reference gases which, where possible, are traceable to the National Bureau of Standards.

Outputs are recorded and monitored continuously on strip chart recorders. Analyzer outputs are also digitized, and on command are sent via telephone link to a Sigma 8 computer to be processed in real time and/or recorded on a computercompatible, cassette-type magnetic tape. The Sigma 8 Data Reduction Program for the mobile laboratory receives data transmitted from the laboratory, converts the data into engineering units, performs calculations and returns the results to a video terminal within the mobile laboratory. Additional information pertaining to the emissions analysis equipment is presented in Appendix B.

4.4 SUPPORTING FLOW VISUALIZATION RIGS

In conjunction with segment rig testing, flow visualization models of certain aspects of the duct burner were used as diagnostic tools. Three models were designed, fabricated and used during the program. These include a water tunnel flow visualization rig, a swirler calibration rig and a fuel injector flow visualization rig. A brief description of these facilities is presented in the following paragraphs.

4.4.1 Water Tunnel Flow Visualization Rig

The water tunnel flow visualization rig was used in stand X-420 for aerodynamic design optimization of the duct burner. The test rig, which is shown in Figure 4-7, duplicates the essential aerodynamic geometry and size of the segment combustion rig. Internal flow restrictors are incorporated to simulate the pressure drop produced by combustion in the pilot secondary stage.

The model itself is constructed of plexiglas, except for the swirler tubes which are the same cast components used in the segment combustion rig. A liquid dye serves as the medium for distinguishing flow patterns. Data are obtained with inlet and local total and static pressure probes to define the flow distribution in the model.

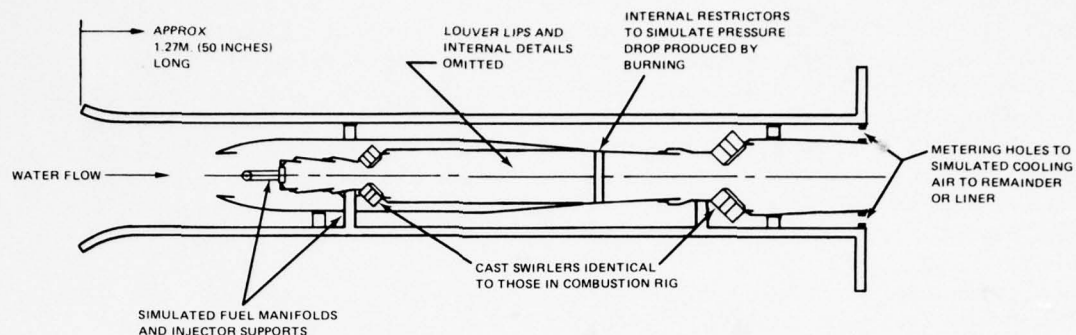


Figure 4-7 Water Flow Visualization Model Duct Burner

4.4.2 Swirler Calibration Rig

The test rig used for flow calibrating the swirlers in the pilot secondary and high power stages is shown schematically in Figure 4-8. This facility is located in stand X-416. Simulating flow conditions in the vicinity of the swirler tubes is accomplished with two independently controlled air sources: one representing shroud flow and the other, mainstream flow; and a variable wall member to change the pressure gradient on the swirler. Rig instrumentation consists of a complement of total and static pressure sensors.

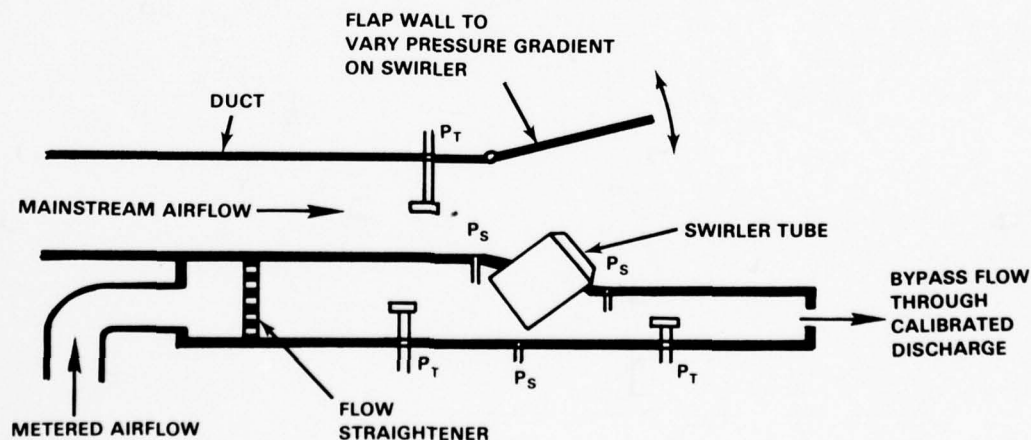


Figure 4-8 Swirler Flow Calibration Rig

4.4.3 Fuel Injector Flow Visualization Rig

The fuel injector rig was used in flow visualization studies to evaluate the spray penetration characteristics of various fuel injectors for use in the duct burner pilot secondary and high power stages. The test rig is shown in Figure 4-9 and consists of a rectangular duct constructed of plexiglas. The duct height is 19.1 cm (7 in), which duplicates the radial depth of a flight engine duct burner at the location of the high power stage. A ramp can be inserted to reduce the height to a dimension consistent the radial height of the high power stage of the segment rig duct burner.

Fuel injectors undergoing evaluation are installed on the wall and spray high-pressure water to simulate fuel into a cold air stream at conditions selected to approximate the dynamics of the fuel dispersion in the duct burner. The rig is equipped with appropriate instrumentation to monitor the air supply total and static pressure and temperature as well as the water flow rate, pressure and temperature.

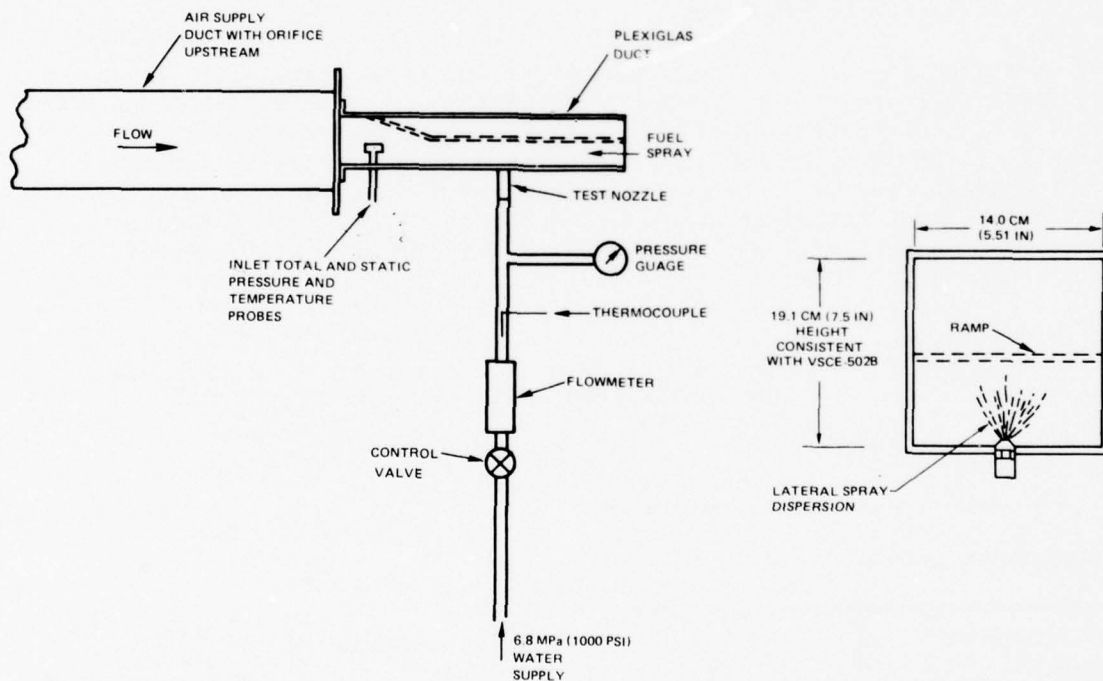


Figure 4-9 Fuel Injector Flow Visualization Rig

SECTION 5.0

EXPERIMENTAL PROCEDURES

5.1 INTRODUCTION

This section presents a definition of the parameters used in assessing the performance and emissions characteristics of the duct burner. Also contained in this section are the test procedures and the test conditions.

The various duct burner performance parameters that are discussed as program results are listed in Table 5-I. Definitions of the calculated parameters are presented in Section 5.2 and the symbols are defined on the Nomenclature list.

TABLE 5-I

SUMMARY OF DUCT BURNER PERFORMANCE PARAMETERS

<u>Parameter</u>	<u>Symbol</u>	<u>Units</u>	<u>Measured</u>	<u>Calculated</u>
Total Airflow	W_{at}	Kg/sec(lb/sec)	X	
Burner Airflow	W_{ab}	Kg/sec(lb/sec)		X
Inlet Total Pres	P_{Tin}	MPa(psia)	X	
Inlet Total Temp	T_{Tin}	$^{\circ}K(^{\circ}R)$	X	
Inlet Mach Number	M_n			X
Airflow Split	% of W_{ab}	%		X
Reference Velocity	V_{Ref}	m/sec(ft/sec)		X
Total Fuel Flow	W_F	Kg/sec(lb/sec)	X	
Fuel Flow Split	% of W_F	%	X	
Fuel/Air Ratio	F/A			X
Burner Total Pres Loss	P/P_{Tin}	% of P_{Tin}	X	
Ideal Burner Exit Temp	$T_{exit;id}$	$^{\circ}K$		X
Max. Metal Temp.		$^{\circ}K(^{\circ}R)$	X	
Fuel Temperature	T_{fuel}	$^{\circ}K(^{\circ}R)$	X	
Carb Bal Fuel/Air Ratio	FA_{CB}			X
Specific Humidity	H	g/kg	X	
Combustion Efficiency	η_c	%		X
Thrust Efficiency	η_t	%		X

5.2 PERFORMANCE PARAMETER DEFINITIONS

The total airflow (W_{at}) is that measured at the venturi in the inlet duct. The duct burner airflow (W_{ab}) is computed from the measurement of the airflow distribution. Sufficient total and static pressure measurements, coupled with known swirler, dilution and cooling component effective flow areas, permitted calculation of the duct burner airflow distribution. The burner exit is defined as a plane located at the entrance of the gas sampling probe tips. Total burner airflow W_{ab} includes all air entering the duct burner upstream of this plane and excludes the cooling flow to the last louver (louver 12) of the rig and that passing through the purge system behind this louver.

The distribution of airflow into the three stages is critical to burner performance and emissions. Definition of the airflow split was accomplished by computing the flow: (1) as a percentage of burner flow, through the end of the prechamber, defined as a plane immediately upstream of the pilot secondary stage fuel injectors; and (2) the flow through the end of the pilot secondary zone, defined as a plane immediately upstream of the fuel injectors in the high power stage.

The inlet Mach number is computed from the measured total rig airflow W_{at} , and inlet total temperature and pressure. The rig inlet area used in this computation is 694.22 cm^2 (107.604 in^2).

Reference velocity is defined as the velocity that would result if the total burner airflow at the rig inlet temperature and static pressure was passed through the duct burner at the maximum cross sectional area. This area occurs in the high power stage and is 441.48 cm^2 (68.43 in^2).

The total pressure loss across the duct burner is defined as the difference between the mean inlet total pressure and the exit total pressure, as defined by the average of 18 individual measurements at the exit plane expressed, as a percent of the inlet total pressure.

In addition to measuring total fuel flow into the duct burner, the fuel flowing into each of the three stages was also measured. This permitted defining the fuel flow split (prechamber/pilot secondary/ high power stage fuel flow) expressed as percent of the total burner fuel flow.

5.2.1 Fuel/Air Ratio

Duct burner fuel/air ratio is reported in two forms: (1) the metered fuel/air ratio defined as the ratio of the measured total fuel flow and the burner airflow W_{ab} ; and (2) the carbon balance fuel/air ratio, which is computed from measured exhaust species concentrations in accordance with the procedures established in SAE ARP 1256 (ref. 12). Following ARP 1256, the carbon balance fuel/air ratio is computed as follows:

$$F/A_{CB} = \frac{M_C + \alpha M_H}{M_{AIR}} \frac{n_{CO} + n_{CO_2}}{100 - \frac{1}{2} + \frac{\alpha}{4} n_{CO} - \frac{\alpha}{4} n_{CO_2}} \quad \text{Eq (1)}$$

where: M_x is the molecular weight of the x^{th} specie
 n_x is the mole fraction of the x^{th} specie
 α is the hydrogen to carbon ratio in the fuel

The metered and carbon balance fuel/air ratio are compared in Figure 5-1. The carbon balance fuel/air ratio consistently exceeds the metered by an increasing amount with increasing power level. While the carbon balance fuel/air ratio is defined from an analysis of the mixed sample from 18 sampling ports on the exit rakes, a varying quantity of liner cooling, and particularly end wall cooling air is not represented in the mixed sample. This quantity of unmixed air increases with increased power level as high power stage liner pressure drops and cooling flow increase. Thus, the carbon balance fuel/air ratio is more representative of mainstream combustion processes while the metered fuel/air ratio implies a mixture of all of the fuel in all the burner airflow. Consequently, consistent comparisons between rig configurations are best made on the metered fuel/air ratio basis.

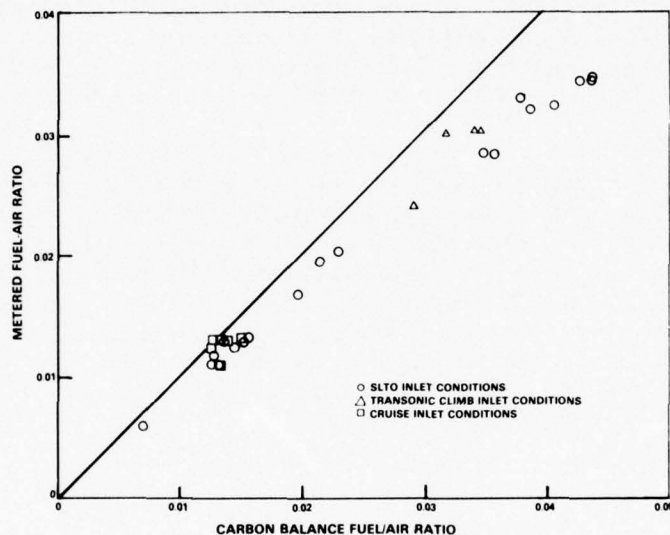


Figure 5-1 Comparison of Metered and Carbon Balance Fuel-Air Ratio

The ideal burner exit temperature is computed on the basis of 100 percent efficient combustion of all fuel to chemical equilibrium. The ideal burner exit temperature is based on the metered fuel/air ratio, for the given burner inlet conditions and burner airflow.

5.2.2 Combustion Efficiency/Exit Temperature

Combustion efficiency is calculated from gaseous emissions data on a deficit basis using measured concentrations of carbon monoxide and total unburned hydrocarbons. The calculation is based on an assumption that the total concentration of unburned hydrocarbons can be assigned the heating value of methane (CH_4) and the equilibrium concentration of carbon monoxide is negligible. The equation is:

$$\eta_c = 1 - \left(\frac{4300 \text{ EI}_{\text{CO}} + 21600 \text{ EI}_{\text{THC}}}{(18600)(1000)} \right) \quad \text{Eq (2)}$$

where: EI_{CO} is the measured carbon monoxide concentration in g/kg fuel
 EI_{THC} is the measured total unburned hydrocarbon concentration in g/kg fuel.

Duct burner exit temperature is obtained from emissions concentration measurements either as a mean temperature, from a fully mixed sample, or as temperature profiles generated from individual probe sampling. This method was chosen over direct temperature measurement with thermocouple probes because local gas temperatures could exceed the temperature capability of this type of conventional instrumentation.

The carbon balance fuel/air ratio and the combustion efficiency are defined from the emission analysis. The duct burner exit temperature then is defined from the ideal temperature rise associated with the carbon balance fuel/air ratio and corrected for combustion inefficiency with Equation 2.

An assessment of the accuracy of the emissions-derived temperature is shown in Figure 5-2. The watercooled aspirating thermocouple probe, positioned at the burner exit plane, was utilized to directly measure the gas temperature with a platinum/platinum-rhodium thermocouple at reduced fuel/air ratios. The aspirated combustion gases were directed to the emissions analysis equipment from which the emissions derived temperature was obtained simultaneously. The agreement between the temperatures is exceptionally good and demonstrates the accuracy of measuring exit temperature by emissions analyses.

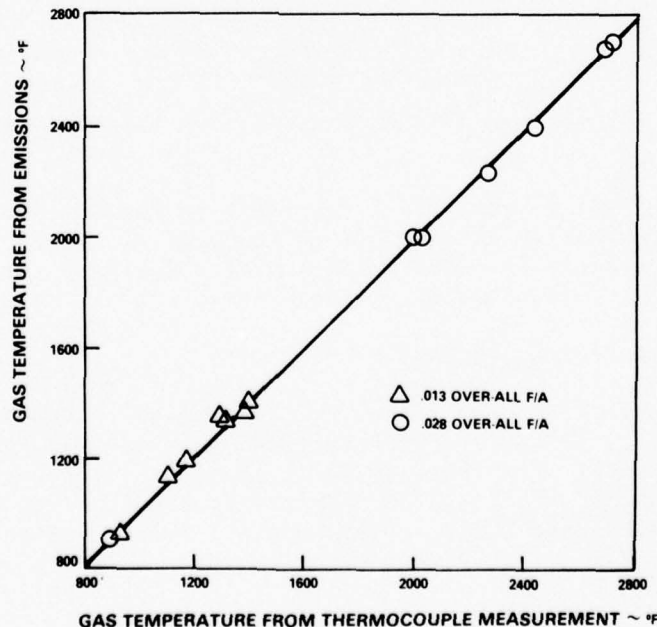


Figure 5-2 Comparison of Exit Gas Temperature Calculated From Local Carbon Balance Fuel-Air Ratio and the Thermocouple Probe Measurement

5.2.3 Thrust Efficiency

Maximum thrust is obtained from a duct burner with a uniform discharge flow profile and severe exit temperature or pressure profiles can have an adverse effect on net thrust. Consequently, while pattern factor is the characteristic parameter for a main combustor, thrust efficiency is utilized to characterize duct burner performance in this regard. Direct definition of thrust efficiency was not possible from the test data because the rig did not incorporate an exhaust nozzle. However, an estimate of thrust efficiency was accomplished by formulating an aerodynamic model to analytically compensate for the effect of an engine fan duct nozzle.

Referring to Figure 5-3, the total pressure and temperature profiles, measured by gas sampling probes, are reconstructed at the sonic throat of the exhaust nozzle by geometric translation of the radial scale. The temperature profiles reflect measured combustion inefficiency and are extrapolated to the measured liner temperatures. Mixing effects that would normally occur in the convergent section of the nozzle were ignored. This added conservatism to the analysis. The nozzle throat profiles are extended to include nozzle cooling air. The temperature of the nozzle cooling air is assumed to be the rig inlet temperature and, again conservatively, no mixing was assumed between this cooling air and combustion products.

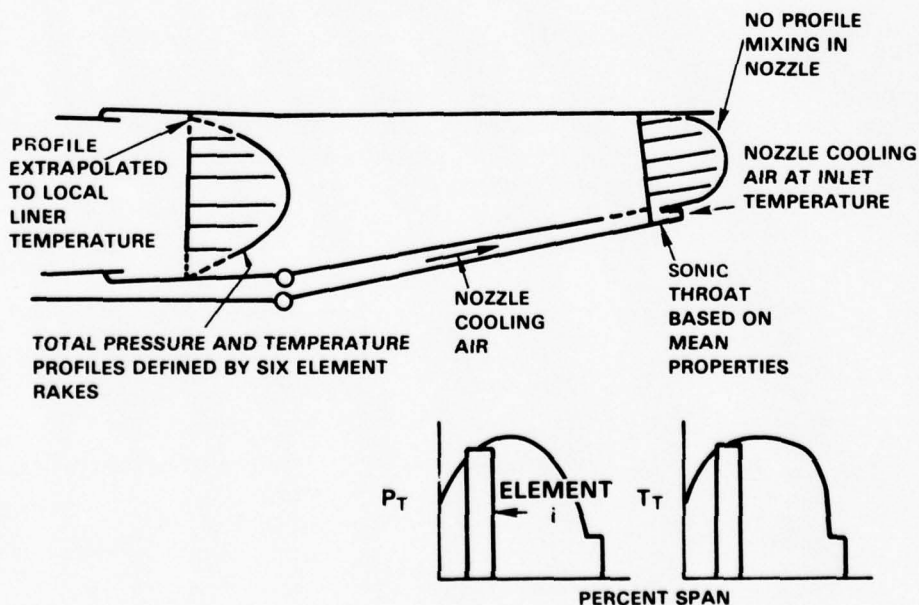


Figure 5-3 Analytical Model for Computing Thrust Efficiency

Evaluating thrust efficiency requires computing the thrust effective temperature, or that temperature corresponding to a uniform flow stream having the same thrust as the actual stream. Actual thrust is computed as:

$$\text{Actual Thrust} = \frac{1}{g_c} \sum_i W_i V_i \quad \text{Eq (3)}$$

where: W_i is the mass flow of the i^{th} element.
 V_i is the flow velocity at the throat of the i^{th} element.

An element here is a radial interval about a single gas sampling probe port, having unit circumferential or transverse width. For a flow field having uniform temperature and pressure at the throat, the thrust is:

$$\text{Thrust} = W \sqrt{\frac{2R}{g_c} \frac{T^*}{(\gamma-1)} \left[1 - \left(\frac{P_s}{P_T^*} \right)^{\frac{\gamma-1}{\gamma}} \right]} \quad \text{Eq (4)}$$

T^* is the thrust effective temperature, P_s is the throat static pressure, and P_T^* the throat total pressure. Equating the actual thrust from Equation 3 with the uniform stream thrust from Equation 4 and, assuming the total pressure mass averaged over the profiles is representative of P_T^* , the thrust effective temperature may be computed. The thrust efficiency is then defined as:

$$\eta_T = \frac{T^* - T_{T_{in}}}{\bar{T}_{enth} - T_{T_{in}}} \quad \text{Eq (5)}$$

where: \bar{T}_{enth} is an enthalpy weighted average temperature obtained from:

$$\bar{T}_{enth} = \frac{\sum_i W_i C_{p_i} T_i}{\sum_i W_i C_{p_i}} \quad \text{Eq (6)}$$

5.2.4 Gaseous Emissions Calculations

Since the rig inlet total pressure deviated from the nominal design levels, the emissions data for oxides of nitrogen and carbon monoxide obtained at the rig test conditions are reported in two forms: (1) as measured and (2) corrected to design inlet conditions. Oxides of nitrogen emissions were also corrected for inlet humidity. The correlations utilized are as follows:

$$\text{Corrected EI}_{\text{CO}} = \text{Measured EI}_{\text{CO}} \times \left(\frac{P_{T\text{meas}}}{P_{T\text{corr}}} \right) \quad \text{Eq (7)}$$

$$\text{Corrected EI}_{\text{NOx}} = \text{Measured EI}_{\text{NOx}} \left(\sqrt{\frac{P_{T\text{corr}}}{P_{T\text{meas}}}} \right) \left(\exp^{0.0188 (H_{\text{meas}} - H_{\text{corr}})} \right) \quad \text{Eq (8)}$$

where: P_T is the inlet total pressure

H is the inlet specific humidity

The specific humidity reference was 6.34 gm/kg for data obtained at simulated takeoff conditions. Since the transonic climb and supersonic cruise operating conditions represent high altitude flight conditions, data obtained at these conditions were referenced to zero specific humidity.

5.3 TEST CONDITIONS

Duct burner segment rig testing consisted of an investigation of emissions, performance and operational characteristics at three critical operating conditions. These included the sea level takeoff design point, transonic climb and supersonic cruise. Duct burner operating conditions for these flight modes in the VSCE-502B study engine are tabulated in Table 3-I, while corresponding rig conditions are listed in Table 5-II. While rig operating pressure was initially specified at flight engine levels, it was necessary to operate the rig at a slightly reduced inlet pressure to compensate for higher than expected air supply system losses. The volumetric flow capacity of the exhaust system in the test facility limited the maximum fuel/air ratio at which the duct burner rig could be operated to about 0.035, as opposed to the 0.0385 design intent. In addition, concern over adequate high power stage fuel injector pressure drop at the reduced flow associated with the transonic climb condition required operation at an increased airflow and pressure when simulating this condition.

TABLE 5-II

DUCT BURNER SEGMENT RIG TEST CONDITIONS

	<u>Takeoff</u>	<u>Transonic Climb</u>	<u>Cruise</u>
Inlet Pres - MPa (psia)	0.229(33.2)	0.229(33.2)	0.229(33.2)
Inlet Temp - °K (°F)	429(313)	445(342)	604(628)
Total Airflow -kg/sec(pps)	6.58(14.5)	4.67(10.3)	4.0(8.8)
Inlet Mach number	0.12	0.087	0.087
Fuel Flow - kg/sec (pps)	0.253 (0.558)	0.14(0.309)	0.052(0.114)
Fuel/Air Ratio	0.035	0.030	0.013
Exit Temp - °K (°F)	1605(2434)	1500(2240)	998(1340)

The comparison of duct burner inlet Mach numbers in the test rig with those in the VSCE-502B on Table 3-I indicates that Mach numbers in the test rig are about 25 percent lower. However, as indicated in Section 3.4.3, this is a consequence of mechanical constraints involved in scaling the full size duct burner to the airflow size of the VCE testbed engine. While these constraints necessitated increasing the duct radial height, which reduced the inlet Mach number, all critical local Mach numbers and velocities in the duct burner proper were maintained equivalent to those in the VSCE-502B study engine.

5.4 TEST PROCEDURES

For each test configuration, pressure loss and burner airflow distribution data were acquired in cold flow (unfired) and over a range of fuel/air ratios. Surveys of exhaust product emissions defined duct burner combustion performance. With these surveys, combustor discharge temperature and emissions profile data were obtained and combustion and thrust efficiencies determined. Data were obtained at the three critical inlet conditions of interest.

Typically, operating power level was increased by sequencing through the three duct burner fuel stages, pausing at representative power levels to record the necessary aerodynamic, combustion and emissions performance data. Throughout the test sequence, rig inlet and exit valves were constantly adjusted to maintain the required inlet conditions. In several instances, maximum high power operation was limited by elevated local burner liner temperatures.

With selected configurations, parametric tests were conducted to investigate the effects of stage fuel flow splits on the emissions and performance characteristics with the objective of defining optimum fuel splits. Tests were also conducted with selected configurations to assess stability and ignition characteristics. These tests were conducted at inlet conditions representative of takeoff. Ignition characteristics were defined over a wide range of prechamber fuel/air ratio. All testing was conducted using fuel that conformed to the American Society for Testing and materials (ASTM) Jet-A specification.

SECTION 6.0

EXPERIMENTAL RESULTS--CONFIGURATION 11

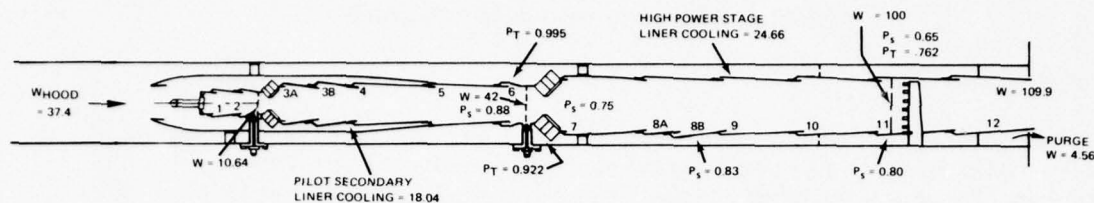
6.1 INTRODUCTION

The experimental evaluation consisted of a performance assessment of twelve duct burner rig configurations and involved over 200 hours of testing. The duct burner was operative for more than 80 percent of this total time. The mechanical arrangement of the twelve rig configurations is summarized in Appendix A. Appendix A also identifies the intent of the design modifications and, where appropriate, the limitations encountered in the evaluation of each configuration. Appendix C includes detailed tabulations of the aerodynamic performance and emissions characteristics of all test configurations.

The majority of modifications made to the duct burner were directed at enhancing performance, emissions, operational characteristics and, as required, the durability of the duct burner toward the program goals, as opposed to evaluation of parametric variations of a particular configuration. Consequently, the presentation of results is made in two parts. This section is restricted primarily to a discussion of results of a configuration evaluated near the end of the test sequence which reflects the extent of achievement of program goals and objectives. Rig Configuration 11 has been selected for this purpose and will be discussed in detail in this section. Results of the remaining configurations will be presented in Section 7.0. In this section the effect of design modifications, in terms of performance changes, leading to Configuration 11 will be discussed.

6.2 DUCT BURNER CONFIGURATION AND AIRFLOW DISTRIBUTION

Figure 6-1 shows the mechanical arrangement of duct burner Configuration 11 and the airflow distribution in the rig as calculated from the measured pressure distribution in the gas path and shrouds and the flow characteristics of the apertures in the liners listed on Figure A-7 of Appendix A. Comparison of the data with the initial design in Figure 3-12 indicates the major revisions introduced into the duct burner as the configuration evolved. The most significant of these is the level of liner cooling flow, which was increased from 12.6 to 18 percent of duct burner airflow in the pilot secondary stage and from 18.5 to 24.66 percent in the high power stage. The increased cooling to the pilot secondary stage was required to offset deterioration of the cooling film integrity on the louvers in this stage. This deterioration was caused by high turbulence generated by the swirling combustion air jets.



COMBUSTION AIR DISTRIBUTION

	W
PRECHAMBER FUEL INJECTOR	2.04
PRECHAMBER BULKHEAD	0.98
COMBUSTION AIR JETS - LOUVRE 1	2.84
PILOT SECONDARY SWIRLER TUBES	
INNER	6.70
OUTER	6.62
HIGH POWER STAGE SWIRLER TUBES	
INNER	15.28
OUTER	18.06

W = PERCENT OF TOTAL FLOW IN BURNER AT EXIT RAKE PLANE

P_s, P_T = LOCAL PRESSURES AS FRACTION OF BURNER INLET TOTAL PRESSURE

COOLING AIR DISTRIBUTION

LOUVER NUMBER	INNER* WALL W	OUTER* WALL W	TOTAL FOR FOUR WALLS W
1	0.958	0.958	1.916
2	1.429	1.429	2.858
3A	2.723	2.723	5.445
3B	1.096	1.096	2.192
4	1.463	1.588	3.051
5	1.339	1.420	2.759
6	2.723	1.870	4.593
7	2.100	1.997	4.097
8A	1.259	1.119	2.378
8B	—	1.151	1.151
9	2.140	3.065	5.205
10	2.473	3.605	6.078
11	2.873	2.878	5.751
12	2.657	2.661	5.318

*INNER AND OUTER WALL COOLING ALSO INCLUDE ONE HALF OF ENDWALL COOLING FLOW

Figure 6-1 Airflow Distribution in Configuration 11 of the Duct Burner Rig

Increasing the cooling flow by itself, however, was inadequate to maintain reasonable metal temperatures on louver 3, the first louver downstream of the swirler tubes in this stage. This louver panel was replaced with two shorter panels on both the inner and outer walls of the burner to provide sufficient cooling film integrity in the high turbulence environment. With these revisions, metal temperatures in the pilot secondary stage were maintained at or below 1200°K (1700°F) at the high inlet temperature of the supersonic cruise condition.

The need for higher cooling flows in the high power stage was due, in part, to the same interaction between the high turbulence level in the combustion gases and the louver cooling films. This situation was complicated by the fuel dispersion process in the high power stage. The fuel injected into this stage was found to concentrate near the outer liner subjecting it to higher heat loads. As in the case of the pilot secondary stage, the long louver 8 on the outer wall of the high power stage was also replaced with two short louvers to maintain cooling film integrity.

The radial fuel dispersion situation in the high power stage also led to other variations in the design prior to definition of Configuration 11. Fuel injectors in this stage were changed from the initial rig configurations an 85 degree hollow cone fuel spray injectors being replaced with injectors producing a flat spray with a 80-degree fan width. With the plane of the spray fan oriented perpendicular to the gas flow, these injectors produced better radial fuel dispersion than the conical spray injectors. The airflow split between the swirler tubes on the inner and outer side of the high power stage was also shifted from a symmetrical split to one favoring the tubes on the outer wall to lean the fuel rich regions on that side of the high power stage.

The airflow in each stage of the duct burner is within one percent of the total combustor airflow of the design intent of Figure 3-12. As a result, reference velocities, bulk equivalence ratios and gas temperatures at the downstream end of the stages were consistent with the initial aerothermal design. However, bulk equivalence ratios in the initial reaction zones at the upstream end of the pilot secondary and high power stages are higher than intended because the additional liner cooling air required in these stages was diverted from the swirler tubes. Table 6-I shows the bulk equivalence ratios in the upstream end of these stages and indicates that the increase, particularly in the pilot secondary stage, is significant. This increase in equivalence ratio could be expected to cause higher gas temperatures in the initial reaction zones that would increase NO_x production rates.

TABLE 6-I
BULK EQUIVALENCE RATIOS IN INITIAL REACTION ZONES AT THE TAKEOFF
OPERATING CONDITION

<u>Stage</u>	<u>Design of Figure 3-12</u>	<u>Configuration 11</u>
Pilot Secondary	0.63	0.80
High Power	0.69	0.75

Comparison of the rig pressure distribution with the design intent in Figure 3-12 indicates that the total pressure loss in the outer shroud passage around the hood enclosing the pilot stages is slightly higher than estimated in the design, while the corresponding loss in the passage on the inner side is below the projected level. This is due primarily to the increased airflow in the outer passage produced by the bias of the swirler tube airflow to this side and the increased cooling air supplied to the outer liner. Measurements were made of total pressure profiles at the entrance to the inner and outer shrouds adjacent to the pilot hood and further downstream in these passages near the inlet

to swirler tubes in the high power stage. The data indicated that there were minimal losses in the shroud entrance regions and that the shrouds were flowing full at the end of the diffusers formed by the sloped contour of the downstream surfaces of the pilot hood. Flow visualization tests conducted on the model described in Section 4.4.1 confirmed the absence of spillage from the pilot hood and stall free operation of the shroud diffuser.

Despite the consistency of the external pressure distribution and the per stage airflow distribution between the test rig and the design intent, the data in Figure 6-1 suggest that the high power stage static pressure is depressed relative to the aerothermal design. The mechanism causing this pressure reduction and attendant increase in overall total pressure loss across the duct burner will be discussed in further detail later in this section and in Section 7.0. Because of the depressed static pressure in the gas path of the high power stage, the pressure drops across the liner in this stage are higher than intended, on the order of 8 to 15 percent, rather than 6 percent. These pressure drops could be reduced by adjusting the flow areas of the meter plates and louvers, but such an effort is a development adjustment beyond the intended scope of the program. With the current high pressure drops, the liner was supplied with the necessary quantity of cooling air without having to increase the size of the metering holes in the louvers.

Figure 3-12 also shows a screech suppression system in louvers 7 and 8 of the outer liner panels. The system consisted of multiple rows of perforations in the liner panels with cover plates installed on the shroud side to limit leakage of liner cooling air through the perforations. Early in the program, this geometry was found to permit recirculation of combustion gases in the cavities causing liner burnout. Since dynamic pressure measurements indicated no propensity for acoustic combustion instabilities, the screech suppression system was removed and the perforated liner panels were replaced with solid louvers.

In the foregoing discussion, the observed airflow distribution in the duct burner was at the maximum fuel/air ratio takeoff condition. The airflow distribution in main burners is generally insensitive to operating conditions but, in augmentor systems, this distribution shifts with the overall fuel/air ratio because the total pressure losses associated with heat addition are an order of magnitude larger and cause variations in the static pressure in the gaspath. Figure 6-2 shows the variation in the airflow in the stages and components of Configuration 11 over the entire operating range. As the fuel/air ratio is increased and the gas-path pressure reduced in the downstream end of the burner the airflow is shown to shift with progressively larger quantities of air entering through the downstream components. The majority of the total airflow shift between unfired ($F/A = 0$) and the maximum fuel/air ratio condition occurs over the range of fuel/air ratios below 0.013, i.e., when the prechamber and pilot secondary stages become operational. Beyond this fuel/air ratio, the per stage flow splits remain essentially constant but air is diverted from the swirler tubes in the high power stage to

the liner cooling system in that stage and the flow to the cooling system in the rig exit components, which simulates the cooling flow for an exhaust nozzle, continues to increase. The magnitude of the flow shifts are not quite as pronounced at the lower reference Mach number associated with supersonic cruise and transonic climb because the magnitude of the variations in gas path pressure are not as large.

From the point of view of duct air utilization, these airflow shifts are desirable since it provides a self-compensating cooling air adjustment. At low fuel/air ratios such as supersonic cruise, a large quantity of combustion air is available in the prechamber and pilot secondary stages to control the combustion processes, while the liner in the high power stage and the exhaust nozzle are not overcooled with an adverse effect on exit temperature profile and thrust efficiency. At the high fuel/air ratios, more cooling air is required for these surfaces and is provided by the flow shift. However, the airflow shift has an adverse effect on ignition and possibly lean stability because the airflow through the prechamber varies by more than 70 percent and makes this stage considerably leaner at the unfired and low fuel flow conditions.

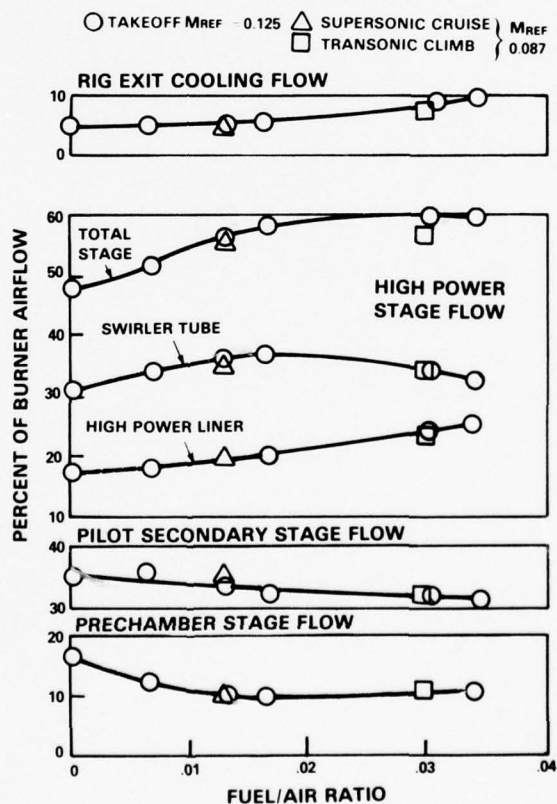


Figure 6-2 Effect of Fuel Air Ratio on Airflow Distribution in the Duct Burner

6.3 EMISSIONS

Table 6-II presents the emissions characteristics of Configuration 11 at the three critical duct burner operating conditions and includes, for comparison, the program goals and the analytically-projected emissions levels determined during the aerothermal design⁽¹⁾. The measured emissions have been corrected to the duct pressure levels of the VSCE-502B study engine and to standard humidity at the appropriate altitude using the procedures defined in Section 5.2.4. Data at supersonic cruise and transonic climb conditions were obtained at the appropriate fuel/air ratios, while data at takeoff were acquired at the maximum fuel/air ratio consistent with the facility exhaust system volumetric flow capacity. All three conditions were evaluated at per stage fuel flow splits consistent with the design fuel schedule in Figure 3-7.

TABLE 6-II
DUCT BURNER EMISSIONS CHARACTERISTICS

	Config* 11	Analytical Projection	Program Goal
<u>OPERATING CONDITIONS</u>			
<u>Supersonic Cruise</u>			
Fuel/Air Ratio	0.013	0.013	0.013
Stage Fuel Flow Split(+)	58/42/0	60/40/0	60/40/0
Emissions Indices (gm/kg)			
CO	2.1	30.0	30.0
THC	0.12	3.0	3.0
NO _x	8.1	2.75	1.0
Combustion Efficiency (%)	99.9	99.0	99.0
<u>Transonic Climb</u>			
Fuel Air Ratio	0.030	0.030	0.030
Stage Fuel Split(+)	26/17/57	27/16/57	27/16/57
Emissions Indices (gm/kg)			
CO	9.5	225.0	30.0
THC	0.04	22.5	3.0
NO _x	3.8	1.22	None Req'd.
Combustion Efficiency (%)	99.8	92.5	99.0
<u>Takeoff</u>			
Fuel/Air Ratio	0.344	0.0385	0.0385
Stage Fuel Split(+)	22/17/61	21/13/66	21/13/66
Emissions Indices (gm/kg)			
CO	11.9	30.0	30.0
THC	0.009	3.0	3.0
NO _x	2.7	1.78	1.0
Combustion Efficiency (%)	99.7	99.0	99.0
Smoke (SAE Smoke Number)	4.2	<15	<15

* Rig emissions measurements corrected to VSCE-502B study engine pressures and standard humidity.

+ Fuel flow to prechamber, pilot secondary and high power stages

Results indicate that at all three operating conditions the combustion efficiency exceeded analytical projections and program goals by wide margins. Emissions of unburned hydrocarbons are extremely low, approaching the thresholds of accurate measurement capability. Carbon monoxide emissions at supersonic cruise are also extremely low, while those measured at transonic climb and takeoff, at which the inlet temperature is lower and the high power stage is operational, are about one third of the projected and goal levels. The NO_x emissions, on the other hand, are in excess of the analytical projections, higher by almost a factor of three at supersonic cruise and transonic climb. At the higher fuel/air ratio takeoff condition, the excess NO_x production reduces to approximately 50 percent of the projected level.

It appears that a significant part, if not the majority, of the differences between the analytically projected and the measured emissions levels is due to rich combustion in the pilot secondary and high power stages. Combustion at higher than intended fuel/air ratios will increase local gas temperatures causing higher NO_x production and carbon monoxide consumption rates. The richer combustion was caused by increases in the bulk equivalence ratios in the initial reaction zones in these stages which were cited on Table 6-I and occurred as a result of reducing the swirler tube airflows to accommodate increased liner cooling requirements. The radial dispersion of fuel across the burner gas path from the injectors in the outer wall of the burner also affected the local equivalence ratio distribution, particularly in the high power stage. Considerable effort was expended during the program to improve the dispersion characteristics of fuel injectors in the high power stage. While 80-degree flat spray type injectors used in Configuration 11 led to considerable improvement in the emissions characteristics and liner heat load relative to other types of injectors used in the earlier portions of the program, further improvement in fuel dispersion with other fuel injector concepts might lead to reduced NO_x emissions at the high fuel/air ratio operating conditions.

Carbon monoxide and unburned hydrocarbon emissions at the transonic climb condition provide some indication of the effect of fuel dispersion on the combustion process in the high power stage. Analytical projections (ref. 1) indicated that combustion efficiency at this condition could be severely deficient because when computed on the basis of a bulk equivalence ratio in the initial reaction zone of this stage gas temperatures were too low to produce a carbon monoxide consumption rate consistent with the available residence time. However, experimental data from Configuration 11 suggest that carbon monoxide emissions at this condition were not only well below the levels necessary to meet the combustion efficiency goals, but also lower than those observed at the higher fuel/air ratio takeoff condition. While the difference in carbon monoxide emissions relative to the takeoff condition may be attributable to longer residence time, the inconsistency with the analytical projection must be attributable to (in this case favorable) fuel dispersion effects. The combined influence of lower total duct airflow and a lower fuel/air

ratio at transonic climb relative to the takeoff condition leads to a reduction in pressure drop across the high powerstage fuel injectors to less than 35 percent of that occurring at takeoff. As will be shown in Section 7.0, this reduction leads to reduced radial penetration of the fuel spray and consequently combustion in a richer environment near the outer wall of the combustor. In turn, this leads to higher local gas temperatures, relative to those projected from the bulk equivalence ratio with carbon monoxide oxidation rates sufficiently high to exceed rather than fall short of the combustion efficiency goal. Of course, this locally rich combustion also leads to the higher NO_x production shown on Table 6-II. Additional evidence of this fuel dispersion phenomenon will be presented in Sections 6.4 and 7.3 where duct burner exit temperature profiles will be discussed.

Further insight into the emissions generating mechanisms is provided by examining the emissions characteristics of the duct burner over the entire fuel/air ratio range. Figure 6-3 shows test data which, with the exception of the point at an overall fuel/air ratio of 0.006 (only the prechamber operational), were obtained from rig Configuration 11. All conditions were established at per stage fuel flow splits consistent with the schedule of Figure 3-7 and, except for the identified supersonic cruise and transonic climb conditions, all other data were obtained at duct burner inlet total pressure, total temperature and air-flow consistent with takeoff conditions. Because of the strong quenching effect of air entering through the high power stage swirlers when this stage is not operational, the composition of combustion products leaving the pilot secondary stage may be considered frozen and the emissions concentrations measured at the rakes representative of those at the end of that stage. A similar assumption regarding the combustion products from the prechamber is also at least qualitatively valid because the pilot secondary swirler tube airflow with this stage inoperative is sufficient to quench prechamber combustion products to temperatures of about 1365°K (2000°F). Data indicate that NO_x production in the prechamber is low, while carbon monoxide and unburned hydrocarbon emissions from this stage are high. The prechamber is designed for an overall equivalence ratio of about unity, but the reaction zone proper operates at an equivalence ratio of 1.8 to 2.0. This is conducive to lower NO_x production rates but the formation of large quantities of carbon monoxide. When the pilot secondary stage is operational, this carbon monoxide and unconsumed hydrocarbons are oxidized in that stage. Data obtained with pilot secondary stage indicate a significant increase in carbon monoxide emissions but minimal changes in NO_x or unburned hydrocarbons with increasing fuel flow to that stage. While increasing the fuel flow to this stage would be expected to enhance carbon monoxide consumption because of the higher equivalence ratio in the reaction zone immediately downstream of the swirler tubes, the presence of an opposite trend implies a possible coupling of the reaction zones in the prechamber and pilot secondary stages. If this is the case, the prechamber and pilot secondary stages are not functioning as discrete stages, as intended. This hypothesis would also explain the threefold increase in supersonic cruise NO_x emissions relative to that projected on the basis of data from experimental Vorbix main combustors. Correcting this situation to uncouple the two stages would require increasing the length of the prechamber stage.

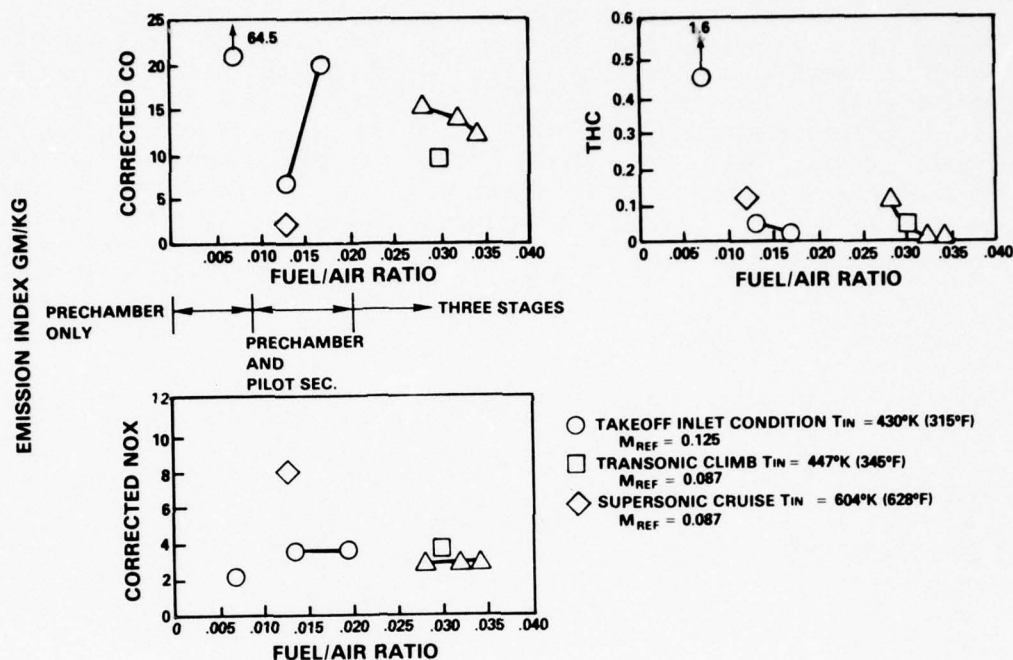


Figure 6-3 Emissions Characteristics of the Duct Burner

It could be alternatively argued that the increase in carbon monoxide emissions with increasing fuel flow to the pilot secondary stage is a result of reduced gas density and hence residence time in this stage. However, between the 0.013 and 0.0168 fuel/air ratio conditions, the residence time in this stage is only decreased 5 percent and it is doubtful that a change in residence time of this magnitude would produce a threefold increase in carbon monoxide emissions.

When the high power stage is operational, increasing the fuel/air ratio by increasing fuel flow reduces both carbon monoxide and unburned hydrocarbon emissions, while it has minimal impact on the overall NO_x emissions level. The trend of reduced carbon monoxide emissions with increasing high power stage fuel flow is attributed to the progressive increase in gas temperature in the high power stage and the consequent increase in the rate of carbon monoxide consumption. Over the range of fuel/air ratios from 0.028 to 0.0344, shown on Figure 6-3, the residence time in this stage was reduced by a factor of about 1.7 because of increased gas velocity. While residence time limitations on carbon monoxide oxidation might still be encountered at higher fuel/air ratios, had the latter been attainable, the lack of a residence time sensitivity in the available data suggests that the equivalence ratio of the reaction zone in the high power stage is a more significant parameter in establishing the CO emissions characteristics at high fuel/air ratios.

The low level of the carbon monoxide emissions at transonic climb compared to those measured at the same fuel/air ratio at the takeoff condition is attributed primarily to the radial stratification of the fuel in the high power stage because of the deteriorated fuel dispersion at low injector pressure drops. The decline in the unburned hydrocarbon emission with increasing fuel flow to the high power stage is also attributed to the dispersion characteristics of the fuel injectors in this stage. As fuel/air ratio is increased, the fuel spray penetration into the gaspath is improved with smaller quantities of fuel being entrained in the cooling air layer adjacent to the liner. This effect is demonstrated in the results of the fuel injector flow visualization studies presented in Appendix D.

When the high power stage is operational, the NO_x emissions index is lower than that observed with only the prechamber and pilot secondary stage operative. The lower NO_x output is attributed to this stage operating in an uncoupled mode. The invariance of the NO_x emissions index as the fuel flow to this stage is increased must be attributed to the effect of compensating factors. These include the reduction in residence time in this stage with increasing gas temperature and potentially more homogeneous mixtures if the fuel is dispersed more uniformly at the higher fuel injector flow rates and pressure drops.

Perturbations of the per stage fuel flow splits were conducted to provide additional information on emissions characteristics. Variations in the prechamber to pilot secondary stage fuel split were performed at an overall fuel/air ratio of 0.013 with rig inlet conditions representative of both supersonic cruise and takeoff. The results are shown in Figure 6-4 and indicate that the sensitivity of emissions to this fuel flow split is minimal with most of the variations approaching the accuracy of measurement. Nevertheless, some trends such as a decrease in NO_x emissions with increasing fuel flow in the prechamber, are discernable. This observation must be attributed to the high nominal equivalence ratios in the prechamber which reduced the flame temperature and consequently the NO_x production in this stage. The general insensitivity of emissions to fuel split supports the proposed concept of coupling of the prechamber and pilot secondary reaction zones because the extremely rich combustion in the prechamber is not completed in the available residence time.

An assessment of emissions sensitivity to the fuel split between the high power stage and the combined prechamber and pilot was conducted, and the results are shown in Figure 6-5. The data reveal weak trends of increasing carbon monoxide and decreasing NO_x emissions indices as more of the fuel is consumed in the high power stage. The variation is to be expected because there is less time available for oxidation of carbon monoxide and the formation of NO_x when the fuel is consumed in the high power stage. The unburned hydrocarbon emissions, while minimal, also decreased with increasing fuel flow to the high power stage because the higher injector pressure drop leads to better fuel spray penetration in this stage and less fuel entrainment in the cooling layer on the outer liner.

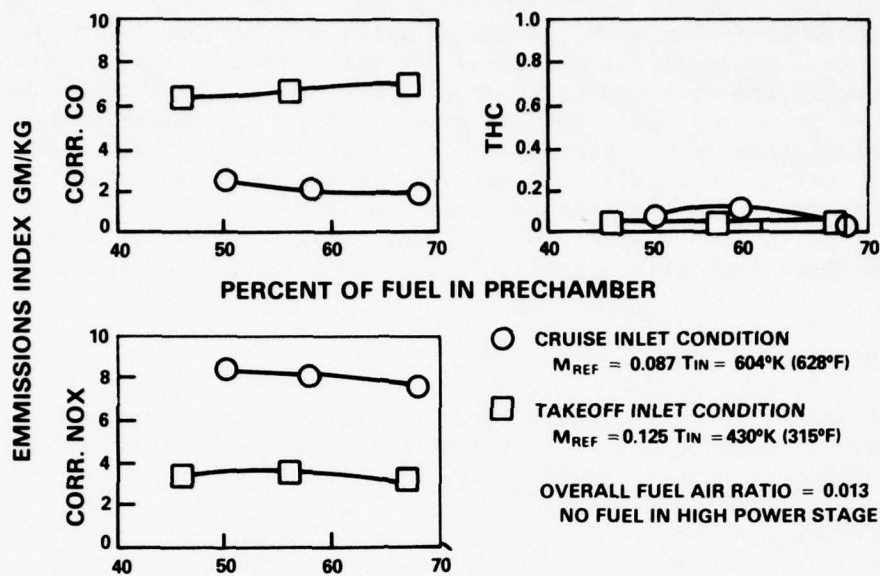


Figure 6-4 Effect of Fuel Flow Split on the Emissions Characteristics of the Combined Prechamber and Pilot Secondary Stages

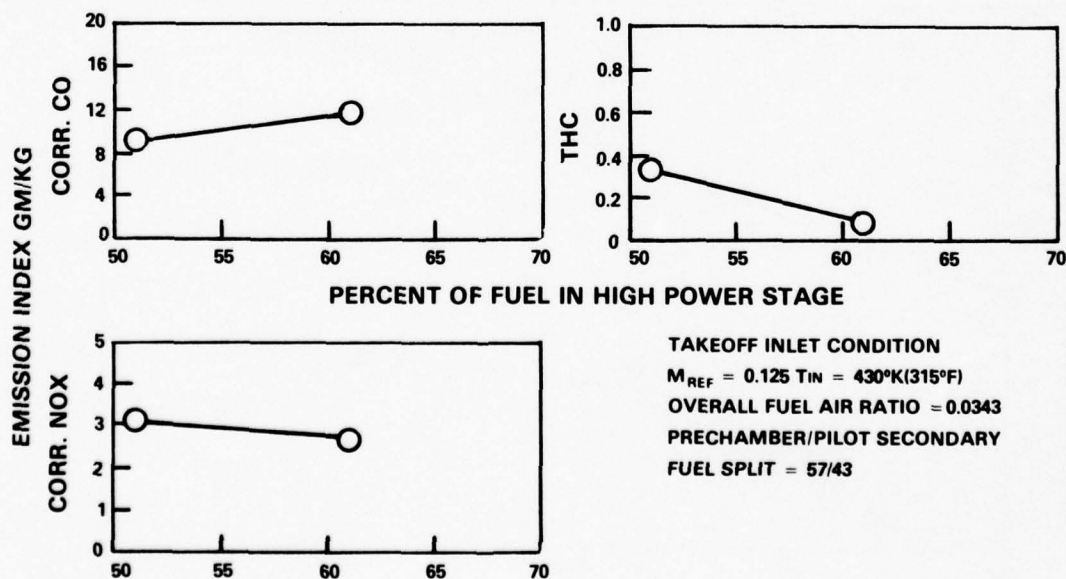


Figure 6-5 Effect of Fuel Split Between Prechamber/Pilot Secondary Stages and the High Power Stage on Emissions

The smoke output from the duct burner rig was well below the goal level with an SAE Smoke Number of 4.2 being observed at the takeoff condition. Because of the low operating pressure, low smoke output is to be anticipated. However, the rich combustion environment in the prechamber was suspected of producing large quantities of particulates because in some configurations that were operated at off design low inlet Mach number conditions, carbon deposition was observed on the louvers in the prechamber. The low overall SAE Smoke Numbers must be attributed to the residence time in the remainder of the duct burner, which was at least twice that typical of main burners, during which the carbon could be oxidized.

6.4 TOTAL PRESSURE LOSS

Figure 6-6 shows the variation in the total pressure loss of Configuration 11 over a range of fuel/air ratios. Data are presented for the inlet reference Mach numbers consistent with the takeoff and the lower flow supersonic cruise and transonic climb conditions. The results follow the anticipated trends of increasing pressure loss with increasing inlet Mach number and fuel/air ratio the latter arising from the total pressure loss associated with heat release in a high Mach number environment. The data indicate that the total pressure loss is considerably above the goal and analytically projected levels with the measured loss at the supersonic cruise condition being 6.76 percent, as opposed to a goal of 4.5 percent.

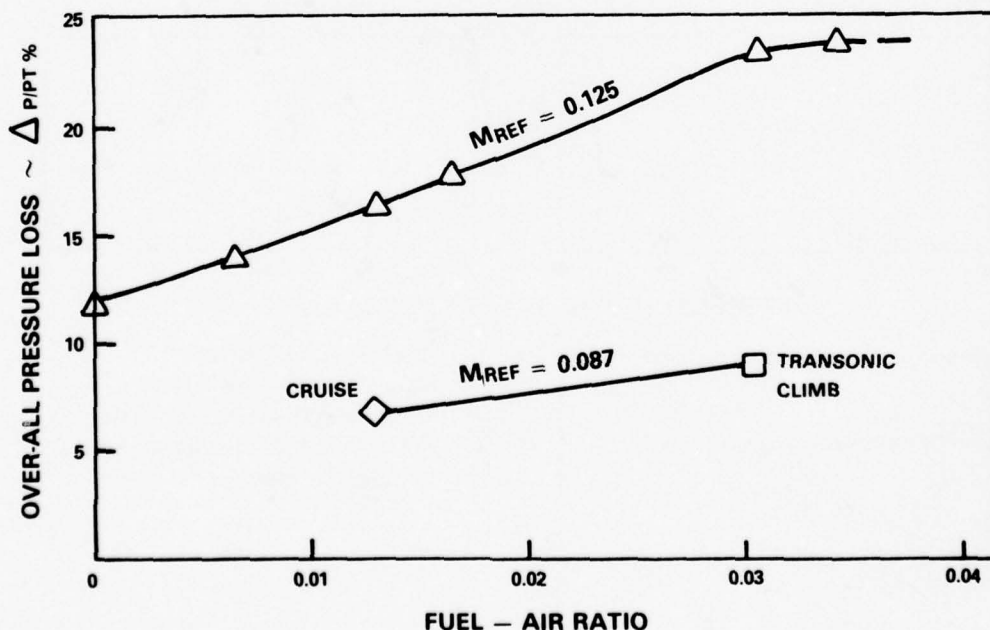


Figure 6-6 Total Pressure Loss Across Configuration 11 of the Duct Burner Rig

The mechanism causing this increase in total pressure loss has been identified and is related to interaction between the jets of combustion air entering the burner through the swirler tubes and the flow of the combustion products inside the burner. Figure 6-7 demonstrates this interaction where the jets act as radial blockages of the gas path and force the hot gas flow from the upstream stage to accelerate into the gaps between the jets and then incur a sudden expansion loss in expanding to fill the entire cross section of the gaspath downstream of this blockage. This blockage phenomenon has been observed in supporting flow visualization model tests. As shown in Figure 6-7, an analysis, modified to include this additional loss mechanism, predicted the static pressure distribution in the gas path to be in close agreement with the experimentally observed distribution. This blockage phenomenon occurs over the entire fuel/air ratio range, including unfired or cold flow conditions and similar agreement between analytically projected and measured static pressure distributions have been found over this range. Pressure losses of this type are incurred at the swirler tubes in both the pilot secondary and the high power stage but, because of the higher gas and combustion air jet velocities, the effects are more pronounced in the high power stage. The analysis indicates the local losses are about 4 times larger in the high power stage than in the pilot secondary.

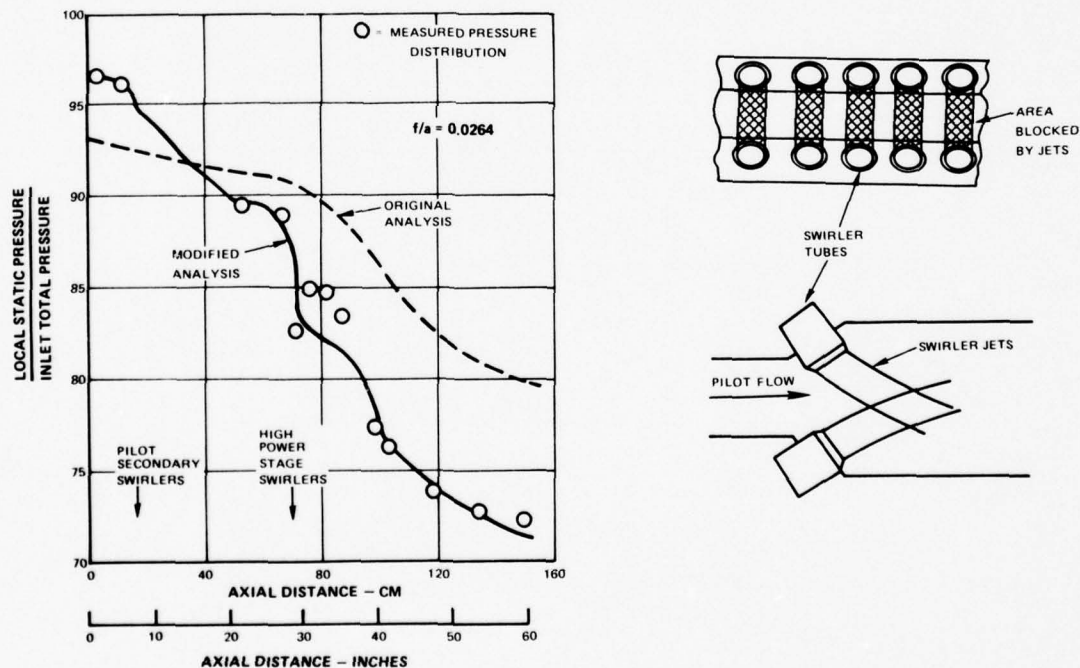


Figure 6-7 Comparison of Predicted and Measured Static Pressure Distributions

In Section 7.4 it will be demonstrated that the duct burner has been found responsive to design revisions that are directed at reducing the intensity of these blockage-induced losses. In one configuration discussed in that section (Configuration 12), the excess total pressure loss was reduced to about half the magnitude shown on Figure 6-6 without significant compromise to the emissions or other performance parameters.

6.5 THRUST EFFICIENCY

The thrust efficiency of the duct burner is related to both the chemical combustion efficiency and the uniformity of the flow at the exhaust nozzle. Figure 6-8 shows total pressure and total temperature profiles measured at the exit rake location in Configuration 11. The data indicate that at the supersonic cruise condition the exhaust gas total pressure and total temperature profiles are extremely uniform with negligible transverse or circumferential variation. This result was due to the vigorous mixing produced by the swirling air jets in the high power stage, which was not operational at this condition.

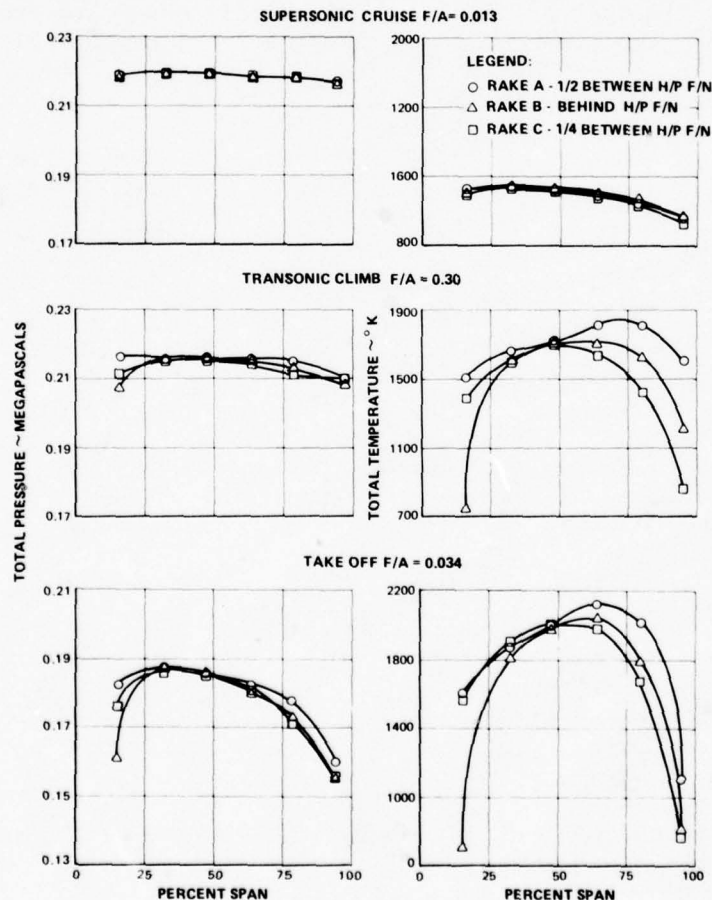


Figure 6-8 Total Pressure and Temperature Profiles at the Exit of the Duct Burner Rig (Configuration 11)

At the transonic climb and takeoff conditions, the high power stage is operational and the exit profiles are dominated by the mixing and combustion phenomena occurring in that stage. With exception of some local temperature differences near the outer wall, circumferential variations in the profiles are small and the dominant profile influence is in the radial direction. The temperature profiles indicate a bias of the peak temperatures toward the outer wall as a result of the previously cited fuel dispersion effect in this stage. In general, the profiles indicate that the circumferential fuel source density and mixing in that direction are adequate.

Computations were made of duct burner thrust efficiency using the flow property data of Figure 6-8 and the analytical procedure of Section 5.3. The thrust efficiency was projected both for a duct burner of the same radial height as the segment rig and installed in the VCE testbed demonstrator and for the larger duct burner sized compatible with the duct stream of the VSCE-502B study engine, as described in Section 3.4.2. The major difference in these two flow sizes is in the quantity of cooling air required for the convergent section of the exhaust nozzle with the larger flow size VSCE-502B configuration using proportionately less air for this purpose because of its lower surface to gas path area ratio. The results of this computation are summarized in Table 6-III.

TABLE 6-III

PROJECTED THRUST EFFICIENCY OF DUCT BURNER TEST CONFIGURATION 11

	Operating Condition		
	Supersonic Cruise	Transonic Climb	Takeoff
Fuel/Air Ratio	0.013	0.030	0.034
Chemical Combustion Efficiency (%)	99.9	99.8	99.7
VSCE-50B Size Engine			
Enthalpy Avg.			
Temperature °K (°F)	1044 (1419)	1399 (2058)	1510 (2259)
Thrust Effective			
Temperature °K (°F)	1032 (1397)	1343 (1975)	1430 (2114)
Thrust Efficiency - %	97.1	94.1	92.6
VCE Testbed Size Engine			
Enthalpy Avg.			
Temperature °K (°F)	1037 (1406)	1370 (2006)	1466 (2179)
Thrust Effective			
Temperature °K (°F)	1013 (1363)	1297 (1874)	1363 (1994)
Thrust Efficiency - %	94.5	92.1	90.1

The difference between enthalpy average temperature, which includes the assumed exhaust nozzle cooling air, and thrust effective temperature is the deficiency associated with the nonuniformity of the total pressure, total temperature and mass flow distribution at the exhaust nozzle throat. This temperature difference is shown to be only 12°K (22°F) at the supersonic cruise condition of the VSCE-502B sized engine, and when combined with the previously established chemical combustion efficiency lead to thrust efficiencies in excess of the goal of 94.5 percent. In the case of the VCE testbed size duct burner, the penalties associated with the larger quantity of nozzle cooling air lead to a loss of about 2.5 percent in thrust efficiency but the goal level is still achieved.

At the higher fuel/air ratio conditions where the high power stage is operational, the duct burner discharge flow nonuniformity effects become more evident and the quantity of nozzle cooling air is higher. This leads to differences between the enthalpy averaged and the thrust effective temperatures of the order of 80 to 100°K (145 to 180°F) at the takeoff condition and thrust efficiencies in the 90 to 93 percent range which are in excess of the 88 percent projected for a VSCE-502B sized duct burner in the preceding analytical studies.

6.6 IGNITION AND STABILITY

Because of the requirement of soft lighting to avoid generating pressure pulses that could propagate upstream in the fan duct and potentially stall the fan, tests were conducted to evaluate the ignition characteristics of the duct burner. Figure 6-9 shows the results of these tests for Configurations 1 and 11. The ignition boundaries for both configurations are similar with the lowest attainable ignition fuel/air ratio coinciding with the reference Mach number for takeoff which would be the normal duct burner starting condition. The boundary for Configuration 11 approaches the goal of an ignition fuel/air ratio of 0.002 at this reference Mach number but is deficient over the remainder of the range of Mach number. Configuration 1 is shown to meet or exceed the ignition goal over a wide range of reference Mach number reaching minimum ignition fuel/air ratio of 0.0014. These configurations had essentially identical prechamber geometries and air loadings, but the difference in the level of the ignition boundary for these two configurations has been traced to differences in the pressure drop across the bulkhead of the prechamber. Configuration 1 had a higher bulkhead pressure drop than Configuration 11 and the resultant higher air velocity through the aerating fuel injectors employed in this stage could have produced finer fuel atomization with an attendant advantage in ignition capability.

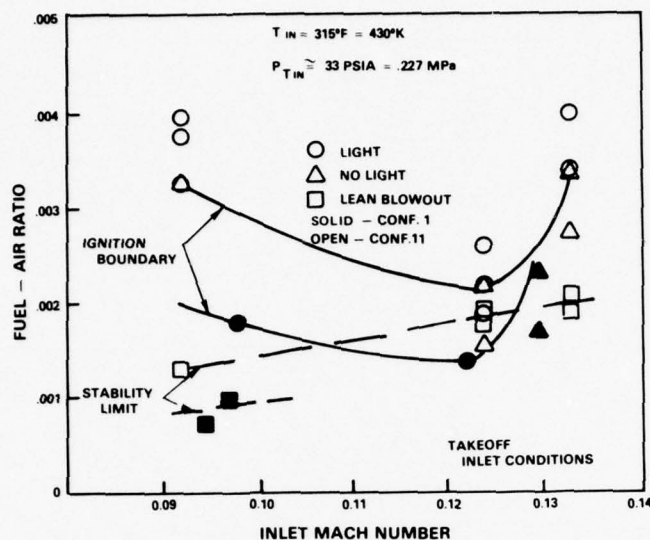


Figure 6-9 Ignition and Lean Blow Out Characteristics of the Duct Burner

Visual examination of the ignition process through a viewing port in the facility's exhaust elbow indicated that, for all conditions at which ignition was achieved, it was accomplished immediately after pressurization of the fuel manifold. In addition, propagation across all fuel injectors in the prechamber was essentially instantaneous. Partial lights, i.e., failure to propagate after achieving ignition at the fuel injector nearest the ignitor, were not observed at any of the conditions tested.

While the duct burner has been evaluated for soft ignition capability against a fuel/air ratio goal, the actual parameter of interest is the magnitude of the pressure pulse that occurs when ignition is achieved. This pulse was observed in Configuration 11 with a Kulite pressure transducer installed in the wall of the duct burner rig case so as to measure variations in the static pressure in the plane of the inlet instrumentation. The signal from the transducer, after suitable amplification, was recorded on a photographic strip chart recorder. Figure 6-10 shows the history of a typical ignition pressure pulse and reveals that the pulse occurred in two phases. The initial pressure rise was rapid, occurring in times of the order of one tenth of a second and was followed by a more gradual adjustment of the pressure to a final higher level. The figure shows the variation of the magnitude of both the initial phase and the overall pressure pulse with the fuel/air ratio at ignition. The data indicate that the strength of the initial pressure pulse is approximately proportional to the ignition fuel/air ratio, while that of the more gradual second phase is essentially a constant increment independent of the fuel/air ratio. The rapid initial pulse would be of concern and, as shown on this figure at the 0.002 ignition fuel/air ratio achieved by this rig configuration, this pressure pulse was estimated at less than two percent of the burner inlet total pressure.

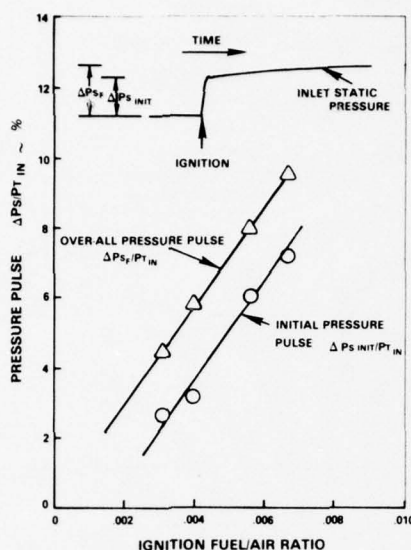


Figure 6-10 Duct Burner Ignition Pressure Pulse

Data were also obtained on the lean blowout limits of the prechamber stage. As shown on Figure 6-9 the lean stability envelopes generally paralleled the ignition boundaries with the minimum stable fuel/air ratios of Configuration 11 being 0.0018 at air inlet properties consistent with the takeoff operating condition.

6.7 ACOUSTIC STABILITY

Previous experience with thrust augmentation systems involving combustion at relatively low pressure levels and high spatial heat release rates has generated concern over the potential for acoustic instabilities of the combustion process. The most serious of these instabilities is screech a potentially destructive oscillatory mode associated with standing waves in the radial direction. Such a resonance would be most likely to occur at high fuel air ratios in the high power stage where the combustion gas velocities and the heat release rate are the highest. Based on the radial dimensions of the duct burner and estimated gas temperatures in this stage, if screech were to occur in the duct burner rig, it would be in the 4000-5000 Hz frequency range. This mode may be suppressed by perforating the liner of the duct burner in the regions of high heat release rate and this approach had been incorporated into the earlier configurations of the test rig. Recirculation of combustion gases in the cavities behind these perforations was encountered in an early test configuration. Consequently, this suppression system was removed and the remaining configurations evaluated without protection from this mode of instability. However, a Kulite pressure transducer in

a water-cooled jacket was installed in the test rig with the sensor aperture protruding through louver 7 in the high power stage of the burner and was used to monitor and record acoustic phenomenon. The data indicated that all of the configurations evaluated were free of any acoustic combustion instability. Figure 6-11 shows a typical spectral distribution of the pressure oscillations recorded at a fuel/air ratio of 0.0344, which is essentially the highest fuel/air ratio achieved during the program. The particular data presented was obtained from Configuration 9 and for reference purposes the spectral distribution recorded at an unfired (fuel/air ratio = 0) condition at the same air inlet conditions is also shown. The data indicate that the increase in oscillatory energy associated with combustion is relatively evenly distributed over the entire frequency range. The intensity of the pressure variations are somewhat higher in the 3000-4000 Hz range but this is not viewed as incipient instability because such instabilities would be much more intense and over a more discrete and narrower frequency range.

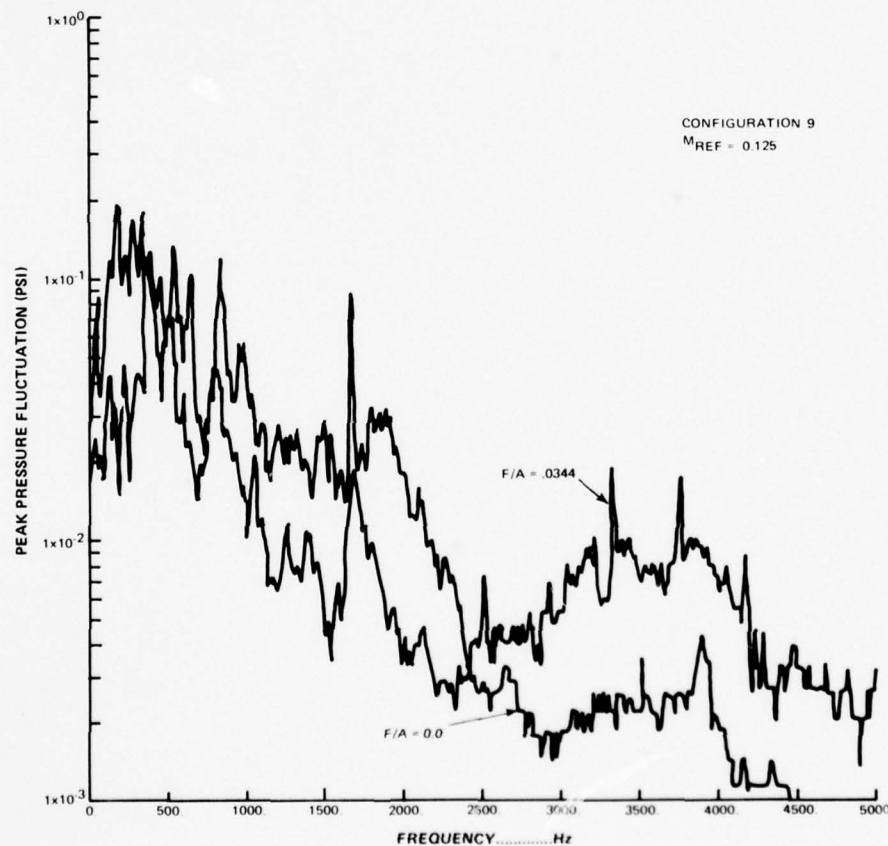


Figure 6-11 Spectral Distribution of Pressure Variation in the High Power Stage of the Duct Burner

The only unusual acoustic phenomena encountered in the entire test sequence was the presence of a discrete tone noise when the rig was operated with combustion in only the prechamber stage near the upper end of its fuel schedule, i.e., at overall fuel/air ratios of 0.006 to 0.010. When the pilot secondary stage was activated this tone was no longer audible. Spectral analyses of the data from the pressure transducer indicated this tone was occurring at a frequency of about 180 Hz and that it was suppressed, and not merely masked by other acoustic signals when the pilot secondary stage was activated. It is unclear whether this tone was mechanically induced by component vibration or an axially oriented acoustic mode within the combustor proper.

SECTION 7.0

EXPERIMENTAL RESULTS - DUCT BURNER EVOLUTION

7.1 INTRODUCTION

In the evolution of the duct burner toward the configuration discussed in Section 6.0, some of the design revisions had significant effects on the performance, emissions and durability of the system. The observed effect of these revisions are discussed in this section. The particular revisions include modifications to the combustor and the fuel systems to eliminate liner overheating and aerothermal perturbations introduced to reduce the total pressure loss across the duct burner. These revision are described in Appendix A.

7.2 BURNER LINER DURABILITY

The operation of the earliest configurations of the duct burner rig indicated that a durability problem existed with the louver panels immediately downstream of the swirler tubes in both the pilot secondary and the high power stages. The problem arose primarily from interaction between the highly turbulent mixing of the combustion gases generated by the swirling air jets and the cooling film on those louvers. While metal temperatures on the louver panels in the pilot secondary stage were acceptable for short duration testing at the lower inlet temperatures associated with the takeoff and transonic climb conditions, they precluded operation at the higher inlet temperature supersonic cruise condition. This situation was more severe in the high power stage and it was impossible to operate this stage at overall fuel/air ratios above 0.026 without exceeding local liner temperatures of 1200°K (1700°F). While the liner temperatures appeared to be essentially equal on the inner and outer walls of the pilot secondary stage, the overtemperature situation in the high power stage was restricted to the outer liner with the highest metal temperatures being encountered in louver 8. This implied that fuel injection into this stage was also involved in the overheating problem. Several revisions were incorporated into the duct burner to alleviate this situation and the effect of these modifications on the metal temperature history of louver 8 of the outer liner are shown in Figure 7-1.

The first revision, incorporated between the evaluation of Configurations 3 and 4 involved a change in the direction of rotation of the swirler tubes in both the pilot secondary and the high power stages. Figure 7-2 shows the orientation of these tubes in Configurations 1 through 3 in what has been designated a counterrotating array. In this orientation, the vortical flows generated by the swirling jets reinforce between adjacent swirler tubes on the same wall and generate secondary flows that are alternatively directed toward the wall and toward the center of the gas path. Based on metal heating patterns, it appeared

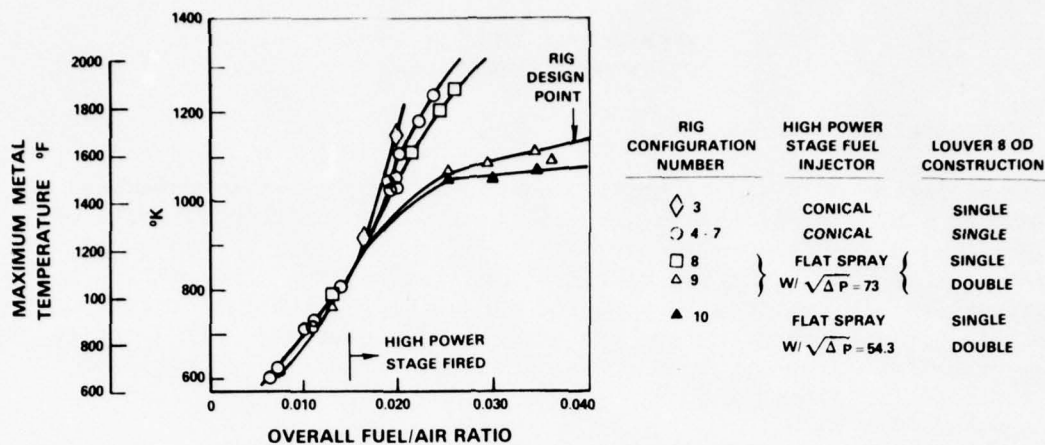
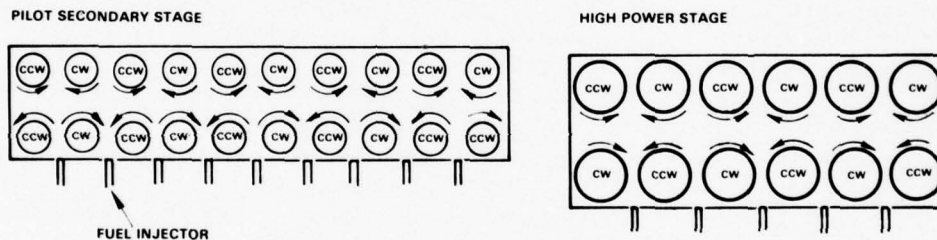


Figure 7-1 Metal Temperature History on Louver 8 of the Outer Liner

CONFIGURATIONS 1 THROUGH 3 – COUNTERROTATING SWIRLERS:



CONFIGURATIONS 4 THROUGH 12 – COROTATING SWIRLERS:

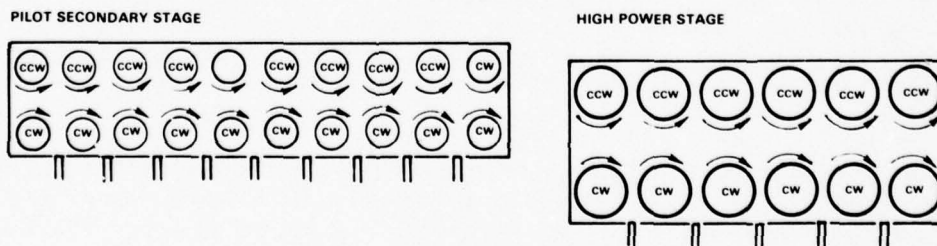


Figure 7-2 Swirler Tube Orientation in the Duct Burner

that hot gases entrained by the swirling jets were impinged on the liner at the transverse positions where these secondary flows were directed toward the wall. In the pilot secondary stage, five and four local streaks occurred on the inner and outer wall, respectively, at positions between the appropriate swirler tubes. The overheating was not as localized in the high power stage, but there was still considerable evidence of a higher heat load on the outer liner at three transverse spaced locations coinciding with the positions of swirler tubes that would produce secondary flows toward the wall. It was also suspected that, in the high power stage, these secondary flows were entraining fuel from the injectors, that were positioned between and immediately upstream of the swirler tubes, and further aggravating the local heat load by intensifying combustion near the outer liner at these positions. To avoid this situation, the swirler tubes in both the pilot secondary and the high power stage were re-oriented to the corotating arrays shown on Figure 7-2, in which the vortical flows are in shear rather than reinforcing directions between the tubes. This approach was successful in that localized overtemperaturing of the liners in both stages was relieved, but, as shown in Figure 7-1, temperatures on louver 8 were still well in excess of acceptable limits. Attempts were made to reduce the temperature of the affected louvers by increasing the cooling flow, but were unsuccessful. Between Configurations 4 and 7 the cooling flow to the outer louver 8 was increased by nearly 30 percent by increasing the flow area of the meter plate in the outer shroud with no appreciable effect on metal temperatures. A similar 50 percent increase in the cooling flow to louver 3 on both the inner and outer wall of the pilot secondary stage produced minimal metal temperature reductions.

The effect of fuel dispersions from the injectors was investigated in a separate effort in which various types of injectors were evaluated in the flow visualization apparatus described in Section 4.4.3. The injector under investigation was mounted on the wall of a plexiglas duct and sprayed water radially into a cold air stream. The air stream velocity and the injector pressure drop were established to simulate the momentum of the fuel droplets relative to that of the combustion gases. While such a simulation is not realistic in terms of intervening vaporization and combustion phenomena, it offered a first order representation of the dynamics of the initial spray penetration and dispersion process. The details of this investigation including photographs of pertinent results are presented in Appendix D.

The results of these flow visualization studies indicated that fuel dispersion from the injectors in the pilot secondary stage was consistent with the design intent in that there was no filming of fuel on the outer wall and the spray appeared to disperse across a radial distance equivalent to the 4.25 cm (1.67 in) height of the gaspath in this stage. A similar evaluation of the 85-degree hollow cone spray injectors used in the high power stage during the evaluation of Configurations 1 through 6 of the duct burner rig indicated that at the conditions where

high outer liner temperatures were encountered the fuel spray did not penetrate significantly beyond the midspan of the gas path and some propensity for fuel film formation on the outer liner was evident. Further investigations conducted in a flow visualization model indicated fuel that penetrated less than 25 percent of the radial height of the gas path was entrained in a strong flow between the high power stage swirler tubes and accumulated in a region adjacent to the louvers 7 and 8 of the outer liner.

The fuel injector flow visualization study progressed to evaluate other injector configurations that would offer better fuel dispersion characteristics in the high power stage. A flat spray type injector, having a 80-degree spray fan with the plane of the fan aligned perpendicular to the gaspath flow direction was selected for evaluation in Configuration 8. In the flow visualization study, this type of injector was found to produce a spray that would penetrate the complete radial height of the burner gas path with considerably less residual spray near the outer liner. As the data in Figure 7-1 indicate, the improvement in fuel dispersion produced by these injectors reduced the metal temperatures of the outer louver 8 by about 65°K (120°F) at the high fuel/air ratio test conditions. As will be shown later in this section, the change to the flat spray fuel injector also had a substantial impact on the combustion process in the high power stage and produced a significant reduction in emissions.

The most significant improvement in liner durability was achieved when shorter louvers were incorporated in place of louvers 3 and 8 in Configuration 9 of the duct burner rig. The length of these panels had been 14.2 cm (5.6 in) and 15.8 cm (6.2 in) on louvers 3 and 8, respectively, and when replaced with two louvers of about half these lengths the integrity of the cooling film was maintained over the entire panel. As shown in Figure 7-1, this permitted operation of the high power stage up to the maximum attainable fuel/air ratio while maintaining reasonable metal temperatures. A similar improvement in cooling film integrity was obtained on louver 3 in the pilot secondary stage permitting operation of the duct burner at the higher inlet temperature supersonic cruise condition without exceeding metal temperatures of 1200°K (1700°F) in this louver.

The fuel injector flow visualization study also revealed that the spray penetration characteristics of the fuel injectors improved with increasing fuel pressure drop. Smaller flow capacity injectors with both 85-degree hollow cone spray (Configuration 7) and flat spray patterns (Configurations 10, 11 and 12) were also evaluated in the combustor rig. The increased pressure drop of the smaller 85-degree hollow-cone injector had no substantial effect on the metal temperatures of louver 8 but, as shown in Figure 7-1, an additional 41°K (75°F) temperature reduction was achieved with the reduced capacity flat spray injector. Extrapolation of the wall temperature history to even the highest takeoff

fuel/air ratios under consideration for the VSCE-502B study engine indicate that with the combination of a lower flow capacity flat spray injector and shorter lower panels the maximum temperature of the liner does not exceed 1140°K (1600°F).

With the exception of the overheating of louvers 3 and 8 because of the high gas path turbulence level and the previously cited problem of combustion gas recirculation in the cavities of the screech suppression system incorporated in the initial rig configurations, no other significant liner cooling problems were encountered. Minor adjustments in cooling flow were introduced, as required, in conjunction with other more significant hardware modifications. Figure 7-3 shows the measured metal temperature distribution in Configuration 11 of the duct burner and indicates that while some additional cooling air redistribution might be desirable, the temperature levels are acceptable at this stage of evolution of the burner.

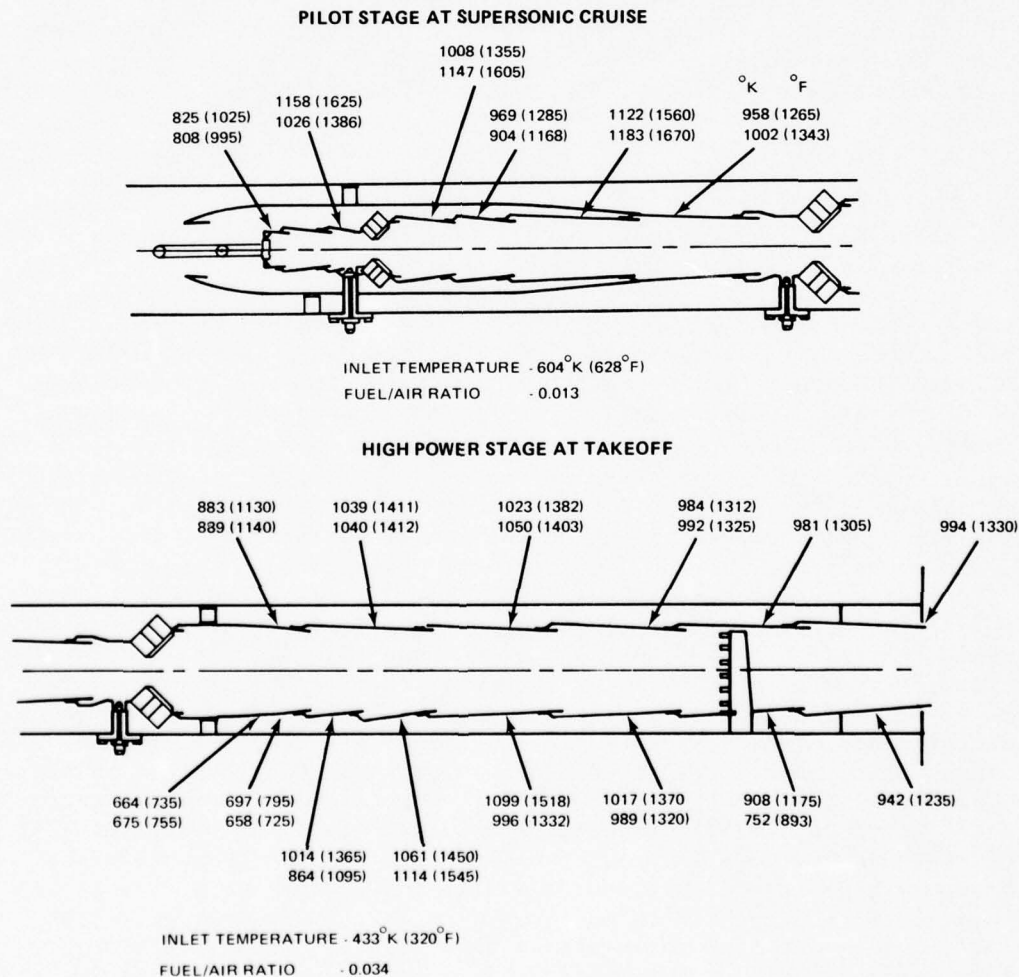


Figure 7-3 Measured Liner Temperature Distribution in Configuration 11 of the Duct Burner

7.3 EFFECT OF FUEL INJECTORS ON EMISSIONS

Emissions at high fuel/air ratios were found to be sensitive to the different types of fuel injectors used in the high power stage. In rig Configuration 7 the effect of increased pressure drop on the 85degree hollow cone type injector was assessed by installing similar smaller flow capacity injectors and in a subsequent test configuration these injectors were replaced with flat spray injectors. Table 7-I shows a comparison of emissions characteristics with these injectors.

The data indicate that with the initially specified hollow-cone injectors (Configuration 6) combustion efficiency at maximum attainable fuel/air ratio, dictated by metal temperatures on louver 8 of the outer liner, was only 92 percent with the majority of the inefficiency being due to high unburned hydrocarbon emissions. Increasing the injector pressure drop by more than four fold in Configuration 7 was expected, on the basis of the flow visualization studies, to produce some improvement in fuel dispersion. While the fuel/air ratio was still restricted to the same levels by the outer liner metal temperature limit some improvement in CO and THC emissions was evident. Substitution of flat spray injectors produced a substantial added reduction in these emissions constituents with both being reduced to levels below the analytical projections and the program goals. The NO_x emissions were shown to increase progressively with these improvements in fuel injection. This is a consequence of the higher bulk gas temperatures associated with improved combustion efficiency, and in the case of Configuration 10, a higher nominal equivalence ratio in this stage.

The mechanism causing the pronounced difference in emissions output with the hollow cone and flat spray fuel injectors is shown in Figure 7-4. This figure shows profiles of the local fuel/air ratio and the concentration of emissions constituents at the duct burner exit. Data are shown for Configuration 7 that employ the low flow capacity hollow cone fuel injectors in the high power stage at conditions identical to those listed in Table 7-I. The data for a configuration with flat spray type injectors were generated during the evaluation of Configuration 11, which was discussed earlier in Section 6.0. These profiles were measured at conditions essentially identical to that listed for Configuration 10 in Table 7-I. These data indicate that, despite considerably higher fuel/air ratio and fuel flow to the high power stage with the flat spray fuel injectors, fuel/air ratio profiles at the exit rakes are quite uniform in the radial direction and indicative of fuel being dispersed across the radial depth of the gas path. Data obtained with the hollow cone injectors when operating at an even higher pressure drop exhibit greater circumferential uniformity but a peak in the local fuel/air ratio near the outer wall. Despite circumferential uniformity of the fuel/air ratio, the data indicate that a large part of the high carbon monoxide and unburned hydrocarbon emissions associated with the use of the hollow cone injectors is attributable to the region axially downstream of the swirler tubes in the high power stage. This observation suggests a reaction quenching effect associated with interaction of the fuel spray with the combustion air jets that is avoided when the fuel is injected

TABLE 7-1

EFFECT OF HIGH POWER STAGE FUEL INJECTOR
ON DUCT BURNER EMISSIONS CHARACTERISTICS

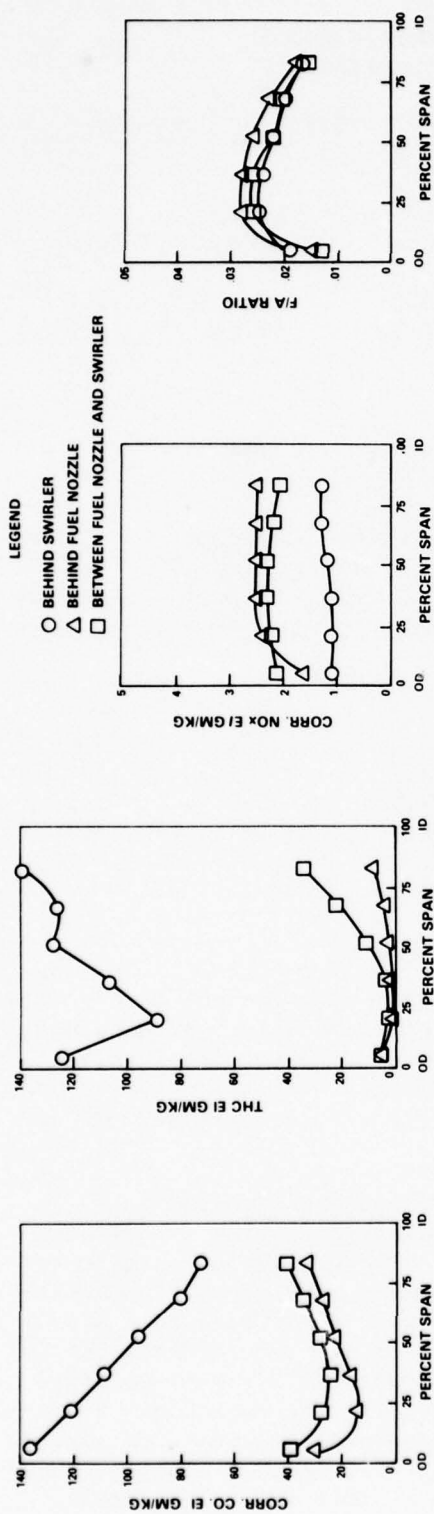
	Analytical Projection	TEST CONFIGURATION		
		6	7	10
Fuel Injector Type:	-	Hollow Cone	Hollow Cone	Flat Spray
Flow Size per injector	-	45.5 (8.3)	19.7 (3.6)	54.3 (9.9)
W/ $P^{1/2}$ $\frac{\text{kg/hr}}{\text{MPa}^{1/2}}$ $\left(\frac{\text{lb/hr}}{\text{psia}^{1/2}} \right)$				
Pressure Drop - MPa (psia)	-	0.80 (116)	3.38 (491)	2.42 (351)
Fuel/Air Ratio	0.0385	0.0203*	0.0196*	0.0328*
Stage Fuel Split	21/13/66	15/19/46	35/20/45	19/21/60
Air Inlet Condition (Ref Table 5-II)	Takeoff	Takeoff	Takeoff	Takeoff
Emissions Index gm/Kg:				
CO	30.00	60.9	47.6	28.0
THC	3.0	56.9	27.4	0.8
NO _x	1.78	1.9	2.1	2.4
Combustion Efficiency - %	99.0	92.0	95.7	99.3
SAE Smoke Number	<15	2.1	-	1.3

* Maximum attainable within liner temperature limits.

through the flat spray injectors. The fact that NO_x emissions were also lower at the rake location where high carbon monoxide and unburned hydrocarbon emissions were observed supports the argument that variations in NO_x emissions with this type of fuel injector are due primarily to local combustion efficiency and hence gas temperature variations.

Test data from rig Configuration 11 in Figure 7-4 also provide an assessment of the current limitations on the emissions characteristics of the duct burner and provide some direction for future evolution of this concept. Unburned hydrocarbon emissions appear to be virtually nonexistent in the core of the flow and reach significant magnitudes only near the outer wall. These levels are probably due to fuel entrainment in the liner cooling air and potentially could be reduced by further improvement of the fuel injector spray characteristics and/or reduction in the liner cooling airflow. The carbon monoxide concentration profiles exhibit some increases near the outer wall but are not indicative of a severe or limiting reaction quenching situation in this area. The radial

CONFIGURATION 7 - HOLLOW CONE INJECTORS



CONFIGURATION 11 - FLAT SPRAY INJECTORS

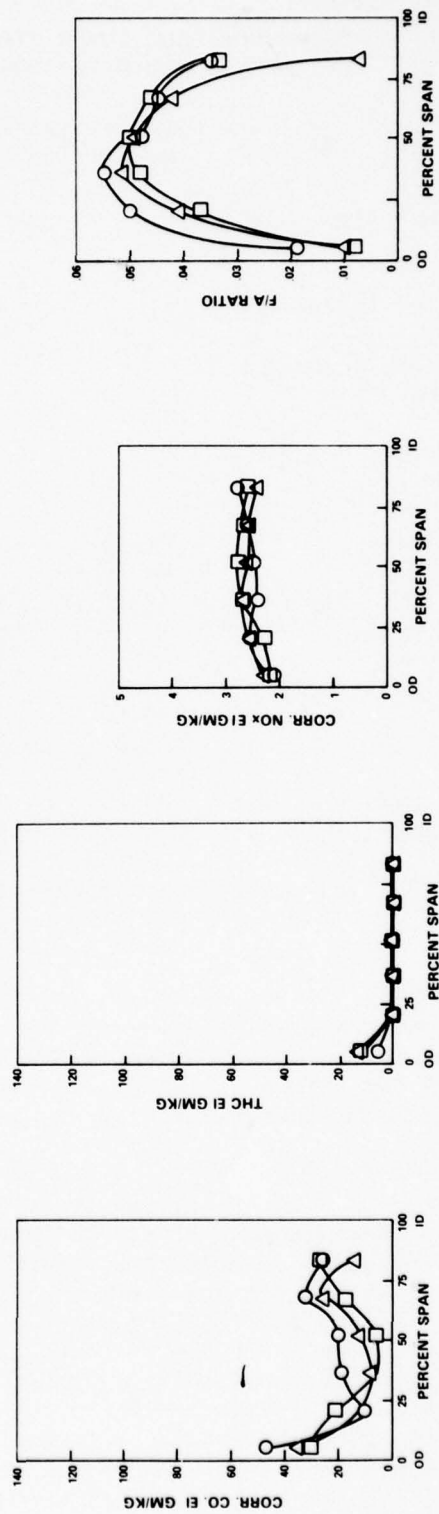


Figure 7-4
 Effect of Conical Spray (Configuration 7) Vs Flat Spray
 (Configuration 11) High Power Fuel Nozzles on Emissions
 Takeoff Inlet Conditions

variations in carbon monoxide concentrations indicate that a fully mixed situation has not been achieved at the exit rake and some of the higher local concentrations might be reduced by improved initial fuel air mixing. The effect of residence time in the high power stage has not been investigated directly in the effort to date and should be included in future tests to assess carbon monoxide NO_x emissions tradeoffs as well as mixing effects.

The sensitivity of emissions to the fuel injection process in the high power stage is important to operation at transonic climb since the duct airflow and high power stage fuel/air ratio are reduced relative to the takeoff condition. In the VSCE-502B study engine, this reduces the injector pressure drop in this stage to only about 12 percent of those attained at takeoff.

Figure 7-5 shows profiles of local fuel/air ratio and emissions concentrations at the rig exit plane as obtained during the evaluation of Configuration 11 at the simulated transonic climb condition (ref. Table 5-3). The pressure drop across the fuel injectors in the high power stage was 0.83 MPa (120 psi) at this condition. Comparison of profiles of fuel/air ratio with those obtained at takeoff indicate more bias of the fuel toward the outer wall and are indicative of somewhat less fuel spray penetration. With exception of the carbon monoxide concentration measured at the rake immediately downstream of a swirler tube, the profiles indicate a high degree of mixture uniformity at the exit rakes. This could be attributed to lower velocities and increased residence time in the high power stage at this operating condition. It is significant that wall quenching is also not a major factor in combustion efficiency at this condition. Visual examination of the reaction zone in the high power stage through the view port in the exhaust elbow showed a more pronounced yellow color in this zone at transonic climb. This would be consistent with richer combustion over a limited extent of the stage as a result of reduced fuel spray penetration.

While the revisions incorporated in the high power stage fuel system to resolve a liner durability problem had a significant effect on emissions, the other modifications introduced for this purpose can only be qualitatively assessed and appear to have a smaller impact. The increases in local cooling flow and the installation of double louvers in critical locations the latter requiring more cooling flow than a single louver of the same length impacted emissions in two ways: (1) the potential for reaction quenching at the wall is increased and (2) air used for cooling must be diverted from the initial reaction zones increasing the equivalence ratio in those zones. In the current investigation, wall reaction quenching was observed but it was not found a limiting factor on attaining combustion efficiency. The enrichment of initial reaction zone because of the diversion of air to liner cooling was recognized in earlier discussions as a significant factor on NO_x emissions but this enrichment was due primarily to the smaller airflow size of the test rig and the VCE testbed, in addition to the need to cool the rig endwalls. The effect of additional diversion of air to liner cooling during the evolution of the burner is masked by other revisions incorporated at the same time.

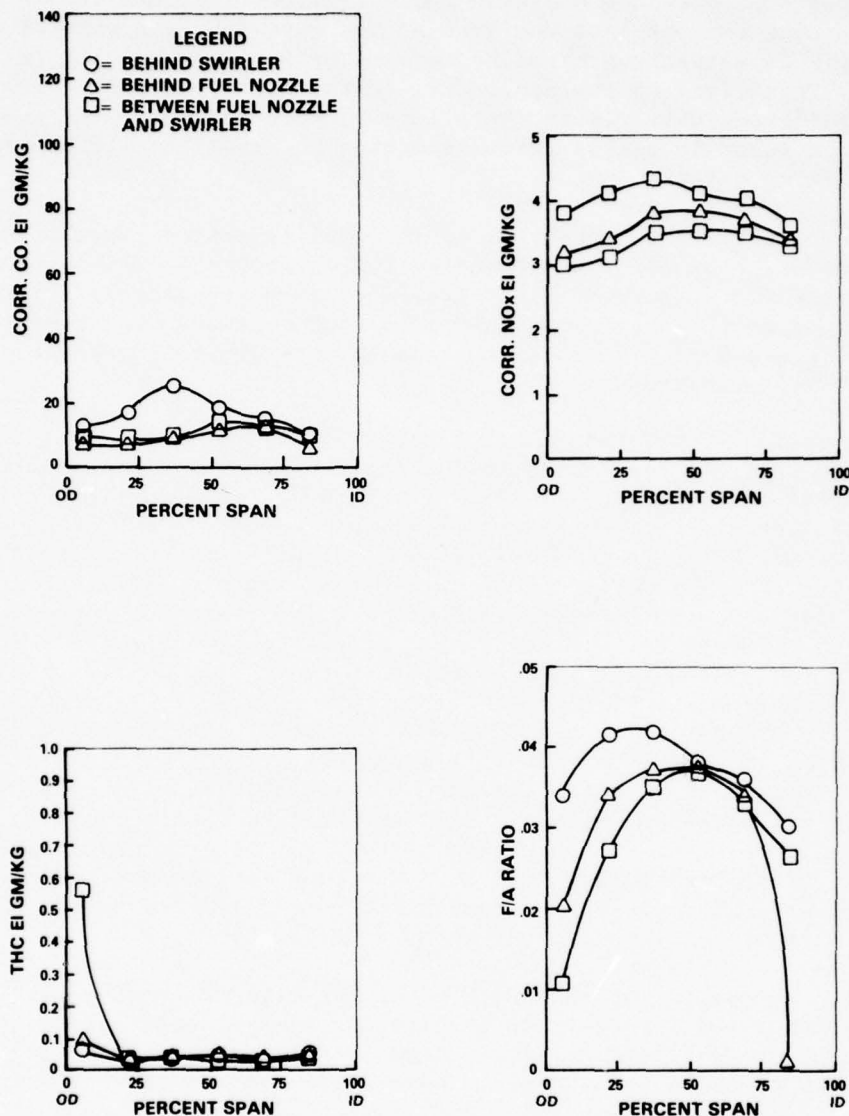


Figure 7-5 VCE Duct Burner Rig Exit Emissions Profiles at Transonic Climb Conditions

The change from counterrotating to corotating swirler orientations between rig Configurations 3 and 4 was found to have a pronounced effect on fuel dispersion with regard to liner heating, and it might be expected that these fuel dispersion effects could also alter the emissions characteristics. This phenomenon was not investigated because emissions measurements were not obtained prior to the change in swirler tube orientation. With improved liner durability, this aspect should be investigated in future test configurations.

7.4 TOTAL PRESSURE LOSS REDUCTION

As indicated in Section 6.4, the total pressure loss across the duct burner, as measured with Configuration 11, was found to be considerably above the analytical projection and goal level. At supersonic cruise, the total pressure loss was 6.76 percent as opposed to a goal of 4.5 percent. It was also indicated in that section that the mechanism causing this increase was identified as expansion losses associated with the flow of the combustion products around the jets of air entering the burner through the swirler tubes.

Modifications introduced into duct burner Configurations 11 and 12 were directed specifically at reducing the total pressure loss, and the testing of these configurations involved assessing overall performance and emissions to identify any adverse effects of the loss reduction. The approach used was based on the results of flow visualization studies conducted on the duct burner model described in Section 4.4.1. The flow visualization study concentrated on the gas path jet flow interactions in the vicinity of the swirler tubes with the intent of minimizing the blockage effects that produced the expansion losses. The first modification deduced from these studies and incorporated in Configuration 11 involved revising the swirler tubes in the high power stage. As shown in Figure 7-6, the tubes employed in Configurations 1 through 10 were designed with a small centertube passing nonswirling air to fill the center of the jet and prevent vortex breakdown when the jet expanded. However, flow visualization studies indicated that, when this passage was plugged, the air jet was more compact and not expanding as rapidly would produce less blockage of the gas path. In Configuration 11 this centertube was capped and flow from the centertube was restricted to a small vent hole in the cap.

The second modification, evaluated in Configuration 12, involved altering the size and cant angle of the swirler tubes in the high power stage. This revision is shown in Figure 7-7 and involved reducing the inclination of the swirler tubes from 45 to 23 degrees relative to the axis of the burner. This change was expected to reduce the total pressure loss by directing the jets into the larger cross sectional area region of the high power stage where the blockage effect on the combustion gases would be less pronounced. Furthermore, inclining the jets further toward the axial direction would direct more of the momentum of the jets into the net momentum of the gas path flow. It was also recognized that blockage produced by the swirler tubes protruding into the gas path was significant. As indicated in Section 3.5, these tubes were oversized to ensure adequate flow capacity and flow rate controlled by the use of conical restrictors on the tube exit. With the flow capacity of these tubes subsequently established by tests on the apparatus in Section 4.4.2 and the airflow requirements of the burner more precisely identified, it was found possible to reduce the diameter of these tubes from 5.08 cm (2.0 in) to 3.94 cm (1.55 in), while providing the required airflow.

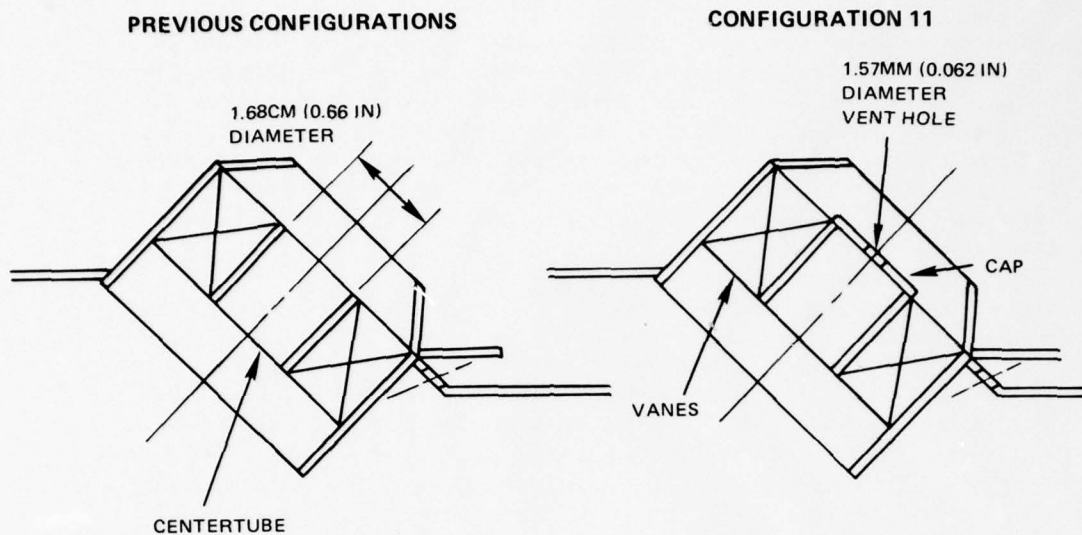


Figure 7-6 Capped Swirler Centertube Employed in Duct Burner Rig Configuration 11

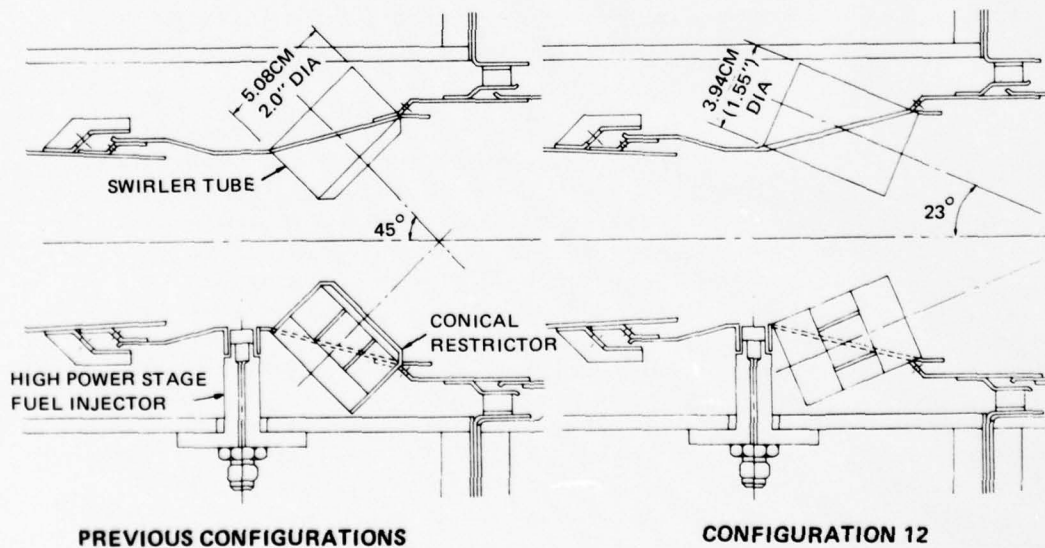


Figure 7-7 Reduced Diameter and Cant Angle Swirler Tubes Employed in Duct Burner Rig Configuration 12

Figure 7-8 shows the test results of Configuration 11, in which these modifications were incorporated. The pressure loss characteristics of Configuration 10 provided a reference. The data indicate that, contrary to expectations, the total pressure loss across Configuration 11 with the capped centertubes in the high power stage was slightly higher than that of the reference Configuration 10. This deviation is apparently due to incomplete compensation for changes in the net airflow area of the duct burner when the swirler tubes were modified and other revisions incorporated into the hardware. Nonetheless, it must be concluded that the capping of the swirler centertubes by itself is inadequate in reducing the total pressure loss. It will be shown in Section 7.5 that this revision, however, produced a significant and favorable effect on carbon monoxide emissions and hence the combustion efficiency.

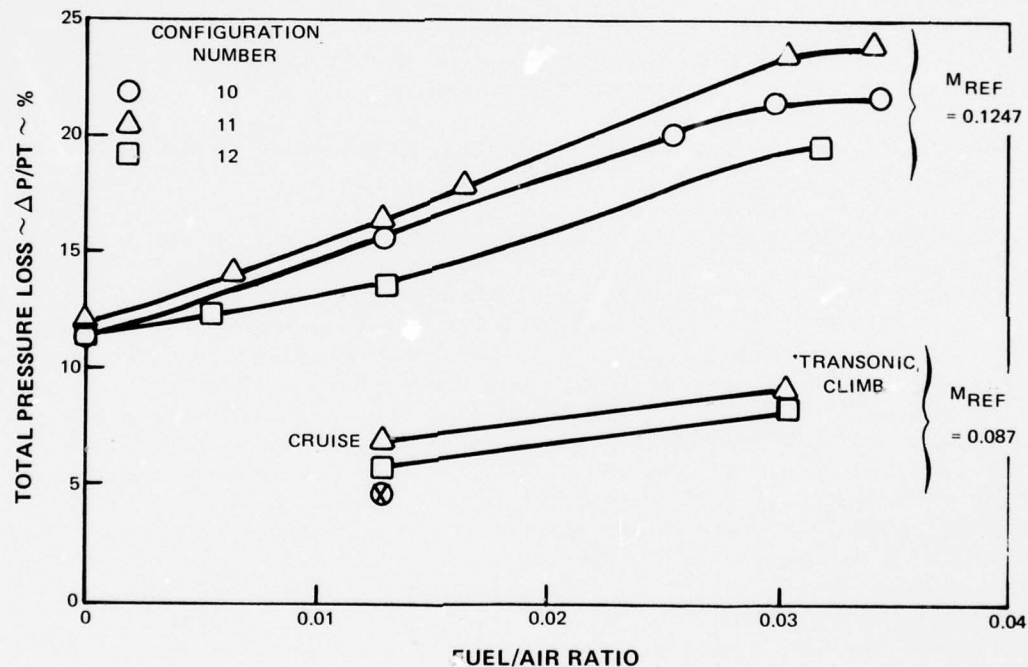


Figure 7-8 Effect of Modifications on the Total Pressure Loss Across the Duct Burner

The data in Figure 7-8 show that reducing the diameter and cant angle of the swirler tubes in Configuration 12 produced a significant reduction in the total pressure loss. Relative to Configuration 11, the total pressure loss at supersonic cruise was reduced from 6.76 percent to 5.86 percent; about forty percent of the excess pressure loss above the goal was eliminated. Recognizing that the same blockage and expansion phenomena occur, but to a lesser degree in the pilot secondary stage, incorporating this type of revision in the components of that stage would have produced an additional reduction in the total pressure loss. It was

analytically estimated that the resultant total pressure loss at supersonic cruise would be in the range of 5.25 to 5.50 percent if these revisions were made.

In the evaluation of Configuration 12, louvers 8 and 9 in the high power stage were found to operate hotter than in previous configurations, and the maximum attainable fuel/air ratio of 0.035 achieved at the takeoff condition with other configurations could not be duplicated because liner temperature limits would be exceeded. Overtemperaturing the liner could be attributed to two causes. First, the reduction in total pressure loss also reduced the pressure drop across the liner of the high power stage and reduced the cooling air flow to these louvers by as much as 23 percent. Secondly, reorientation of the swirler tubes brought the swirling combustion air jets closer to the liner and increased the turbulent activity near the wall. This could have caused a more rapid deterioration of the cooling film on this louver. In either case, some additional redistribution of cooling air will be required as the system pressure loss is reduced toward the goal level.

7.5 EFFECT OF TOTAL PRESSURE LOSS ON EMISSIONS AND OTHER PERFORMANCE PARAMETERS

In conventional main burners, the total pressure loss across the combustion system consists primarily of the liner pressure drop. Since liner drop dictates the available momentum of combustion or dilution air jets and is the dominant source of turbulence for internal mixing, there is concern that in reducing the total pressure loss across the duct burner the favorable emissions and performance characteristics obtained to date might be adversely affected. This need not be the case because, in the duct burner, a significant part of the losses are due to heat addition at high velocity levels or are parasitic in nature and may not contribute the turbulence level and hence the mixing in the combustor. With the exception of the reduction in pressure drop across the high power stage liner in Configuration 12, the revisions discussed in Section 7.4 did not produce any significant shifts in burner airflow distribution or the pressure drops across critical airflow metering components. Table 7-II presents a summary of the emissions and performance characteristics of Configurations 10, 11 and 12 and indicates that the only significant effect of the modifications was an improvement in the combustion efficiency, through a substantial reduction in the carbon monoxide and unburned hydrocarbon emissions when the swirler center tubes were plugged in Configuration 11. Modifications to the size and inclination of the high power stage swirler tubes that produced a forty percent reduction in the excess total pressure loss at supersonic cruise in Configuration 12 are shown to lead to small, and in most cases, negligible changes in the emissions and thrust efficiency of the burner. It is concluded that the expansion losses that caused the excess system total pressure loss are parasitic in nature and contribute little to the mixing mechanisms in the duct burner. Consequently, in future efforts these losses may be minimized further without any severe adverse effect on the emissions and other performance characteristics.

TABLE 7-II

EFFECT OF DUCT BURNER MODIFICATIONS ON EMISSIONS CHARACTERISTICS

	Configuration Number		
	<u>10</u>	<u>11</u>	<u>12</u>
<u>High Power Stage Swirler Tube:</u>			
Diameter - cm (in)	5.08 (2.0)	5.08 (2.0)	3.94 (1.55)
Cant Angle (deg.)	45	45	23
Centertube	Open	Plugged	Partial Plugged
<u>Operating Conditions:</u>			
Supersonic Cruise:			
Fuel/Air Ratio	-	0.013	0.013
Total Pressure Loss (%)	-	6.76	5.86
Emissions Indices (gm/kg)			
CO	-	2.1	2.4
THC	-	0.12	0.26
NO _x	-	8.1	6.8
Combustion Efficiency (%)	-	99.9	99.9
Thrust Efficiency (%)*	-	97.1	97.4
Transonic Climb:			
Fuel/Air Ratio	0.024	0.030	0.030
Total Pressure Loss (%)	7.89	9.02	8.25
Emissions Indices (gm/kg)			
CO	7.2	9.5	10.0
THC	0.07	0.04	0.04
NO _x	3.1	3.8	3.6
Combustion Efficiency (%)	99.8	99.8	99.8
Thrust Efficiency (%) *	-	94.1	93.6
Takeoff:			
Fuel/Air Ratio	0.0328	0.344	0.0319
Total Pressure Loss (%)	21.42	23.83	19.51
Emissions Indices (gm/kg)			
CO	28.0	11.9	12.9
THC	0.86	0.009	0.105
NO _x	2.4	2.7	3.0
Combustion Efficiency (%)	99.3	99.7	99.7
Thrust Efficiency (%)*	92.6	92.6	-

NOTES: Rig emissions measurements corrected to VSCE-502B study engine pressures and standard humidity.

* Thrust efficiency computed on basis of exhaust nozzle cooling flows consistent with the VSCE-502B study engine.

SECTION 8.0

SUMMARY OF EXPERIMENTAL RESULTS

The objectives of this program were to determine the performance of a three-stage duct burner operating on the Vorbix combustor principle and to refine this duct burner configuration to provide acceptable performance and durability for use in the VCE Testbed Program. Based on the results of this effort these objectives have been achieved.

The results demonstrated that emissions of carbon monoxide and unburned hydrocarbons from the duct burner were substantially below the program goals and analytical projections. Combustion efficiencies in excess of 99.7 percent at all three critical operation conditions -supersonic cruise, transonic climb and takeoff were obtained. Emissions of oxides of nitrogen were moderate, but in excess of the program goals and analytical projections. However, analysis indicates that because overall NO_x emissions are dominated by the main burner, duct burner NO_x emissions of the level observed would not compromise the ability of the engine to comply with the proposed Environmental Protection Agency (EPA) emissions standards for Class T-5 engines in the airport vicinity.

Analytical projections based on observed burner exit total temperature and pressure profiles indicate that duct burner thrust efficiency at supersonic cruise is in excess of 97 percent, as opposed to a goal of 94.5 percent. Similar analysis of data obtained at the transonic climb and takeoff conditions indicate thrust efficiencies 4 to 6 percent higher than initial analytical projections.

The total pressure loss across the duct burner exceeded the program goal with the measured loss at supersonic cruise being 6.76 percent compared to a goal of 4.5 percent. However, the mechanism causing this elevated pressure loss was identified, and in one of the configurations evaluated, 40 percent of the excess total pressure loss was eliminated without significantly compromising emissions and thrust efficiency characteristics. On this basis, the mechanism causing the excess pressure loss appears parasitic in nature and a further reduction without compromising other performance or emissions aspects should be achievable.

The soft ignition capability of the duct burner was also demonstrated. Ignition was achieved at fuel/air ratios as low as 0.002 with resulting static pressure pulses of less than two percent of the burner inlet total pressure. The absence of any combustion-related acoustic instabilities was also demonstrated over the entire duct burner operating range.

SECTION 9.0

CONCLUDING REMARKS

In the course of evolving the duct burner toward achieving the performance and emissions goals, areas were identified where additional exploratory effort and development beyond the scope of the current program is warranted. The heat load on the duct burner liners, particularly in the upstream end of the pilot secondary and high power stage, were found to be high and sensitive to swirler tube and fuel injector configuration as a result of interactions between the fuel spray and the combustion air jets. While acceptable metal temperature levels were achieved in these tests through judicious modifications to the liner cooling system and the use of fuel injector configurations with improved spray characteristics, further efforts are required in this area to ensure adequate liner durability over the entire operating range. Fuel spray/swirler jet interactions were found to have a pronounced effect on emissions and burner exit temperature uniformity and the potential for additional improvement of these aspects provide further incentive for optimizing the configuration of these components.

To produce a viable duct burner for commercial application, the technology evolved during this program must be extended to reduce the complexity and improve long term durability. On the basis of this test experience, a two-stage system could be an alternative approach and substantiation of this type of configuration through additional rig testing should be a main consideration for future effort. Successful completion of such an effort would produce a duct burner with considerably fewer fuel injectors and swirler tubes and a simpler fuel control system.

The duct burner has demonstrated adequate durability for experimental programs, but the louver-type liner construction may not be compatible with the long term durability requirements of commercial aircraft applications. This situation is particularly significant in the pilot stages which are operational at the maximum inlet temperatures and local fuel/air ratios over the entire supersonic cruise portion of the mission. Alternative cooling concepts and advanced materials should be pursued in future programs.

APPENDIX A

DUCT BURNER CONFIGURATIONS

The VCE Duct Burner Segment Rig Program involved the experimental evaluation of twelve configurations. The basic design features of the duct burner are discussed in Section 3 and 4, and were incorporated in Configuration 1. The detailed description of the geometrical features affecting airflow distribution and various modifications implemented to improve duct burner performance are outlined for each configuration in this Appendix.

Configurational details are illustrated in the form of scheme charts, which include tabulating cooling and combustion airflow areas, on Figure A-1 to A-8. Endwall cooling is distinguished from liner louver cooling with the latter parameters listed to the upper left, and the former to the lower right sections of the tables.

Two orientations of the pilot secondary and high power swirlers were utilized: counterrotational and corotational. These orientations are shown schematically in Figure 7-2. Similarly, two types of high power stage fuel injectors were utilized: hollow-cone, conical spray injectors in the early configurations, and flat spray fuel injectors in the latter configurations.

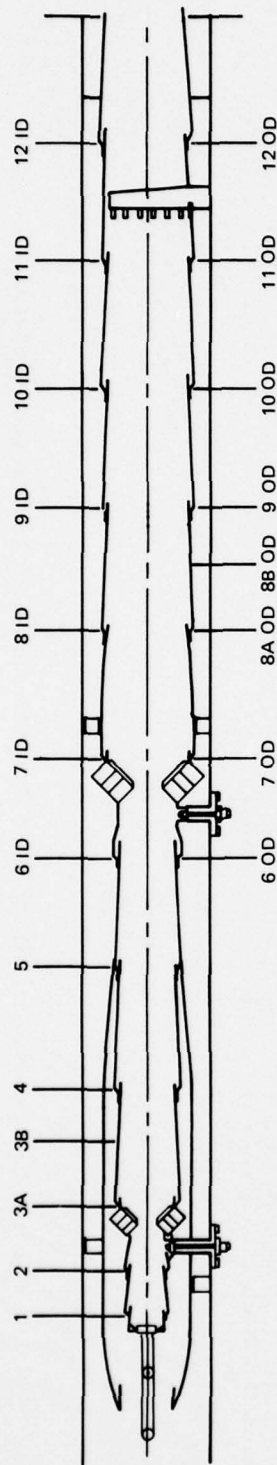
Configuration 1

The scheme chart illustrating the air distribution details of Configuration 1 is shown in Figure A-1. This configuration incorporated the basic design features of the VCE duct burner described in Sections 3 and 4.

The experimental evaluation of this configuration showed higher than anticipated system pressure losses and an improper airflow distribution. Testing was terminated prematurely due to a rupture of the front hood segment-to-rear hood attachment while operating at above design rig inlet Mach numbers.

Configuration 2

A more positive hood-to-burner liner attachment scheme was incorporated into Configuration 2 to prevent recurrence of hood distortion resulting from the substantial pressure differentials acting on the hood surfaces. In addition, an effort to reduce system pressure losses and to direct increased airflow to the high power stage was made by substantially increasing the high power swirler effective flow area. These modifications reduced system pressure loss, but losses remained well above design goals. Excessive pressure losses in the shrouds were also noted. Testing was terminated because of a burnout in the screech suppression section of the high power stage liner.



COUNTER - ROTATIONAL SWIRLERS

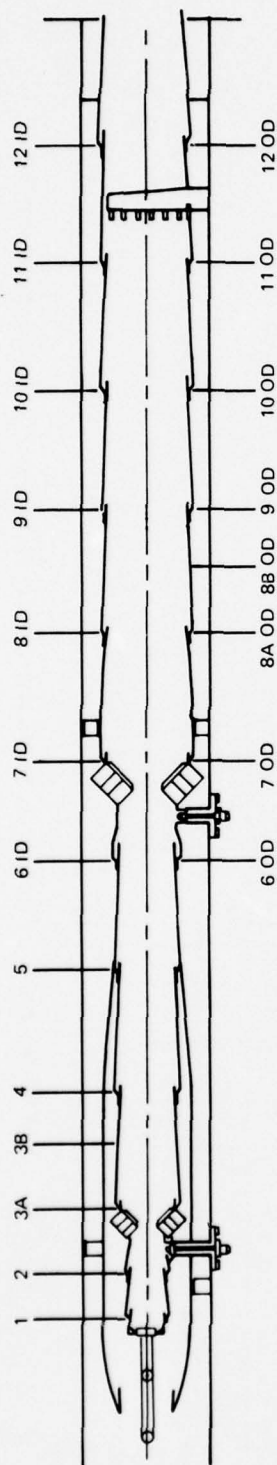
PRECHAMBER NOZZLE SWIRLER	0.645 AC _D (CM ²)
NOZZLE LEAKAGE	0.089
BULKHEAD COOLING	1.350
PRECHAMBER DILUTION	2.760
PILOT SEC. SWIRLER - I.D.	5.790
PILOT SEC. SWIRLER - O.D.	5.790
HIGH POWER SWIRLER - I.D.	9.650
HIGH POWER SWIRLER - O.D.	9.650
REAR CAVITY PURGE - I.D.	1.329
REAR CAVITY PURGE - O.D.	1.329

CONICAL SPRAY PILOT SECONDARY AND HIGH POWER FUEL

LOUVER	DIA. CM	#OF HOLES	AREA (AC _D)/CM ²	LOUVER	DIA. CM	#OF HOLES	AREA (AC _D)/CM ²
1	.312	96	6.748	11 I.D.	.462	31	5.335
2	.432	62	10.445	12 I.D.	.345	42	4.316
3A	.292	92	11.232	6 O.D.	.305	47	11.503
3B	—	—	—	7 O.D.	.356	40	14.651
4	.199	144	4.464	8A O.D.	.401	36	4.825
5	.218	128	4.768	8B O.D.	—	—	—
6 I.D.	.305	47	10.219	9 O.D.	.401	36	4.723
7 I.D.	.356	40	15.155	10 O.D.	.419	35	4.942
8 I.D.	.401	36	4.677	11 O.D.	.462	31	12.496
9 I.D.	.401	36	4.723	12 O.D.	.345	42	4.316
10 I.D.	.419	35	4.942				

LOUVERS 1 THROUGH 5 HAVE SAME HOLES ON O.D. AND I.D.

Figure A-1 Liner Hole Pattern for Duct Burner Configuration 1



COUNTER - ROTATIONAL SWIRLERS

PRECHAMBER NOZZLE SWIRLER	9 AT 0.645 AC _D (CM ²)
NOZZLE LEAKAGE	9 AT 0.089
BULKHEAD COOLING	20 AT 1.350
PRECHAMBER DILUTION	18 AT 2.760
PILOT SEC. SWIRLER - I.D.	10 AT 5.790
PILOT SEC. SWIRLER - O.D.	10 AT 5.790
HIGH POWER SWIRLER - I.D.	6 AT 12.90
HIGH POWER SWIRLER - O.D.	6 AT 12.90
REAR CAVITY PURGE - I.D.	20 AT 1.329
REAR CAVITY PURGE - O.D.	20 AT 1.329

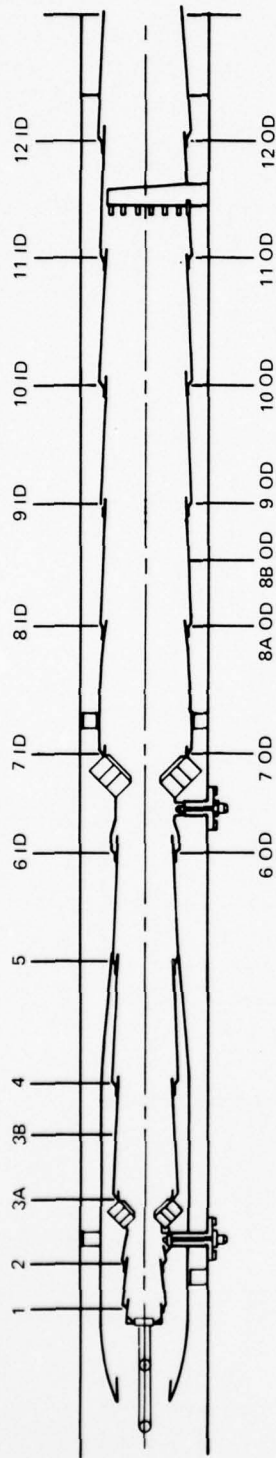
MODIFICATIONS: REFERENCE CONFIGURATION 1

- INCREASED HIGH POWER SWIRLER FLOW

LOUVER	DIA. CM	#OF HOLES	AREA (AC _D)CM ²	LOUVER	DIA. CM	#OF HOLES	AREA (AC _D)CM ²
1	.312	96	6.748	11 I.D.	.462	31	5.335
2	.432	62	10.445	12 I.D.	.345	42	4.316
3A	.292	92	11.232	6 O.D.	.305	47	11.503
3B	—	—	—	7 O.D.	.356	40	14.651
4	.199	144	4.464	8A O.D.	.401	36	4.825
5	.218	128	4.768	8B O.D.	—	—	—
6 I.D.	.305	47	10.219	9 O.D.	.401	36	4.723
7 I.D.	.356	40	15.155	10 O.D.	.419	35	4.942
8 I.D.	.401	36	4.677	11 O.D.	.462	31	12.496
9 I.D.	.401	36	4.723	12 O.D.	.345	42	4.316
10 I.D.	.419	35	4.942				

LOUVERS 1 THROUGH 5 HAVE SAME HOLES ON O.D. AND I.D.

Figure A-2 Liner Hole Pattern for Duct Burner Configuration 2



COUNTER - ROTATIONAL SWIRLERS

PRECHAMBER NOZZLE SWIRLER	9 AT 0.645 AC _D (CM ²)
NOZZLE LEAKAGE	9 AT 0.089
BULKHEAD COOLING	20 AT 1.350
PRECHAMBER DILUTION	18 AT 2.760
PILOT SEC. SWIRLER - I.D.	10 AT 5.790
PILOT SEC. SWIRLER - O.D.	10 AT 5.790
HIGH POWER SWIRLER - I.D.	6 AT 8.40
HIGH POWER SWIRLER - O.D.	6 AT 8.40
REAR CAVITY PURGE - I.D.	20 AT 1.329
REAR CAVITY PURGE - O.D.	20 AT 1.329

CONICAL SPRAY PILOT SECONDARY AND HIGH POWER FUEL NOZZLES

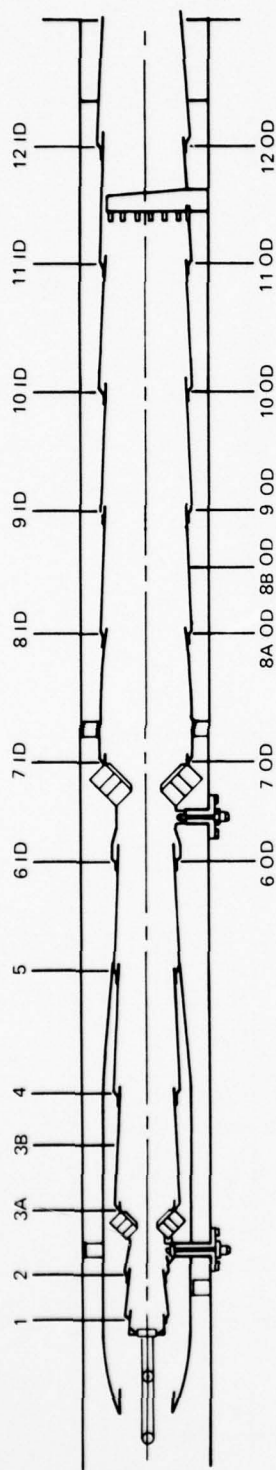
MODIFICATIONS: REFERENCE CONFIGURATION 2

- REPLACED SCREECH LINERS
- DECREASED HIGH POWER SWIRLER FLOW AREA
- OPENED HIGH POWER OD METER PLATE

LOUVER	DIA. CM	#OF HOLES	AREA (AC _D)CM ²	LOUVER	DIA. CM	#OF HOLES	AREA (AC _D)CM ²
1	.312	96	6.748	11 I.D.	.462	584	5.335
2	.432	62	10.445	12 I.D.	.345	584	4.316
3A	.292	92	11.232	6 O.D.	.305	394	11.503
3B	—	—	—	7 O.D.	.409	465	15.542
4	.199	144	4.464	8 A O.D.	.401	546	4.677
5	.218	128	4.768	88 O.D.	—	—	—
6 I.D.	.305	47	10.219	9 O.D.	.401	558	4.723
7 I.D.	.356	40	15.155	10 O.D.	.419	559	4.942
8 I.D.	.401	36	4.677	11 O.D.	.462	584	12.496
9 I.D.	.401	36	4.723	12 O.D.	.345	584	4.316
10 I.D.	.419	35	4.942				

LOUVERS 1 THROUGH 5 HAVE SAME HOLES ON O.D. AND I.D.

Figure A-3 Liner Hole Pattern for Duct Burner Configuration 3



CO-ROTATIONAL SWIRLERS

PRECHAMBER NOZZLE SWIRLER	9 AT 0.645 AC _D (CM ²)
NOZZLE LEAKAGE	9 AT 0.089
BULKHEAD COOLING	20 AT 1.350
PRECHAMBER DILUTION	18 AT 2.760
PILOT SEC. SWIRLER - I.D.	10 AT 5.790
PILOT SEC. SWIRLER - O.D.	10 AT 5.790
HIGH POWER SWIRLER - I.D.	6 AT 6.450
HIGH POWER SWIRLER - O.D.	6 AT 6.450
REAR CAVITY PURGE - I.D.	20 AT 1.329
REAR CAVITY PURGE - O.D.	20 AT 1.329

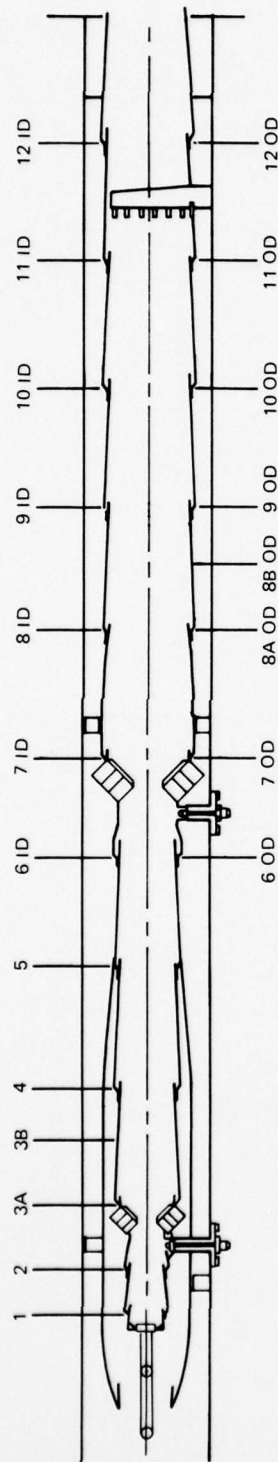
MODIFICATIONS: REFERENCE CONFIGURATION 3

- CHANGED FROM COUNTER - TO CO-ROTATIONAL SWIRLERS
- DECREASED HIGH POWER SWIRLER FLOW AREA
- OPENED HIGH POWER OD METER PLATE
- ELIMINATED JOINT LEAKAGE IN LOUVER 3
- REMOVED HIGH POWER O.D. METER PLATE (CONF 5)

LOUVER	DIA. CM	#OF HOLES	AREA (AC _D)/CM ²	LOUVER	DIA. CM	#OF HOLES	AREA (AC _D)/CM ²
1	.312	96	6.748	11 I.D.	.462	31	5.335
2	.432	62	10.445	12 I.D.	.345	42	4.316
3A	.292	92	6.006	6 O.D.	.305	47	11.503
3B	—	—	—	7 O.D.	.409	40	15.542
4	.199	144	4.464	8A O.D.	.401	36	4.677
5	.218	128	4.768	8B O.D.	—	—	—
6 I.D.	.305	47	10.219	9 O.D.	.401	36	4.723
7 I.D.	.356	40	15.155	10 O.D.	.419	35	4.942
8 I.D.	.401	36	4.677	11 O.D.	.462	31	12.496
9 I.D.	.401	36	4.723	12 O.D.	.345	42	4.316
10 I.D.	.419	35	4.942				

LOUVERS 1 THROUGH 5 HAVE SAME HOLES ON O.D. AND I.D.

Figure A-4 Liner Hole Pattern for Duct Burner Configurations 4 and 5



CO-ROTATIONAL SWIRLERS

PRECHAMBER NOZZLE SWIRLER	9 AT 0.645 AC _D (CM ²)
NOZZLE LEAKAGE	9 AT 0.089
BULKHEAD COOLING	20 AT 1.350
PRECHAMBER DILUTION	18 AT 2.760
PILOT SEC. SWIRLER - I.D.	10 AT 5.810
PILOT SEC. SWIRLER - O.D.	10 AT 5.810
HIGH POWER SWIRLER - I.D.	6 AT 7.145
HIGH POWER SWIRLER - O.D.	6 AT 8.210
REAR CAVITY PURGE - I.D.	20 AT 1.329
REAR CAVITY PURGE - O.D.	20 AT 1.329

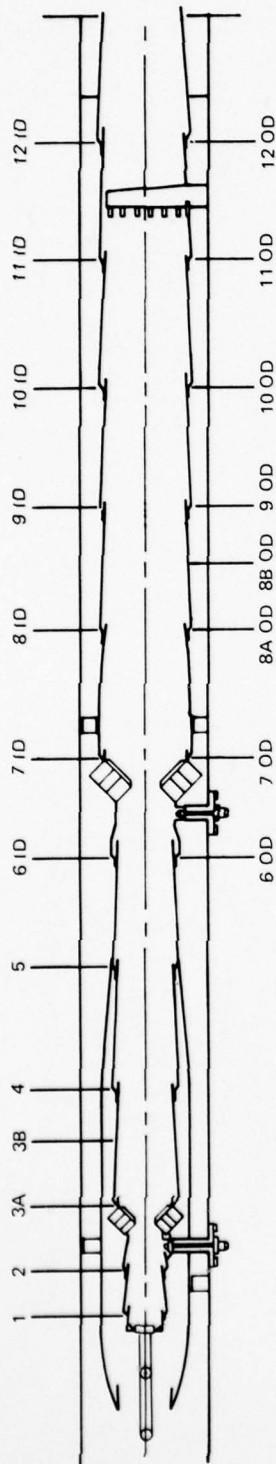
MODIFICATIONS: REFERENCE CONFIGURATION 4

- INCREASED LVR 3 COOLING
- INCREASED HIGH POWER SWIRLER FLOW AREA
- SEALED JOINT AT LVR6
- DECREASED PILOT SECONDARY SWIRLER FLOW AREA
- INSTALLED METER PLATE ON LVR 9
- INSTALLED HIGH ΔP CONICAL SPRAY HIGH POWER FUEL NOZZLES, (CONF. 7)
- INSTALLED FLAT SPRAY HIGH POWER FUEL NOZZLES (CONF 8)

LOUVER	DIA. CM	#OF HOLES	AREA (AC _D)/CM ²	LOUVER	DIA. CM	#OF HOLES	AREA (AC _D)/CM ²
1	.312	96	6.748	11 I.D.	.462	31	5.335
2	.432	62	10.445	12 I.D.	.345	42	4.316
3A	.345	92	8.387	6 O.D.	.485	47	9.671
3B	—	—	—	7 O.D.	.409	40	15.542
4	.199	264	4.464	8A O.D.	.401	36	4.677
5	.218	287	4.768	8B O.D.	—	—	—
6 I.D.	.452	47	7.439	9 O.D.	.401	36	4.723
7 I.D.	.356	40	15.155	10 O.D.	.419	35	4.942
8 I.D.	.401	36	4.677	11 O.D.	.462	31	12.496
9 I.D.	.401	36	4.723	12 O.D.	.345	42	4.316
10 I.D.	.419	35	4.942				

LOUVERS 1 THROUGH 5 HAVE SAME HOLES ON O.D. AND I.D.

Figure A-5 Liner Hole Pattern for Duct Burner Configurations 6, 7 and 8



CO-ROTATIONAL SWIRLERS

PRECHAMBER NOZZLE SWIRLER	9 AT 0.645 AC_D (CM ²)
NOZZLE LEAKAGE	9 AT 0.089
BULKHEAD COOLING	20 AT 1.350
PRECHAMBER DILUTION	18 AT 3.225
PILOT SEC. SWIRLER - I.D.	10 AT 5.810
PILOT SEC. SWIRLER - O.D.	10 AT 5.810
HIGH POWER SWIRLER - I.D.	6 AT 7.145
HIGH POWER SWIRLER - O.D.	6 AT 8.210
REAR CAVITY PURGE - I.D.	20 AT 1.329
REAR CAVITY PURGE - O.D.	20 AT 1.329

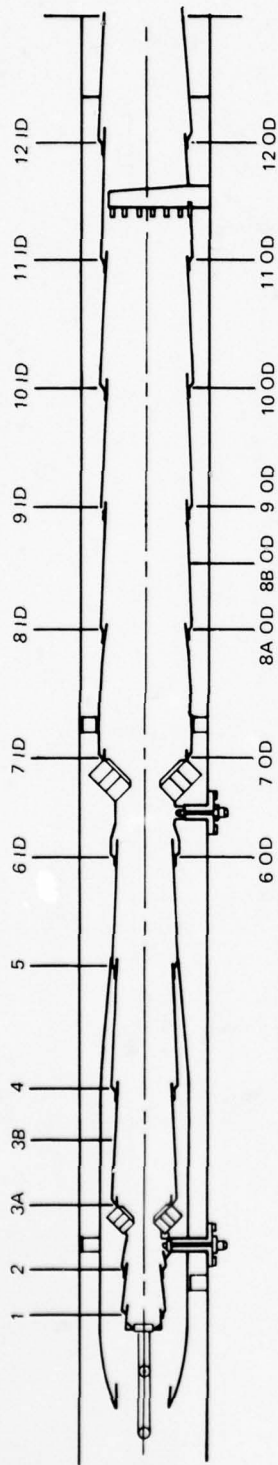
MODIFICATIONS: REFERENCE CONFIGURATION 8

- INSTALLED DOUBLE LOUVERS IN LVR'S 3 AND 8
- INCREASED PRECHAMBER DILUTION HOLE AREA
- INSTALLED HIGH ΔP FLAT SPRAY HIGH POWER FUEL NOZZLES (CONF 10)

LOUVER	DIA. CM	#OF HOLES	AREA (AC_D)CM ²	LOUVER	DIA. CM	#OF HOLES	AREA (AC_D)CM ²
1	.312	96	6.748	11 I.D.	.462	31	5.335
2	.432	62	10.445	12 I.D.	.485	42	4.316
3A	.345	61	5.586	6 O.D.	.409	47	9.671
3B	.282	92	4.761	7 O.D.	.295	40	15.542
4	.199	144	4.464	8A O.D.	.401	48	3.362
5	.218	128	4.768	8B O.D.	.295	48	2.652
6 I.D.	.452	47	7.439	9 O.D.	.401	36	4.723
7 I.D.	.356	40	15.155	10 O.D.	.419	35	4.942
8 I.D.	.401	36	4.677	11 O.D.	.462	31	12.496
9 I.D.	.401	36	4.723	12 O.D.	.345	42	4.316
10 I.D.	.419	35	4.942				

LOUVERS 1 THROUGH 5 HAVE SAME HOLES ON O.D. AND I.D.

Figure A-6 Liner Hole Pattern for Duct Burner Configurations 9 and 10



CO-ROTATIONAL SWIRLERS

PRECHAMBER NOZZLE SWIRLER	9 AT 0.645 AC _D (CM ²)
NOZZLE LEAKAGE	9 AT 0.089
BULKHEAD COOLING	20 AT 1.350
PRECHAMBER DILUTION	18 AT 2.760
PILOT SEC. SWIRLER - I.D.	10 AT 4.200
PILOT SEC. SWIRLER - O.D.	10 AT 4.200
HIGH POWER SWIRLER - I.D.	6 AT 7.400
HIGH POWER SWIRLER - O.D.	6 AT 11.010
REAR CAVITY PURGE - I.D.	20 AT 1.329
REAR CAVITY PURGE - O.D.	20 AT 1.329

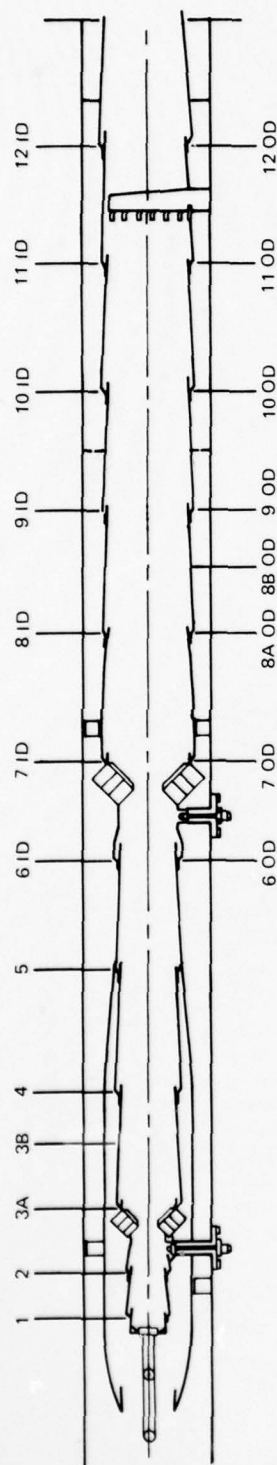
MODIFICATIONS: REFERENCE CONFIGURATION 10

- REDUCED PRECHAMBER DILUTION
- INCREASED LVR'S 3A, 3B, 4, 5, 9 OD AND 10 OD COOLING
- SEALED JOINT IN LVR 7
- DECREASED PILOT SECONDARY SWIRLER FLOW
- PLUGGED SWIRLER CENTER HOLES IN PILOT SECONDARY AND HIGH POWER STAGES
- INCREASED OD/ID HIGH POWER SWIRLER FLOW SPLIT

LOUVER	DIA. CM	#OF HOLES	AREA (AC _D /CM ²)	LOUVER	DIA. CM	#OF HOLES	AREA (AC _D /CM ²)
1	.312	96	6.748	11 I.D.	.462	31	5.335
2	.432	62	10.445	12 I.D.	.345	42	4.316
3A	.404	92	10.671	6 O.D.	.485	47	9.671
3B	.399	61	6.323	7 O.D.	.508	40	7.484
4	.290	142	8.606	8A O.D.	.295	48	3.362
5	.274	128	7.070	88 O.D.	.295	48	2.652
6 I.D.	.452	47	7.439	9 O.D.	.508	36	6.942
7 I.D.	.356	40	15.155	10 O.D.	.526	35	7.187
8 I.D.	.401	36	4.677	11 O.D.	.462	31	12.496
9 I.D.	.401	36	4.723	12 O.D.	.345	42	4.316
10 I.D.	.419	35	4.942				

LOUVERS 1 THROUGH 5 HAVE SAME HOLES ON O.D. AND I.D.

Figure A-7 Lirer Hole Pattern for Duct Burner Configuration 11



CO-ROTATIONAL SWIRLERS

PRECHAMBER NOZZLE SWIRLER	9 AT 0.645 AC _D (CM ²)
NOZZLE LEAKAGE	9 AT 0.089
BULKHEAD COOLING	20 AT 1.350
PRECHAMBER DILUTION	18 AT 2.760
PILOT SEC. SWIRLER - I.D.	10 AT 4.200
PILOT SEC. SWIRLER - O.D.	10 AT 4.200
HIGH POWER SWIRLER - I.D.	6 AT 9.690
HIGH POWER SWIRLER - O.D.	6 AT 9.690
REAR CAVITY PURGE - I.D.	20 AT 1.329
REAR CAVITY PURGE - O.D.	20 AT 1.329

CONICAL SPRAY P/S AND H/P FUEL NOZZLES

MODIFICATIONS: REFERENCE CONFIGURATION 11

- CANTED HIGH POWER SWIRLERS FROM 45° TO 23°; REDUCED SWIRLER DIAMETER
- DECREASED OD/ID HIGH POWER SWIRLER FLOW SPLIT

LOUVERS 1 THROUGH 5 HAVE SAME HOLES ON O.D. AND I.D.

Figure A-8 Liner Hole Pattern for Duct Burner Configuration 12

AD-A078 057

PRATT AND WHITNEY AIRCRAFT GROUP EAST HARTFORD CONN
EXPERIMENTAL EVALUATION OF A LOW EMISSIONS HIGH PERFORMANCE
JAN 79 R P LOHMANN , R J MADOR
PWA-5513-32

F/G 21/5
DUC--ETC(U)

NAS3-20602

NASA-CR-159694

NL

UNCLASSIFIED

2 OF 2
AD-
A078057



Configuration 3

Sidewall dams were installed to limit flow communication between the inner and outer shrouds, a phenomenon responsible, in part, for the excessive total pressure losses, particularly in the shroud diffuser passages. Additional instrumentation was installed to more precisely study shroud losses as well as to permit an expanded definition of pressure and temperature distributions in the high power stage. The metering plate located in the shrouds just downstream of the high power swirlers to control shroud airflow pressure under the liner in the high power stage was opened in the outer shroud to increase cooling flow to the downstream louvers. The screech suppression liners were entirely replaced with conventional louvers.

Experimental testing of Configuration 3 indicated some reduction in shroud pressure losses and improved flow split. Visual observation as well as temperature instrumentation, however, showed that high power combustion was limited to the region near the outer wall, a result of inadequate high power fuel penetration and the interaction of counter-rotating swirler flows. Testing was terminated at a fuel/air ratio of 0.024 due to elevated high power stage outer liner temperatures.

Configuration 4

To further reduce shroud pressure losses, the hood contour was modified to lengthen and smooth the shroud diffusers. Cooling air leakage at the prechamber-to-pilot secondary flange was eliminated by welding, and consequently, sealing this joint. The pilot secondary and high power swirlers were all reoriented to the corotational scheme shown in Figure 7-2. High power stage swirler flow was decreased and the meter plate at louver 7 in the outer shroud was opened to increase the supply pressure for cooling the hot high power stage liners.

The experimental evaluation of Configuration 4 resulted in the achievement of acceptable shroud pressure losses and airflow split. While operation to an increased fuel/air ratio was achieved, excessive high power stage outer liner temperature continued to restrict operation to well below the takeoff fuel/air ratio.

Configuration 5

The metering plate at louver 7 in the outer shroud was entirely removed and a short test series conducted to assess the effect of maximizing the supply pressure for cooling the high power louvers. This modification has an essentially inconsequential effect on liner temperature.

Configuration 6

In Configuration 6, minor modifications, including the installation of a second metering plate in the high power stage shrouds at louver 10, were made to the airflow distribution primarily to increase cooling flow to louvers 3, 8 and 9 because these louvers consistently exhibited elevated temperatures. A seal was installed at the pilot secondary to high power inlet section slip joint to minimize flow leakage.

In the experimental evaluation of Configuration 6, excessive Louver 8 wall temperatures persisted and a severe high power fuel penetration and dispersion problem was reconfirmed. Emissions measurements were made and indicated carbon monoxide and unburned hydrocarbon emissions were in excess of goals at the highest achievable fuel/air ratios.

Configuration 7

In an effort to address the poor high power stage fuel penetration, smaller flow capacity, hollow cone, conical spray fuel nozzles were installed. Fuel injector visualization studies (Appendix D) showed that improved penetration could be achieved by increasing injected fuel momentum i.e. fuel injector pressure drop. Some reduction in the temperature of outer louver 8 was realized permitting operation at higher fuel/air ratios. This was temperature reduction and a reduction in the emissions relative to Configuration 6 emphasized the need to further improve fuel penetration.

Configuration 8

The fuel injector visualization studies identified a major improvement in penetration with flat spray fuel injectors. Consequently, this type of injector was installed in the high power stages in Configuration 8. While improvements in wall temperature were noted, operation at high fuel air ratio was still limited. A substantial reduction in CO and THC emissions was observed at the high fuel/air ratios.

Configuration 9

Throughout the earlier test series, maximum temperatures on louver 8 had limited the attainable fuel/air ratio at takeoff inlet conditions. It was also apparent that transonic climb and supersonic cruise operation condition could not be attained without seriously distressing louver 3 in the pilot secondary stage. Consequently, louvers 3 and 8 in Configuration 8 were replaced with two short louvers with a corresponding increase in cooling to these sections. With these modifications, operation to a fuel/air ratio of 0.0344 was achieved with a significant reduction in the louver temperatures. The temperatures on louvers 9 and 10 on the outer liner then became the limiting factor on overall fuel/ air ratio.

Configuration 10

Improved high power stage fuel penetration was addressed in Configuration 10 by installing smaller flow capacity, flat spray fuel nozzles. Testing at takeoff inlet conditions was easily repeated and operation at transonic climb operation was achieved.

Configuration 11

While the flat spray fuel injectors aided in improving high power stage combustion, temperature levels on several burner liners remained excessive. Consequently, the cooling airflow to louvers 3A, 3B, 4, 5, and the outer wall panels of louvers 9 and 10 was increased. To compensate, swirler airflow was decreased by reducing the conical skirt diameter as well as closing off the swirler center-holes with the latter expected to produce a reduction in pressure loss. In addition, the flow split between the inner and outer high power stage swirlers tubes was biased significantly to the outer to preferentially direct air in the region of highest fuel density.

While the system pressure loss was not decreased, emissions measurements of Configuration 11 were the best observed and were below most of the program goals. Both transonic climb and supersonic cruise operation were achieved and a full compliment of aerodynamic, combustion and emissions performance data were acquired. A complete description of Configuration 11 test results is presented in Section 6.

Configuration 12

In Configuration 12, attention was primarily focused on system pressure loss. The high power swirlers were canted away from the burner centerline to reduce the gas path flow expansion losses. In addition, the inner to outer high power stage swirler airflow split was returned to more realistic levels of Configuration 9 and 10.

The experimental evaluation confirmed that the reduction in pressure loss was accomplished without compromising emissions or other performance parameters but that additional cooling air redistribution would be required to compensate for the pressure loss reduction.

APPENDIX B

EXHAUST GAS ANALYSIS

B.1 Gas Analysis Instrumentation

The Pratt & Whitney Aircraft emission analysis mobile laboratory is a specially designed vehicle capable of measuring gaseous jet engine and rig exhaust constituents. The instrumentation and sample handling system were designed to conform with the specifications in SAE ARP 1256, and conforms to specifications in the Federal Register Vo. 38, No. 136, July 17, 1973. The mobile laboratory is completely self contained, and incorporates the latest on-line gas analysis instruments for the measurement of carbon dioxide, carbon monoxide, oxides of nitrogen, total unburned hydrocarbons, and oxygen. These include:

- o Carbon dioxide, carbon monoxide and nitric oxide measured with Beckman Model 315A Non-Dispersive Infrared (NDIR) instruments.
- o NO_x measured with a TECO chemiluminescence analyzer.
- o Total unburned hydrocarbons measured with a Beckman Model 402 heated input flame ionization detector.
- o Oxygen measured with a Scott paramagnetic O₂ Analyzer.

The combustor rig exhaust gas sample is distributed to the various instruments, with each instrument having its own flow metering system. The sample handling system is shown schematically in Figure B-1. The measurement ranges and accuracy characteristics of the individual instruments are summarized in Table B-I. All instruments have several ranges of sensitivity, making them capable of measurements over wide ranges of fuel/air ratio.

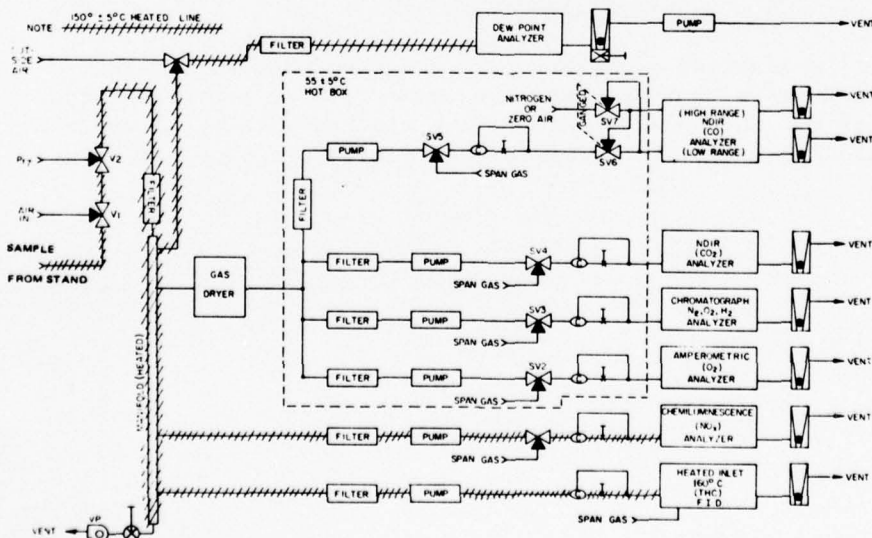


Figure B-1 Mobile Laboratory Gas Analysis System

TABLE B-I

<u>Component</u>	<u>Range</u>	INSTRUMENTATION	
		<u>Instrument and Detection-Method</u>	<u>Instrument Error % Full Scale</u>
THC	0-1 ppmv	Flame Ionization Detector	+5.0
	Intermediate ranges		+1.0
	0-10%	Beckman Model 402	+1.0
NO _x	0-2.5 ppmv	Chemiluminescence	+1
	0-10 ppmv	TECO Model 10A	+1
	0-25 ppmv		+2.5
	0-100 ppmv		+2.5
	0-250 ppmv		+2.5
	0-1000 ppmv		+2.5
CO	0-2500 ppmv		+2.5
	0-100 ppmv	Non Dispersive Infra Red	+2.0
	0-1000ppmv	Beckman Model 315A	+1.0
	0-1%		+1.0
CO ₂	0-7%		+1.0
	0-2%	Non Dispersive	+1.0
	0-5%	Beckman Model 315A	+1.0
O ₂	0-18%		+1.0
	0-1%	Parametric	+1.0
	0-5%	Scott Model 250	+1.0
	0-10%		+1.0
	0-25%		+1.0

Each instrument is provided with "sample" and "calibration" operating modes. The Mobile Laboratory carries its own calibration, zero, and span gases.

The Mobile Laboratory utilizes a heated stainless steel metal bellows sample pump to exact the sample into the sample measurement train. A vacuum type bypass pump is also incorporated into the sampling system to minimize the residence time of the sample in the sample line. The sample is then distributed to the various instruments.

Three systems are available for data logging and processing. The primary data system consists of an on-line Sigma 8 computer, providing essentially real-time data recording and analysis. The gas analyzer outputs are digitized and, on command, are sent via a telephone line to the Sigma 8 computer located in the Engineering building at East Hartford, where emission data reduction is carried out utilizing equations compar-

able to those specified in ARP 1256. After the data have been processed, they are presented visually on a digital scope display in the mobile laboratory or printed, on command, in the computer graphics laboratory. As a backup data system, the analyzer outputs are also digitized and on command recorded on cassette-type magnetic tape. The tape is compatible with an IBM 370 computer, which is available for off-line special data reduction and validation programs. The third system consists of two Texas Instruments four pen records which monitor the output of the instruments and provide a continuous real time record for either immediate inspection or subsequent analysis. This system is especially helpful when troubleshooting problems during the test.

B.2 CALIBRATION GASES

The basic accuracy of exhaust gas concentration measurements depends on the availability of accurately known reference gases. The calibration, zero, and span gases used in this study are the result of a continuing in-house program to develop and maintain accurate standard gases.

ARP 1256 specifies calibration gas certified by the vendor to an accuracy of one percent and span gas to a stated accuracy of +2 percent. It has been Pratt & Whitney Aircraft's experience that gases, while purchased to a certified or stated accuracy, are occasionally significantly different due to errors in blending or inherent instability of the gas in its container. Errors in blending lead to a consistent bias as long as that particular calibration gas is used. Instability normally leads to a reduction in actual concentration levels to an unpredictable new level. To relieve this situation, a set of reference standards are maintained in the Pratt & Whitney Aircraft Standards Laboratory which are carefully, and frequently in the case of unstable gases, analyzed by various appropriate analytical techniques. Where practical, additional analyses are performed by other agencies. These reference materials are maintained as transfer standards.

A summary of calibration gases and methods used for verification analysis is given in Table B-II.

Instruments utilized for the analyses specified in Table B-II are:

1. Gas Chromatographs (g.c.): Hewlett packard Research Grade 7620A with FID; Perkin Elmer 800 with Thermal Conductivity detector; Perkin Elmer 820 with FID and Thermal Conductivity detectors; Barber Coleman cryogenic chromatograph with Thermal Conductivity detector.
2. TECO Model 10A Chemiluminescence Analyzer.
3. Mass Spectrometer: CEC Model 21-130

TABLE B-II
CALIBRATION GASES

Gas	Source	Stability in Range of Interest	Analysis
H/C	NBS	Stable	g.c., FID, Mass spectrometer
CO	Vendor	Unstable in low concentrations	NDIR, G.c., mass spectrometer
CO ₂	Vendor	Stable	NDIR, G.c., mass spectrometer
NO	Vendor	Stable	PDS, Saltzman with oxidizer, mass spectrometer, NDIR, Chemiluminescence
NO ₂	Vendor	Unstable	PDS, Saltzman, mass spectrometer, NDUV, Chemiluminescence
O ₂	NBS/Air	Stable	g.c. mass spectrometer, amperometric

g.c.: gas chromatograph
FID : Flame Ionization Detector

B.3 SMOKE MEASUREMENT

Combustor exhaust smoke concentration is determined using a smoke measuring system that conforms to specifications of the Society of Automotive Engineers Aerospace Recommended Practice 1179 and the Environmental Protection Agency. The smoke measuring system (smoke meter) is a semiautomatic electromechanical device that incorporates a number of features to permit recording smoke data with precision and relative ease of operation. Dimensions of the filter holder and a schematic of the sampling system are shown in Figure B-2. The filter holder has been constructed with a 2.54 cm diameter spot size, a diffusion angle of 0.127 radian and a converging angle of 0.48 radian.

The unit is designed to minimize variability resulting from operator to operator differences. One of these features is a time controlled, solenoid activated main sampling valve (Valve A, See Figure B-2) having "closed", "sample", and "bypass" positions. This configuration permits close control of the sample size over relatively short sample times. In addition, this timing system operates a bypass system around a positive displacement volume measurement meter to ensure that the meter is in the circuit only when a sample is being collected or during the leak check mode. Other design features include automatic temperature control for the sample line and filter holder, and silicon rubber filter holders with support screens for ease of filter handling.

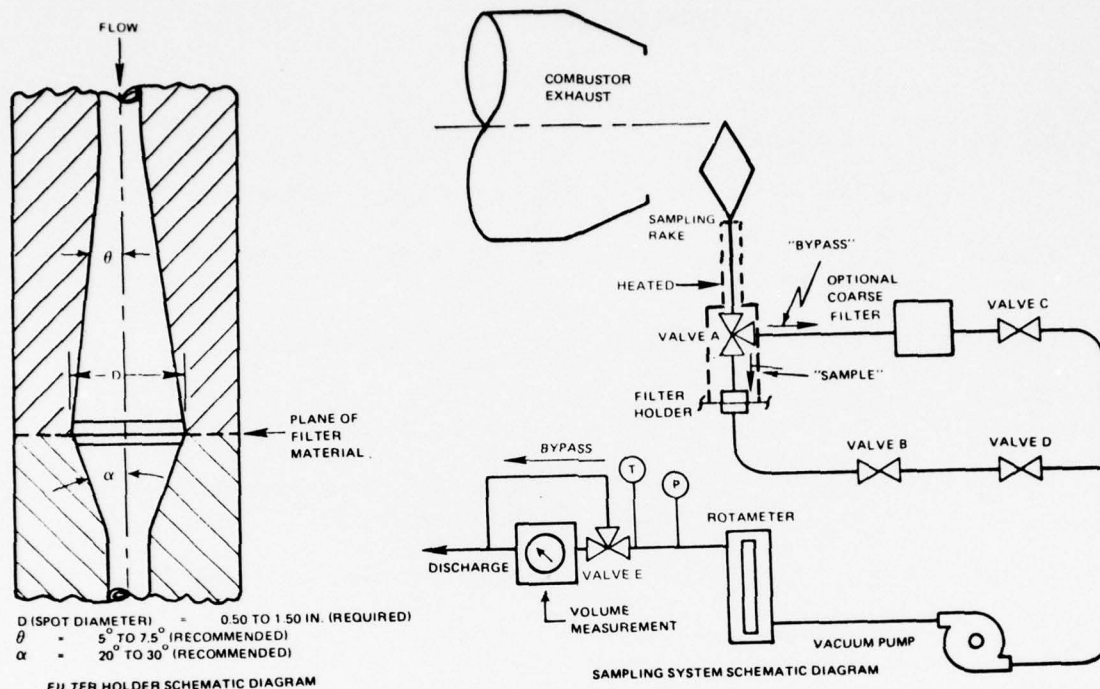


Figure B-2 Smoke Meter (78-8047)

A Photovolt Model 670 reflection meter with a type Y search unit conforming to ASA Ph 2.17-1958 "Standard for Diffuser Reflection Density" is used to determine the reflectance of the clean and stained filters.

Calibration of the reflectance meter is accomplished through the use of a set of Hunter Laboratory, NBS traceable, reflectance plaques which range in 15 steps from 3 to 96 percent. Clean Whatman No. 4 filter paper has a nominal reflectance value of 80 percent, which is within this range. The measured reflectance values are leastsquares fitted, tested for linearity, and the gas sample weight flow per unit filter area are computed by an IBM 370 digital computer.

APPENDIX C

EXPERIMENTAL DATA SUMMARY

All reported data acquired during the VCE duct burner segment rig test program are summarized in this appendix. Table C-1 presents a compilation of aerodynamic performance data and Table C-2 presents a tabulation of the emission performance data. All the listed parameters are defined in Section 5.

TABLE C-1
TEST RESULTS - AERODYNAMIC PERFORMANCE

Conf /Pt	Inlet Press MPa	Inlet Temp DEGK	Total Airflow KG/S	Inlet Mach Number	Burner Airflow KG/S	Airflow Split PC/PS/HP	Reference Velocity M/S	Fuel-Air Ratio	Total Fuel Flow KG/S	Fuel Flow Split PC/PS/HP	Press Loss PCT PTIN	Ideal Exit Temp DEGK	Max Metal Temp DEGK	Max Temp Loc
1-1	0.207	329.6	2.880	0.0522	0.0	0/0/0	--	0.0	0.0	0/0/0	1.690	--	--	
1-2	0.197	361.1	4.614	0.0924	4.451	15/33/52	53.320	0.0	0.0	0/0/0	5.860	--	--	
1-3	0.225	390.6	7.110	0.1284	6.842	17/35/48	75.847	0.0	0.0	0/0/0	13.470	--	--	
1-4	0.141	389.3	4.913	0.1431	0.0	0/0/0	--	0.0	0.0	0/0/0	21.480	--	--	
1-5	0.167	389.9	6.093	0.1504	0.0	0/0/0	--	0.0	0.0	0/0/0	29.670	--	--	
1-6	0.204	383.3	7.696	0.1542	0.0	0/0/0	--	0.0	0.0	0/0/0	31.930	--	--	
1-7	0.200	386.1	7.572	0.1557	7.249	23/48/29	92.122	0.0	0.0	0/0/0	36.120	--	--	
1-8	0.172	365.6	3.878	0.0892	3.715	14/28/58	51.469	0.0052	0.0192	100/0/0	7.460	578.	625.	LVR 1
1-9	0.185	366.5	3.745	0.0804	3.553	12/29/59	46.000	0.0122	0.0434	43/57/0	6.640	846.	742.	LVR 7
1-10	0.202	433.1	5.711	0.1224	5.457	17/37/46	76.630	0.0077	0.0418	75/25/0	14.710	738.	681.	LVR 5
1-11	0.169	436.1	4.636	0.1191	4.520	24/52/24	76.331	0.0100	0.0430	100/0/0	29.590	826.	--	
2-1	0.198	358.3	2.752	0.0543	0.0	0/0/0	--	0.0	0.0	0/0/0	1.210	--	--	
2-2	0.197	366.7	4.576	0.0922	4.410	15/32/53	53.591	0.0	0.0	0/0/0	5.080	--	--	
2-3	0.226	380.6	6.662	0.1199	6.451	18/37/45	71.276	0.0	0.0	0/0/0	8.840	--	--	
2-4	0.224	383.3	7.083	0.1289	0.0	0/0/0	--	0.0	0.0	0/0/0	10.450	--	--	
2-5	0.231	428.9	6.329	0.1182	6.042	11/30/59	73.579	0.0070	0.0423	100/0/0	9.670	709.	764.	LVR 3
2-6	0.231	430.0	6.358	0.1190	6.047	8/27/65	73.847	0.0139	0.0841	56/44/0	12.380	962.	1150.	LVR 5
2-7	0.229	432.2	6.337	0.1196	5.884	9/28/63	72.701	0.0261	0.1538	31/23/46	16.480	1363.	1508.	LVR 7
3-1	0.201	375.0	3.614	0.0722	0.0	0/0/0	--	0.0	0.0	0/0/0	3.010	--	--	
3-2	0.199	380.6	4.524	0.0919	4.346	14/37/49	54.213	0.0	0.0	0/0/0	5.000	--	--	
3-3	0.228	376.7	6.699	0.1184	6.433	14/37/49	69.443	0.0	0.0	0/0/0	8.520	--	--	
3-4	0.226	380.6	7.129	0.1282	6.849	14/37/49	75.603	0.0	0.0	0/0/0	10.190	--	--	
3-5	0.227	444.4	6.194	0.1197	5.886	10/36/54	75.459	0.0074	0.0436	100/0/0	9.960	739.	978.	LVR 3
3-6	0.230	441.7	6.235	0.1188	5.899	11/34/55	74.332	0.0107	0.0633	67/33/0	10.650	859.	1092.	LVR 3
3-7	0.227	436.1	6.243	0.1195	5.918	10/34/56	74.496	0.0113	0.0670	66/34/0	--	875.	1156.	LVR 3
3-8	0.226	454.4	6.087	0.1192	5.738	8/35/57	75.391	0.0165	0.0945	42/23/35	--	1244.	1111.	LVR 3
3-9	0.226	447.2	6.055	0.1176	5.676	10/34/56	73.383	0.0194	0.1099	35/19/46	--	1370.	1172.	LVR 8
4-1	0.201	375.0	3.580	0.0713	0.0	0/0/0	--	0.0	0.0	0/0/0	3.640	--	--	
4-2	0.200	383.3	4.489	0.0912	4.294	16/41/43	53.785	0.0	0.0	0/0/0	6.080	--	--	
4-3	0.229	369.4	6.806	0.1187	6.506	15/41/44	68.641	0.0	0.0	0/0/0	10.630	--	--	
4-4	0.226	380.6	7.122	0.1281	6.810	15/41/44	75.208	0.0	0.0	0/0/0	12.770	--	--	
4-5	0.229	426.7	6.322	0.1185	6.004	12/39/49	73.170	0.0068	0.0408	100/0/0	--	699.	947.	LVR 3
4-6	0.229	426.1	6.342	0.1188	5.992	11/37/52	72.929	0.0104	0.0625	66/34/0	--	834.	1259.	LVR 3
4-7	0.229	430.6	6.296	0.1185	5.907	10/34/56	72.670	0.0142	0.0838	57/43/9	--	972.	1159.	LVR 5
4-8	0.230	430.6	6.296	0.1182	5.869	11/35/54	71.993	0.0207	0.1215	32/25/43	--	1190.	1139.	LVR 3
4-9	0.229	429.4	6.303	0.1184	5.844	11/35/54	71.621	0.0224	0.1311	29/23/48	--	1245.	1242.	LVR 8
4-10	0.229	429.4	6.303	0.1184	5.826	11/36/53	71.403	0.0240	0.1398	26/22/52	--	1294.	1283.	LVR 8
5-1	0.229	430.6	6.280	0.1186	5.984	15/39/46	73.809	0.0	0.0	0/0/0	--	--	--	
5-2	0.228	430.6	6.264	0.1187	5.761	10/35/55	71.281	0.0246	0.1417	28/23/49	--	1314.	1219.	LVR 8
5-3	0.228	430.6	6.315	0.1198	5.791	10/34/56	71.763	0.0264	0.1526	29/21/50	--	1368.	1278.	LVR 8
5-4	0.229	430.6	6.281	0.1185	5.842	0/0/0	--	0.0215	0.1256	31/24/45	15.180	--	1133.	LVR 3
5-5	0.201	430.0	6.265	0.1347	5.824	0/0/0	--	0.0217	0.1263	31/24/45	19.610	--	1042.	LVR 3

TABLE C-1 (Cont'd)
TEST RESULTS - AERODYNAMIC PERFORMANCE

Conf /PT	Inlet Press MPa	Inlet Temp DECK	Total Airflow KG/S	Inlet Mach Number	Burner Airflow KG/S	Airflow Split PC/PS/HP	Reference Velocity M/S	Fuel-Air Ratio	Total Fuel Flow KG/S	Fuel Flow Split PC/PS/HP	Press Loss PCT PTIN	Ideal Exit Temp DECK	Max Metal Temp DECK	Max Temp Loc
6-1	0.200	380.6	3.572	0.0720	3.431	15/34/51	41.511	0.0	0.0	0/0/0	3.660	--	--	
6-2	0.199	383.3	4.487	0.0913	4.317	15/34/51	54.173	0.0	0.0	0/0/0	6.030	--	--	
6-3	0.229	373.3	6.737	0.1183	6.476	15/34/51	69.128	0.0	0.0	0/0/0	10.560	--	--	
6-4	0.227	385.0	7.136	0.1283	6.858	15/34/51	76.156	0.0	0.0	0/0/0	12.500	--	--	
6-5	0.230	435.0	6.277	0.1182	5.967	11/33/56	73.778	0.0075	0.0447	100/0/0	12.290	733.	994.	LVR 3
6-6	0.230	435.0	6.277	0.1184	5.933	10/32/58	73.472	0.0119	0.0708	63/37/0	--	896.	1174.	LVR 3
6-7	0.230	435.0	6.281	0.1182	5.873	10/33/57	72.580	0.0204	0.1201	35/19/46	--	1186.	1189.	LVR 8
6-8	0.229	435.0	6.567	0.1244	6.117	10/32/58	76.036	0.0222	0.1356	32/22/46	--	1241.	1203.	LVR 8
6-9	0.229	432.2	6.578	0.1244	6.217	10/33/57	76.915	0.0112	0.0697	64/36/0	--	868.	1128.	LVR 3
6-10	0.231	433.3	6.291	0.1180	5.945	10/33/57	73.072	0.0111	0.0662	64/36/0	13.000	866.	1133.	LVR 3
6-11	0.230	433.3	6.282	0.1183	5.871	11/33/56	72.423	0.0203	0.1191	35/19/46	--	1179.	1137.	LVR 8
6-12	0.230	433.3	6.273	0.1182	5.929	10/33/57	73.211	0.0111	0.0656	64/36/0	--	864.	1148.	LVR 3
6-13	0.229	433.3	6.273	0.1184	5.928	0/0/0	--	0.0117	0.0662	72/28/0	--	--	--	
6-14	0.230	433.9	6.274	0.1182	5.929	0/0/0	--	0.0111	0.0656	56/44/0	--	--	--	
7-1	0.228	425.0	6.295	0.1182	5.878	11/33/56	71.619	0.0196	0.1153	35/20/45	15.210	1150.	1111.	LVR 8
8-1	0.229	380.6	7.027	0.1246	6.773	16/34/50	73.741	0.0	0.0	0/0/0	--	--	--	
8-2	0.231	436.1	6.737	0.1268	6.332	10/32/58	78.356	0.0247	0.1566	28/22/50	--	1323.	1244.	LVR 8
8-3	0.228	435.3	6.562	0.1248	6.243	11/31/58	77.974	0.0133	0.0828	56/44/0	--	944.	1172.	LVR 3
8-4	0.226	430.8	6.490	0.1239	6.079	11/32/57	75.825	0.0292	0.1773	24/19/57	--	1453.	1269.	LVR 10
8-5	0.228	430.6	6.613	0.1254	6.168	10/33/57	76.389	0.0257	0.1585	29/18/53	21.250	1348.	1300.	LVR 8
9-1	0.202	386.1	3.609	0.0727	--	0/0/0	--	0.0	0.0	0/0/0	3.750	--	--	
9-2	0.199	394.4	4.450	0.0921	--	0/0/0	--	0.0	0.0	0/0/0	6.130	--	--	
9-3	0.229	377.2	6.995	0.1237	6.727	17/34/49	72.698	0.0	0.0	0/0/0	11.470	--	--	
9-4	0.226	394.4	7.041	0.1292	--	0/0/0	--	0.0	0.0	0/0/0	12.580	--	--	
9-5	0.230	431.1	6.624	0.1244	6.374	17/35/48	78.207	0.0	0.0	0/0/0	11.430	--	--	
9-6	0.228	433.3	6.614	0.1256	6.312	11/34/55	78.507	0.0066	0.0418	100/0/0	13.480	698.	1075.	LVR 3B
9-7	0.228	433.3	6.579	0.1249	6.236	10/32/58	77.555	0.0129	0.0806	57/43/0	15.430	930.	1247.	LVR 3A
9-8	0.228	433.3	6.597	0.1253	--	0/0/0	--	0.0256	0.0800	47/53/0	15.520	--	1159.	LVR 3A
9-9	0.228	433.3	6.596	0.1252	6.156	10/32/58	76.574	0.0129	0.1574	24/25/51	19.870	1346.	1167.	LVR 3A
9-10	0.229	433.3	6.565	0.1249	6.118	10/32/58	76.184	0.0262	0.1600	24/24/52	20.010	1364.	1136.	LVR 3A
9-11	0.229	433.3	6.581	0.1247	6.092	10/32/58	75.601	0.0296	0.1804	20/22/58	21.330	1468.	1139.	LVR 3A
9-12	0.231	433.3	6.480	0.1215	5.952	10/31/59	73.121	0.0344	0.2050	18/21/61	21.610	1608.	1225.	LVR 9
9-13	0.196	433.3	5.457	0.1209	5.179	10/32/58	75.176	0.0131	0.0679	46/54/0	14.670	937.	1158.	LVR 3A
9-14	0.200	433.3	5.423	0.1171	4.994	12/31/57	70.672	0.0365	0.1821	17/20/63	20.040	1665.	1272.	LVR 9

TABLE C-1 (Cont'd)

TEST RESULTS - AERODYNAMIC PERFORMANCE

Conf	Inlet Press MPa	Inlet Temp DEGR	Total Airflow KG/S	Inlet Mach Number	Burner Airflow KG/S	Airflow Split PC/PS/HP	Reference Velocity M/S	Fuel-Air Ratio	Total Fuel Flow KG/S	Fuel Flow Split PC/PS/HP	Press Loss PCT PTIN	Ideal Exit Temp DEGR	Max Metal Temp DEGR	Max Temp Loc
10-1	0.228	430.6	6.584	0.1247	6.146	10/32/58	76.159	0.0259	0.1592	23/26/51	19.750	1354.	1094.	LVR 8B
10-2	0.228	431.1	6.590	0.1247	6.095	10/32/58	75.370	0.0299	0.1821	20/22/58	21.370	1475.	1142.	LVR 10
10-3	0.231	433.3	6.505	0.1222	5.968	11/31/58	73.424	0.0345	0.2058	18/21/61	21.420	1610.	1219.	LVR 9
10-4	0.229	433.3	6.566	0.1245	6.266	0/0/0	--	0.0060	0.0376	100/0/0	--	--	--	--
10-5	0.228	433.3	6.577	0.1248	6.237	0/0/0	--	0.0124	0.0772	48/52/0	--	--	--	--
10-6	0.228	433.3	6.521	0.1239	5.998	10/31/59	74.685	0.0328	0.1968	19/21/60	22.170	1562.	1186.	LVR 10
10-7	0.233	450.0	4.569	0.0861	4.293	12/31/57	54.066	0.0240	0.1031	20/29/51	7.890	1311.	1269.	LVR 8A
11-1	0.201	380.0	3.566	0.0715	--	0/0/0	--	0.0	0.0	0/0/0	3.690	--	--	--
11-2	0.200	386.9	4.502	0.0919	--	0/0/0	--	0.0	0.0	0/0/0	6.160	--	--	--
11-3	0.229	372.2	7.063	0.1241	6.779	16/35/49	72.320	0.0	0.0	0/0/0	11.820	--	--	--
11-4	0.228	386.4	7.102	0.1277	6.819	16/35/49	75.868	0.0	0.0	0/0/0	12.620	--	--	--
11-5	0.229	430.6	6.606	0.1247	6.347	17/35/48	78.263	0.0	0.0	0/0/0	11.830	--	--	--
11-6	0.229	430.6	6.585	0.1243	6.277	12/36/52	77.403	0.0065	0.0409	100/0/0	14.070	692.	751.	LVR 2
11-7	0.229	430.8	6.594	0.1247	6.249	10/33/57	77.192	0.0130	0.0130	57/43/0	16.460	931.	1028.	LVR 4
11-8	0.228	431.1	6.589	0.1247	6.223	10/32/58	76.975	0.0165	0.1024	50/50/0	17.820	1050.	1137.	LVR 4
11-9	0.229	431.1	6.594	0.1246	6.079	10/32/58	75.081	0.0305	0.1853	25/19/56	23.470	1492.	1022.	LVR 4
11-10	0.230	432.5	6.606	0.1245	6.239	11/33/56	76.969	0.0130	0.0812	56/44/0	--	952.	1008.	LVR 4
11-11	0.230	431.4	6.615	0.1242	6.218	0/0/0	--	0.0168	0.1045	51/49/0	--	--	1044.	LVR 4
11-12	0.230	431.7	6.590	0.1240	6.095	0/0/0	--	0.0281	0.1715	27/21/52	--	--	1147.	LVR 8B
11-13	0.230	432.5	6.579	0.1241	6.036	0/0/0	--	0.0321	0.1937	23/19/58	--	--	1100.	LVR 8B
11-14	0.230	433.3	6.552	0.1236	5.963	11/31/58	73.695	0.0343	0.2046	22/17/61	--	1605.	1114.	LVR 8B
11-15	0.231	430.0	6.597	0.1230	5.991	11/31/58	72.902	0.0342	0.2046	22/17/61	23.830	1598.	1094.	LVR 8B
11-16	0.232	429.7	6.566	0.1223	5.962	0/0/0	--	0.0344	0.2049	28/21/51	--	--	1175.	LVR 8B
11-17	0.231	429.7	6.608	0.1236	6.271	0/0/0	--	0.0129	0.0810	46/54/0	--	--	1000.	LVR 4
11-18	0.229	430.3	6.649	0.1254	6.309	0/0/0	--	0.0130	0.0822	67/33/0	--	--	1017.	LVR 4
11-19	0.234	448.9	4.588	0.0860	4.273	11/32/57	53.438	0.0304	0.1298	25/17/58	9.020	1503.	1183.	LVR 8A
11-20	0.234	447.5	4.676	0.0975	4.338	9/32/59	54.091	0.0299	0.1298	26/17/57	--	1488.	1167.	LVR 8A
11-21	0.234	602.8	4.076	0.0885	3.874	10/35/55	65.038	0.0128	0.0496	57/43/0	6.760	1075.	1183.	LVR 4
11-22	0.233	600.0	4.041	0.0880	3.840	10/35/55	64.538	0.0129	0.0496	58/42/0	--	1076.	1197.	LVR 4
11-23	0.234	600.0	4.072	0.0883	3.869	0/0/0	--	0.0129	0.0498	68/32/0	--	--	1125.	LVR 2
11-24	0.234	601.9	4.022	0.0874	3.821	0/0/0	--	0.0131	0.0501	50/50/0	--	--	1197.	LVR 3A
11-25	0.235	602.2	4.031	0.0871	3.814	11/34/55	63.696	0.0123	0.0469	57/43/0	--	1057.	1139.	LVR 2
12-1	0.197	381.7	3.561	0.0730	--	0/0/0	--	0.0	0.0	0/0/0	3.590	--	--	--
12-2	0.199	383.3	4.482	0.0913	--	0/0/0	--	0.0	0.0	0/0/0	5.920	--	--	--
12-3	0.228	390.0	6.888	0.1242	6.592	16/36/48	73.876	0.0	0.0	0/0/0	11.340	390.	--	--
12-4	0.227	383.9	7.104	0.1276	--	0/0/0	--	0.0	0.0	0/0/0	12.130	--	--	--
12-5	0.229	432.2	6.560	0.1242	6.272	15/36/49	77.726	0.0	0.0	0/0/0	11.210	433.	--	--
12-6	0.228	430.8	6.558	0.1241	6.216	0/0/0	--	0.0055	0.0344	100/0/0	12.390	--	--	--
12-7	0.228	431.9	6.574	0.1249	6.181	11/34/55	76.814	0.0132	0.0815	55/45/0	13.640	938.	1042.	LVR 4
12-8	0.227	431.4	6.574	0.1250	6.048	0/0/0	--	0.0283	0.1710	27/27/51	18.760	1253.	1253.	LVR 8B
12-9	0.228	431.4	6.585	0.1248	6.004	9/33/58	74.408	0.0319	0.1916	23/19/58	19.510	1534.	1292.	LVR 8B
12-10	0.233	446.7	4.659	0.0876	4.292	9/33/58	53.733	0.0301	0.1293	26/17/57	8.250	1494.	1286.	LVR 8B
12-11	0.232	599.7	3.987	0.0871	3.767	11/35/54	63.459	0.0131	0.0493	58/42/0	5.860	1092.	1167.	LVR 4

TABLE C-2
TEST RESULTS EMISSIONS AND COMBUSTION PERFORMANCE

CONF /PT	INLET PRES MPa	INLET TEMP OK	BURNER AIRFLOW kg/sec	METERED F/A RATIO	FUEL TEMP OK	FUEL SPLIT Pc/ps/hp	CARBON BAL F/A RATIO	CO ₂ %	SPECIF HUMID g/kg	CO EI g/kg	THC EI g/kg	NOX EI g/kg	COMB EF/IC	CORR EI g/kg	CORR NOX EI g/kg	CORR COMB EFFIC	SAE SMOKE NUMBER
6-10	0.231	433.3	5.945	0.0111	292	64/36/0	0.0136	2.766	13.569	4.180	0.429	2.248	99.8	3.7	2.7	99.9	-
6-11	0.230	433.3	5.871	0.0203	292	35/19/46	0.0231	4.278	15.648	68.998	56.855	1.512	91.8	60.9	1.9	92.0	2.1
6-12	0.230	433.3	5.929	0.0111	289	64/36/0	0.0129	2.633	15.092	5.233	0.253	2.024	99.8	4.6	2.5	99.9	-
6-13	0.229	433.3	5.928	0.0117	291	72/28/0	0.0130	2.649	15.092	5.208	0.265	2.003	99.8	4.6	2.5	99.9	-
6-14	0.230	433.9	5.929	0.0111	292	56/44/0	0.0134	2.720	15.648	4.980	0.310	2.164	99.8	4.4	2.7	99.9	-
7-1	0.228	425.0	5.878	0.0196	305	35/24/45	0.0215	4.138	9.508	54.373	27.386	1.859	94.9	47.6	2.1	95.7	-
8-5	0.228	430.6	6.168	0.0257	300	29/18/53	0.0366	7.085	10.612	50.178	2.829	2.115	98.4	43.9	2.5	98.7	2.0
10-4	0.229	433.3	6.266	0.0060	311	100/0/0	0.0071	1.406	6.754	73.446	1.630	1.949	98.1	64.5	2.1	98.3	-
10-5	0.228	433.3	6.237	0.0124	314	48/52/0	0.0147	2.979	6.754	4.460	0.123	2.669	99.9	3.9	2.9	99.9	-
10-6	0.228	433.3	5.998	0.0328	303	19/21/60	0.0380	7.434	6.756	31.997	0.858	2.225	99.2	28.0	2.4	99.3	1.3
10-7	0.233	430.0	4.293	0.0240	301	20/29/51	0.0293	5.853	6.759	5.639	0.066	3.073	99.9	7.2	3.1	99.8	2.2
11-10	0.230	432.5	6.239	0.0130	299	56/44/0	0.0138	2.801	4.361	7.645	0.049	3.535	99.8	6.7	3.6	99.8	-
11-11	0.230	431.4	6.218	0.0168	307	51/49/0	0.0198	3.962	4.363	22.445	0.017	3.446	99.5	19.8	3.6	99.5	-
11-12	0.230	431.7	6.095	0.0281	296	27/21/52	0.0359	7.100	4.361	17.085	0.115	2.735	99.6	15.1	2.8	99.6	-
11-13	0.230	432.5	6.036	0.0321	297	23/19/58	0.0408	8.030	4.360	15.908	0.010	2.859	99.6	14.0	2.9	99.7	-
11-14	0.230	433.3	5.963	0.0343	298	22/17/61	0.0440	8.641	4.360	12.728	0.001	2.769	99.7	12.1	2.8	99.7	-
11-15	0.231	430.0	5.991	0.0342	291	22/19/61	0.0429	8.422	2.988	13.375	0.009	2.714	99.7	11.9	2.7	99.7	4.2
11-16	0.232	429.7	5.962	0.0344	298	28/21/51	0.0440	8.643	2.999	10.192	0.033	3.107	99.8	9.1	3.1	99.8	-
11-17	0.231	429.7	6.271	0.0129	303	46/54/0	0.0152	3.093	3.001	7.172	0.059	3.404	99.8	6.4	3.4	99.8	-
11-18	0.229	430.3	6.309	0.0130	303	67/33/0	0.0153	3.104	3.002	8.001	0.051	3.137	99.8	7.0	3.1	99.8	-
11-20	0.234	447.5	4.338	0.0299	293	26/17/57	0.0320	6.422	4.360	7.405	0.040	3.980	99.8	9.5	3.8	99.8	4.9
11-22	0.233	600.0	3.840	0.0129	308	58/42/0	0.0140	2.856	8.473	2.338	0.120	6.579	99.9	2.1	8.1	99.9	-
11-23	0.234	600.0	3.869	0.0129	308	68/32/0	0.0129	2.639	8.476	2.015	0.043	6.202	99.9	1.9	7.6	99.9	-
11-24	0.234	601.9	3.821	0.0131	308	50/50/0	0.0136	2.774	8.476	2.704	0.083	6.857	99.9	2.5	8.4	99.9	-
11-25	0.235	602.2	3.814	0.0123	304	57/43/0	0.0127	2.594	3.004	1.614	0.033	5.695	99.9	1.5	6.3	99.9	4.2
12- 7	0.228	431.9	6.181	0.0132	298	55/45/0	0.0158	3.205	2.336	6.061	0.492	3.122	99.8	5.3	3.3	99.8	-
12- 8	0.227	431.4	6.048	0.0283	286	27/22/51	0.0350	6.923	1.215	14.532	0.215	2.827	99.6	12.7	2.8	99.7	-
12- 9	0.228	431.4	6.004	0.0319	292	23/19/58	0.0390	7.688	2.336	14.721	0.105	3.034	99.6	12.9	3.0	99.7	-
12-10	0.233	446.7	4.292	0.0301	288	26/17/67	0.0351	6.977	1.664	7.826	0.044	3.931	99.8	10.0	3.6	99.8	11.8
12-11	0.232	599.7	3.767	0.0131	300	58/42/0	0.0151	3.070	1.213	2.593	0.257	6.398	99.9	2.4	6.8	99.9	-

APPENDIX D

FUEL INJECTOR SPRAY EVALUATION

During the course of the experimental evaluation of the duct burner, it became evident that excessive local liner heat loads in the high power stage were caused by inadequate dispersion of the fuel injected into this stage. A flow visualization study was conducted to investigate this phenomenon and identify fuel injector configurations that would produce greater radial penetration and dispersion of the fuel in this stage. The investigation was conducted on the apparatus described in Section 4.4.3 in which water was sprayed across a cold airstream from a fuel injector mounted in the wall of the plexiglas duct. While it was recognized such an approach does not include the effects of vaporization and combustion on droplet trajectories, it provided a basis for assessing the gross effects of injector configuration on fuel dispersion.

A total of twelve different injectors of varying spray configuration and flow size, as listed on Table D-I, was evaluated in this apparatus. In conducting the tests, the parameter controlling the dynamics of fuel dispersion was considered to be the ratio of the pressure drop across the injector, as it relates to fuel droplet momentum, to the dynamic pressure of the airstream. In conducting the tests, dynamic pressure of the airstream was established at the level encountered in the gas path of the duct burner rig at the plane of the high power stage fuel injectors and the test injector operated over a range of pressure drops which, after adjustment for the differences in density between Jet A and water, correspond to those encountered in rig or engine operation.

Figure D-1 shows the variation of maximum fuel spray penetration with the injector pressure drop to airstream dynamic pressure ratio for selected injectors, while Figure D-2 shows photographs of the spray at particular conditions of interest. With reference to Table D-I, injectors A, B and C were of identical configuration and varied only in flow size. Injector B was that initially used in the high power stage of the duct burner rig. As suspected from the duct burner rig tests, these injectors were found to produce poor radial dispersion of the fuel with the spray not penetrating more than 5 cm (2 in) into the airstream. A weak trend of increasing penetration with increasing flow size is evident from the data of Figure D-1. Injectors D and E were selected for evaluation because the spray was confined closer to the axis of the injector providing more radially directed momentum. However, tests of these injectors revealed no significant improvement in spray penetration relative to injectors B or C. Injectors F and G incorporated a swirl chamber as opposed to conical metering element construction, and because the internal pressure drop is considerably smaller in this type of nozzle, more of the overall pressure drop would be expected to be available as droplet momentum at the nozzle discharge. Evaluation of these injectors also indicated minimal improvement in spray penetration over conventional conical spray injectors.

TABLE D-1
FUEL INJECTORS EVALUATED IN SPRAY VISUALIZATION TESTS

		Injector Flow Size		Radial Duct Height		
		$\frac{\text{kg/hr}}{\sqrt{\text{MPa}}}$	$\frac{\text{lb/hr}}{\sqrt{\text{psia}}}$	cm.	(inches)	
A	85° Hollow Cone Spray	10.38	(1.89)	10.15	(4.0)	Used in pilot secondary stage of rig.
B	85° Hollow Cone Spray	45.5	(8.3)	10.15	(4.0)	Used in high power stage Configurations 1 to 6
				10.15	(4.0)	
C	85° Hollow Cone Spray	73.0	(13.3)	10.15	(4.0)	
D	45° Hollow Cone	37.8	(6.9)	10.15	(4.0)	
E	45° Solid Cone	37.8	(6.9)	10.15	(4.0)	
F	50° Solid Cone Swirl Chamber	78.3	(14.3)	10.15	(4.0)	
G	110° Hol Cone Swirl Chamber	71.1	(13.0)	10.15	(4.0)	
H	65° Flat Spray	29.6	(5.4)	10.15	(4.0)	
I	80° Flat Spray	62.5	(11.4)	10.15	(4.0)	Used in high power stage in Configs. 10, 11 and 12
				10.15	(4.0)	
J	75° Flat Spray	74.0	(13.5)	10.15	(4.0)	
K	46° Solid Cone Swirl Chamber	274	(50.0)	19.0	(7.5)	Simulate high power stage in VSCE-502B engine.
L	65° Flat Spray	261	(47.5)	19.0	(7.5)	Simulate high power stage in VSCE-502B engine.

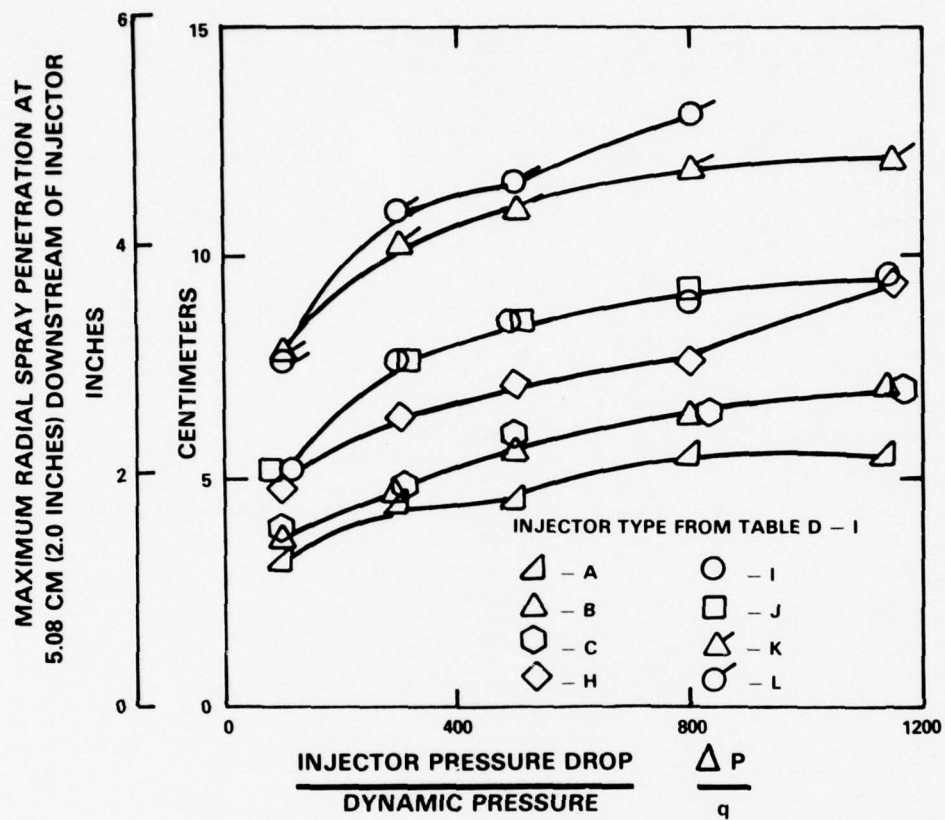


Figure D-1 Fuel Injector Spray Penetration Characteristics

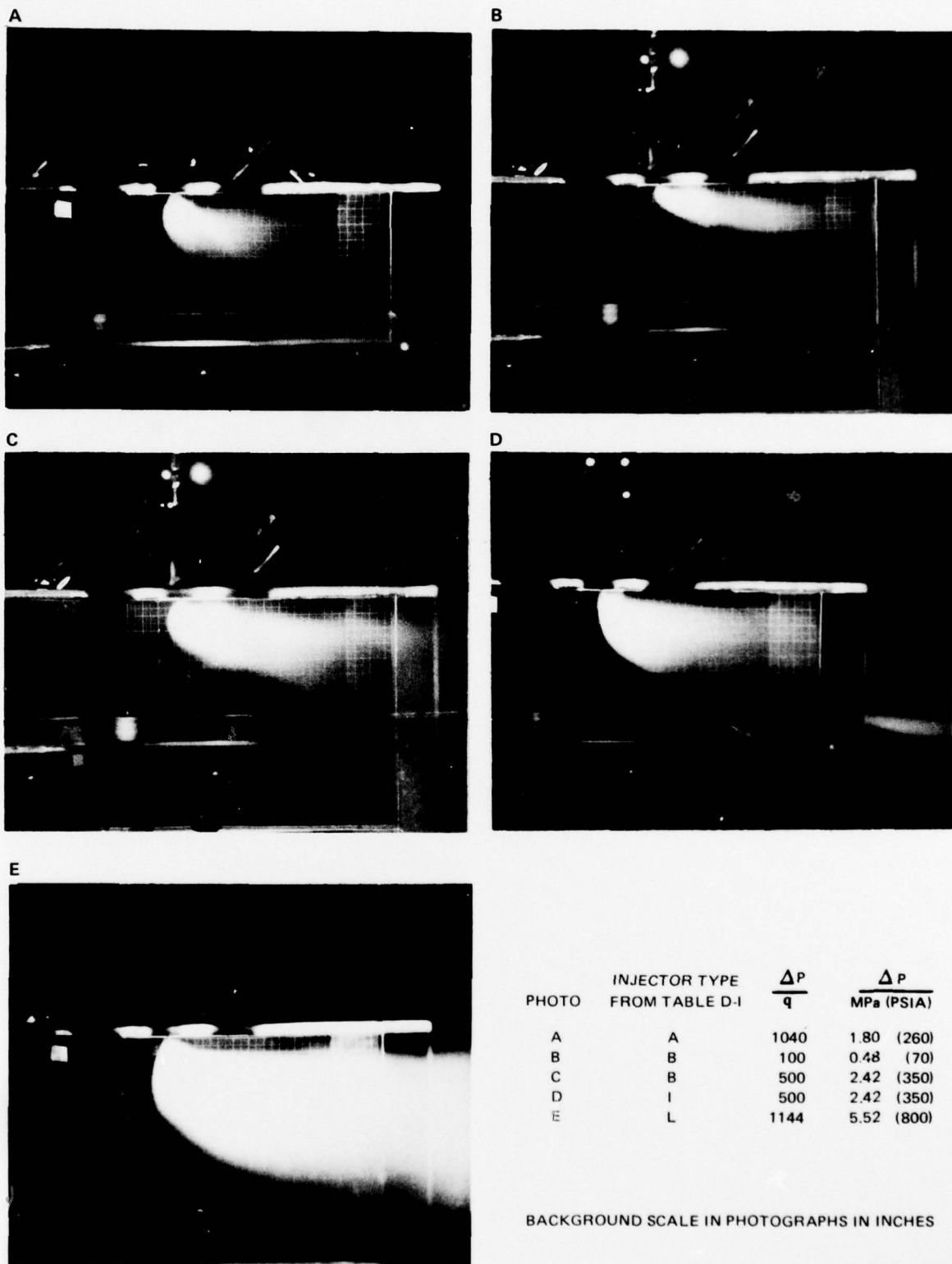


Figure D-2 Fuel Injector Spray Patterns

The flat spray injectors H, I and J are shown in Figure D-1 and produce significantly deeper spray penetration than the conical spray type and also demonstrate a slight trend toward improved penetration with increasing flow size. The penetration is shown sufficient to completely traverse the 7 cm (2.75 in) radial height of the inlet to the high power stage. Based on these results, flat spray injectors were installed in Configuration 8, and injectors of this type were used in the high power stage throughout the remainder of the program.

Because of observed increases in spray penetration with increases in injector flow size, the evaluation was extended to investigate injectors of larger flow size representative of those that would be used in a full scale duct burner for the VSCE-502B. These injectors, K and L on Table D-I, had about four times the flow capacity of those used in the duct burner rig and were evaluated in a duct having a radial depth of 19 cm (7.5 in), which is comparable to the inlet of the high power stage of a duct burner in the VSCE-502B. As shown in Figure D-2, the penetration characteristics of these injectors were considerably better than those of the smaller size injectors. While the data shown in this figure indicate the spray did not completely traverse the duct, significantly deeper penetration was observed further downstream.

Figure D-2 shows photographs of spray patterns observed during the tests. Photograph A shows the spray produced by the small hollow cone injector A of Table D-I. This injector was used in the pilot secondary stage and the photograph was taken at airflow and injector pressure drops consistent with the normal operating mode of this injector in the rig. The radial height of this stage is 4.24 cm (1.67 in) and the spray is shown to readily penetrate and disperse over this distance. Photographs B and C show the hollow cone injector B used in the high power stage of the duct burner rig in the initial configurations. In photograph B, the injector pressure drop is low and the confinement of the spray to the outer wall is demonstrated. Increasing the pressure drop, as in photograph C, improves penetration somewhat, but considerably better penetration is achieved with the flat spray injector shown in photograph D. Photograph E shows the spray produced by a large flat spray injector sized for the VSCE-502B when operating at a high pressure drop. All of the photographs reveal that, at 5.08 cm (2 in) downstream of the injector, the spray is continuing to penetrate the airstream. This length had been chosen as a reference for this study because it corresponds to the injector-swirler tube discharge spacing in the duct burner rig. The observation suggests that increasing the axial spacing between the injectors and the swirler tubes in the rig might enhance fuel dispersion.

NOMENCLATURE

A	Flow Area	cm ² (in ²)
C _D	Discharge Coefficient	
CO	Carbon Monoxide	
F/A	Fuel to Air Ratio	
M _{ref}	Mach Number at Maximum Cross-Sectional Area of Fan Duct Neglecting Blockage by the Duct Burner	
NO _x	Oxides of Nitrogen	
P _S	Static Pressure	MPa (psia)
P _T	Total Pressure	MPa (psia)
q	Dynamic Pressure	MPa (psia)
THC	Total Unburned Hydrocarbons	
T _T	Total Temperature	°K (°F)
V _{ref}	Velocity at a Cross-Section of the Duct Burner in the Absence of Combustion	m/sec (ft/sec)
W _A	Airflow	kg/sec (lb/sec)
W _{AB}	Burner Air Flow	kg/sec (lb/sec)
W _F	Duct Burner Fuel Flow	kg/sec (lb/sec)
η _c	Chemical Combustion Efficiency	
η _T	Thrust Efficiency	
φ	Equivalence Ratio	

REFERENCES

1. Lohmann, R.P., Riecke, G.T., "Analytical Screening of Low Emissions High Performance Duct Burners for Supersonic Cruise Aircraft Engines", NASA CR-135157, March 1977.
2. Westmoreland, J.S., Godston, J., "VCE Testbed Program Planning and Definition Study, Final Report", NASA CR-135362, January 1978.
3. Howlett, R.A., Johnson, J., Sabatella, J., Sewall, T. "Advanced Supersonic Propulsion Study, Phase III Final Report", NASA CR-135148, December 1976.
4. Kozlowski, H., Packman A.B. "Aero/Acoustic Tests of Duct Burning Turbofan Exhaust Nozzles" NASA CR-2628, July 1976.
5. Roberts, R., Fiorentino, A.J., Green, W., "Experimental Clean Combustor Program, Phase III, Final Report", NASA CR-135253, October 1977.
6. Control of Air Pollution from Aircraft and Aircraft Engines, Part II Supersonic Engines, Federal Register, Vol. 41, No. 159, August 16, 1976.
7. Grobecker, A.J., Coroniti, S.C., Cannon, R.H. Jr., "Report of Findings, The Effect of Stratospheric Pollution by Aircraft, Final Report" U.S. Department of Transportation Climatic Impact Assessment Program, DOT-TST-75-58, December 1974.
8. Roberts, R., Peduzzi, A., Vitti, G.E., "Experimental Clean Combustor Program, Phase I, Final Report", NASA CR-134756, October 1975.
9. Roberts, R., Peduzzi, A., Vitti, G.E., "Experimental Clean Combustor Program, Phase II, Final Report", NASA CR-134969, November 1976.
10. Roberts, R., Fiorentino, A.J., Green, W., "Pollution Reduction Technology Program, Can Annular Engines, Final Report", NASA CR-135027, May 1976.
11. Markowski, S.J., Lohmann, R.P., Reilly, R.S., "The Vorbix Burner A New Approach to Gas Turbine Combustors", Transactions of the ASME, Journal of Engineering for Power, Vol. 98, No. 1, January 1976.
12. "Procedure for the Continuous Sampling and Measurement of Gaseous Emissions from Aircraft Turbine Engines," SAE Aerospace Recommended Practice 1256, October 1971.

DISTRIBUTION LIST

	Copies
I. NASA	
1. NASA Lewis Research Center 21000 Brookpark Rod Cleveland, OH 44135	
Attn: Report Control Office MS 5/5	1
Technology Utilization MS 3/19	1
Library MS 60/3	2
D. Gauntner MS 301/2	1
J. E. Dilley MS 500/305	1
W. L. Stewart MS 3/5	1
R. A. Rudey MS 60/4	1
D. A. Petrash MS 60/6	1
L. A. Diehl MS 60/6	1
E. A. Lezberg MS 60/4	1
R. E. Jones MS 60/6	1
R. W. Niedzwicki MS 54/6	1
J. Grobman MS 54/6	1
USAF Office MS 501/3	1
Propulsion Lab., USARTL (AVRADCOM) MS 77/5	2
Author or Project Manager.	28
NASA Headquarters	1
Attn: RTP-6/Manager, Propulsion Office 600 Independence Avenue, S.W. Washington, DC 20546	
3. NASA Scientific & Technical Information Facility	25
Attn: Accessioning Department P.O. Box 8757 Baltimore/Washington International Airport MD 21240	
II. OTHER GOVERNMENT AGENCIES	
1. Air Force Office of Scientific Research	1
Attn: B. T. Wolfson Bolling AFB Washington, DC 20332	
2. Arnold Engineering & Development Center	1
Attn: E. L. Hively Code D1/R Arnold Air Force Station, TN 37389	

DISTRIBUTION LIST (Cont'd)

	Copies
II. OTHER GOVERNMENT AGENCIES (Cont'd)	
3. ARO Incorporated Attn: Library Arnold Air Force Station, TN 37389	1
4. Bureau of Mines Bartlesville Energy Research Center Attn: Richard Hurn P. O. Box 1398 Bartlesville, OK 74003	1
5. Chief Army Research Office Attn: Mr. J. Murray P. O. Box 12211 Research Triangle Park, NC 27709	1
6. Commander U. S. Army Aviation R&D Command Attn: DRDAV-EQP (Mr. Larry Bell) P. O. Box 209 St. Louis, MO 63166	1
7. Commander U. S. Army Fuels & Lubricants Research Lab Southwestern Research Institute P. O. Drawer 28510 San Antonio, TX 78284	1
8. Defense Documentation Center Cameron Station 5010 Duke Street Alexandria, VA 22314	1
9. Director, Applied Tech. Laboratory Attn: DAVDL-ATL-AT (Mr. R. Bolton) U. S. Army Research & Tech. Lab. (AVRADCOM) Ft. Eustis, VA 23604	1
10. Environmental Protection Agency Attn: Mr. Richard Munt 2565 Plymouth Road Ann Arbor, MI 48105	1

DISTRIBUTION LIST (Cont'd)

	Copies
II. OTHER GOVERNMENT AGENCIES (Cont'd)	
Environmental Protection Agency Attn: Library 2565 Plymouth Road Ann Arbor, MI 48105	1
11. Environmental Protection Agency Attn: Library Mail Drop 65 Research Triangle Park, NC 27111	1
12. Environmental Protection Agency Attn: George Kittredge 401 Main Street S.W. Washington, DC 20460	1
13. FAA Headquarters Attn: N. Krull 800 Independence Avenue SW Washington, DC 20591	1
FAA Headquarters Attn: Library 2100 Second Street, SW Washington, DC 20591	1
14. Jet Propulsion Laboratory Attn: M. Clayton MS 125-224 4800 Oak Grove Drive Pasadena, CA 91103	1
15. Naval Air Propulsion Center Attn: Mr. Anthony Klarman PE-71 P. O. Box 7176 Trenton, NJ 03628	1
Naval Air Propulsion Test Center Attn: Mr. Bill Wagner TE-43 P. O. Box 7176 Trenton, NJ 08628	1
16. Naval Ordnance Systems Command Attn: Mr. John W. Murrin Department of Navy Arlington, VA 20360	1

DISTRIBUTION LIST (Cont'd)

	Copies
II. OTHER GOVERNMENT AGENCIES (Cont'd)	
17. Wright-Patterson Air Force Base Attn: E. E. Bailey AFAPL/DO Wright-Patterson AFB, OH 45433	1
Wright-Patterson Air Force Base Attn: Thomas Jackson AFAPL/SFF Wright-Patterson AFB, OH 45433	1
Wright-Patterson Air Force Base Attn: Robert Henderson AFAPL/TBC Wright-Patterson AFB, OH 45433	1
18. FAA/NAFE Attn: W. Westfield, ANA-410 Atlantic City, NJ 08405	1
III. UNIVERSITIES	
1. Cornell University Attn: Prof. F. Gouldin Sibley School of Mechanical & Applied Engineering Upson & Gruman Halls Ithaca, NY 14850	1
2. Massachusetts Institute of Technology Attn: Prof. J. Heywood Department of Mechanical Engineering Cambridge, MA 02139	1
3. Northwestern University Attn: Prof. C. K. Law Department of Mechanical Engineering & Astronautical Sciences Evanston, IL 60201	1
4. Pennsylvania State University Prof. G. M. Faeth Dept. of Mechanical Engineering 208 Mech. Eng. Bldg. University Park, PA 16802	1
5. Purdue University Attn: Prof. A. M. Mellor School of Mechanical Engineering West Lafayette, IN 47907	1

DISTRIBUTION LIST (Cont'd)

	Copies
III. UNIVERSITIES (Cont'd)	
Purdue University Attn: Prof. A. H. Lefebvre School of Mechanical Engineering West Lafayette, IN 47907	1
6. Department of Mechanical Engineering Attn: Prof. J. Odgers Laval University Quebec, CANADA Gik 7P4	1
7. University of California Attn: Prof. R. F. Sawyer Department of Mechanical Engineering Berkeley, CA 94720	1
8. University of California Attn: Prof. G. Scott Samuelson Mechanical and Environmental Eng. Irvine, CA 92717	1
9. University of Illinois at Urbana-Champaign Attn: Prof. R. A. Strehlow Dept. of Aeronautical & Astronautical Engineering 101 Transportation Building Urbana, IL 61801	1
10. University of Michigan Attn: Prof. A. Nicholls Department of Aerospace Engineering Gas Dynamics Lab. North Campus Ann Arbor, MI 48105	1
University of Michigan Attn: Prof. C. W. Kauffman Department of Aerospace Engineering Gas Dynamics Lab. North Campus Ann Arbor, MI 48105	1
11. University of Southern California Associate Dean of Engineering Attn: Prof. Melvin Gerstein School of Engineering Los Angeles, CA 90007	1

DISTRIBUTION LIST (Cont'd)

	Copies
III. UNIVERSITIES (Cont'd)	
12. University of Virginia Attn: Prof. Sam S. Fisher Dept. of Mech. and Aero. Eng. Charlottesville, VA 22901	1
IV. INDUSTRY	
1. Avco/Lycoming Corp. Attn: G. Opdyke 550 South Main Street Stratford, CT 06497	1
Avco/Lycoming Attn: Library 550 South Main Street Stratford, CT 06497	1
2. Battelle Columbus Laboratories Attn: Mr. David W. Locklin 505 King Avenue Columbus, OH 43201	1
Battelle Columbus Laboratories Attn: Library 505 King Avenue Columbus, OH 43201	1
3. Calspan Corporations Attn: Library 4455 Genesee Street Buffalo, NY 14221	1
4. Curtiss-Wright Corporation Attn: S. Moskowitz One Passaic Street Wooldridge, NY 07075	1
Curtiss-Wright Corporation Attn: Library One Passaic Street Wooldridge, NY 07075	1

DISTRIBUTION LIST (Cont'd)

	Copies
IV. INDUSTRY (Cont'd)	
5. Detroit Diesel Allison Div. Attn: J. Tomlinson Department 8882, Plant 8 Speed Code U27A P. O. Box 894 Indianapolis, IN 46202	1
Detroit Diesel Allison Div. Attn: A. Novick Department 8882, Plant 8 Speed Code U27A P. O. Box 894 Indianapolis, IN 46202	1
6. Garrett/AiResearch Company Attn: J. M. Haasis 402 South 36th Street Phoenix, AZ 85034	1
Garrett/AiResearch Company Attn: Library 402 South 36th Street Phoenix, AZ 85034	1
7. General Applied Science Laboratories Attn: G. Roffe Merrick and Stewart Avenues Westbury, NY 11590	1
General Applied Science Laboratories Attn: Library Merrick and Stewart Avenues Westbury, NY 11590	1
8. General Electric Company Attn: C. C. Gleason H-52 Aircraft Engine Group Evendale, OH 45215	1
General Electric Company Attn: D. Bahr H-52 Aircraft Engine Group Evendale, OH 45215	1

DISTRIBUTION LIST (Cont'd)

	Copies
IV. INDUSTRY (Cont'd)	
General Electric Company Attn: E. Ekstedt H-52 Aircraft Engine Group Evendale, OH 45215	1
General Electric Company Attn: Tech. Info. Ctr. N-32 Aircraft Engine Group Evendale, OH 45215	1
9. General Electric Company Attn: Library Gas Turbine Engineering Department One River Road No. 53-324 Schenectady, NY 12345	1
General Electric Company Attn: Dr. Richard Roberts Energy Systems & Technology Division Bld. #2 Room 543 One River Road Schenectady, NY 12345	1
General Electric Company Attn: Mr. Norman R. Dibelius Energy Systems & Technology Division Bld. #53 Room 331 One River Road Schenectady, NY 12345	1
10. International Harvester Company Attn: W. A. Compton Solar Division P. O. Box 80966 San Diego, CA 92138	1
International Harvester Company Attn: Library Solar Division P. O. Box 80966 San Diego, CA 92138	1
11. Northern Research & Engineering Corp. Attn: Library 219 Vassar Street Cambridge, MA 02139	1

DISTRIBUTION LIST (Cont'd)

	Copies
IV. INDUSTRY (Cont'd)	
12. Parker Hannifin Corp. Attn: H. C. Simmons 17325 Euclid Avenue Cleveland, OH 44112	1
Parker Hannifin Corp. Attn: Library 17325 Euclid Avenue Cleveland, OH 44112	1
13. Teledyne CAE Attn: C. Rogo 1330 Laskey Road Toledo, OH 43697	1
Teledyne CAE Attn: Library 1330 Laskey Road Toledo, OH 43697	1
14. United Technologies Corporation Attn: Library Pratt & Whitney Aircraft Group 400 Main Street East Hartford, CT 06108	1
15. United Technologies Corporation Attn: J. P. Rusnak Pratt & Whitney Aircraft Group Government Products Division Box 2691 West Palm Beach, FL 33402	1
United Technologies Corporation Attn: Library Pratt & Whitney Aircraft Group Government Products Division Box 2691 West Palm Beach, FL 33402	1
16. United Technologies Research Center Attn: R. Pelmas Silver Lane East Hartford, CT 06108	1

DISTRIBUTION LIST (Cont'd)

	Copies
IV. INDUSTRY (Cont'd)	
United Technologies Research Center Attn: H. Couch Silver Lane East Hartford, CT 06108	1
United Technologies Research Center Attn: Library Silver Lane East Hartford, CT 06108	1
17. Westinghouse Electric Corp. Attn: Mr. S. M. Decorso Gas Turbine Systems Division Lester Branch Box 9175 Philadelphia, PA 19113	1
Westinghouse Electric Corp. Attn: Library Gas Turbine Systems Division Lester Branch Box 9175 Philadelphia, PA 19113	1
18. Westinghouse Electric Corp. Attn: Mr. Richard M. Chamberlain Research and Development Center Pittsburgh, PA 15235	1
Westinghouse Electric Corp. Attn: Library Research and Development Center Pittsburgh, PA 15235	1
19. Williams Research Attn: M. Bak 2280 West Maple Walled Lake, MI 48088	1
Williams Research Attn: Library 2280 West Maple Walled Lake, MI 48088	1

5-
FIL